Image Histogram Features for Nano-scale Particle Detection and Classification

A thesis

submitted in partial fulfilment

of the requirements for the Degree

of

Doctor of Philosophy

in the

University of Canterbury

by

Kapila K Pahalawatta

Department of Computer Science and Software Engineering

University of Canterbury

2014

Sāraṁ ca sārato ňatvā
asāraṁ ca asārato
te sāraṁ adhigacchanthi
sammā samkappa gocarā

What is real they deem as real, what is unreal they deem as unreal, - they who abide in the pasture ground of right thoughts, arrive at the real
(Lord Buddha).

With love
to Patalee and Janindu

ACKNOWLEDGEMENTS

I express my deepest gratitude for the advice, guidance and suggestions given to me by my supervisor, Assoc. Prof. Richard Green, Department of Computer Science and Software Engineering, University of Canterbury, in the task of carrying out this research. I gratefully appreciate the knowledge, training and the guidance I received from his deep involvements in the computer vision field. Without his supervision and constant help this dissertation would not have been possible.

My special thanks to Assoc. Prof. R. Mukundan, my associate supervisor for his helpful advice. I like to take this opportunity to thank Mr. Hamish House, the director of NZi3 (National ICT Innovation Institute), the other staff members of NZi3, and also to the department of Computer Science and Software Engineering for their enormous support during my stay in NZi3.

In addition, I would like to acknowledge and thank FRST (now MSI) and Schneider Electric (the world leader in Electrical Distribution and global number 2 in Automation & Control) for their PhD TIF scholarship supporting this research.

Finally, to my wife Patalee and to my son Janindu who was of enormous help and support in the culmination of this work which was probably not fully appreciated at the time, thank you indeed.

Publications

1. Kapila K. Pahalawatta and Richard Green, “Particle Detection and Classification in Photoelectric Smoke Detectors using Image Histogram Features”, *International Conference on Digital Image Computing: Techniques and Applications*, December 2013, pp. 1-8.

2. Kapila K. Pahalawatta and Richard D. Green, “Detection and classification of nano-scale particles with image histograms”, *27th International Conference Image and Vision Computing New Zealand*, November 2012, pp. 446-451.

3. Kapila K. Pahalawatta and Richard Green, “Histogram Maximum Value Index Based Nano-scale Particle Classification”, *International Conference Image and Vision Computing New Zealand (IVCNZ)*, November 2011, pp. 214-219.

4. Kapila K. Pahalawatta and Richard Green, "Classifying Airborne Particles", *International Conference on Digital Image Computing: Techniques and Applications (DICTA),* December 2011, pp. 376-381.

5. Kapila K. Pahalawatta and Richard Green, “Nano-scale particle classification using image histogram maximum value index of Rayleigh scattered images”, *25th International Conference Image and Vision Computing New Zealand (IVCNZ),* November 2010, pp. 1-6.

ABSTRACT

This research proposes a method to detect and classify the smoke particles of common household fires by analysing the image histogram features of smoke particles generated by Rayleigh scattered light. This research was motivated by the failure of commercially available photoelectric smoke detectors to detect smoke particles less than 100 nm in diameter, such as those in polyurethane (in furniture) fires, and the occurrence of false positives such as those caused by steam.

Seven different types of particles (pinewood smoke, polyurethane smoke, steam, kerosene smoke, cotton wool smoke, cooking oil smoke and a test Smoke) were selected and exposed to a continuous spectrum of light in a closed particle chamber. A significant improvement over the common photoelectric smoke detectors was demonstrated by successfully detecting and classifying all test particles using colour histograms. As Rayleigh theory suggested, comparing the intensities of scattered light of different wavelengths is the best method to classify different sized particles. Existing histogram comparison methods based on histogram bin values failed to evaluate a relationship between the scattered intensities of individual red, green and blue laser beams with different sized particles due to the uneven particles movements inside the chamber.

The current study proposes a new method to classify these nano-scale particles using the particle density independent intensity histograms feature; Maximum Value Index. When a Rayleigh scatter (particles that have the diameter which is less than one tenth of the incident wavelength) is exposed to a light with different wavelengths, the intensities of

scattered light of each wavelength is unique according to the particle size and hence, a single unique maximum value index in the image intensity histogram can be detected.

Each captured image in the video frame sequence was divided into its red, green and blue planes (single R, G, B channel arrays) and the particles were isolated using a modified frame difference method. Mean and the standard deviation of the Maximum Value Index of intensity histograms over predefined number of frames (N) were used to differentiate different types of particles. The proposed classification algorithm successfully classified all the monotype particles with 100% accuracy when N ≥ 100. As expected, the classifier failed to distinguish wood smoke from other monotype particles due to the rapid variation of the maximum value index of the intensity histograms of the consecutive images of the image sequence since wood smoke is itself a complex composition of many monotype particles such as water vapour and resin smoke. The results suggest that the proposed algorithm may enable a smoke detector to be safer by detecting a wider range of fires and reduce false alarms such as those caused by steam.

TABLE OF CONTENTS

LIST OF FIGURES

LIST OF TABLES

1 – INTRODUCTION

Classification of digital images have recently become a widely used tool in many day to day human activities such as biometrics authentication, medical diagnosis and medical imaging for studying biological systems, crime prevention, military, geographical information and remote sensing systems, and also in many industrial and engineering applications. Usually, the classification algorithms analyse the numerical properties of various image features and organize data into categories. Most of the existing classification algorithms are constructed to classify the images of solid objects which are represented by a group of connected pixels in images.

With the aim of developing a new generation intelligent household smoke alarm, in the present study, a new kind of classification algorithm was constructed to classify much smaller airborne nano-scale particles which are represented by individual pixels in the images. The following section (section 1.1) discusses an overview of image histogram based classification techniques. The problem, the solution and the objectives of the study are introduced in the sections 1.2, 1.3 and 1.4 respectively. Finally, in the section 1.5, a guide to the theses is presented.

1.1 IMAGE CLASSIFICATION TECHNIQUES

In the past, a variety of content based image classification/retrieval methods have been proposed to classify different groups of images according to the application type. These methods include geometric feature-based methods (Kekre *et al*., 2010; Wiskott *et al*., 1997; Brunelli, & Poggio, 1993), template-based methods (Ahuja & Tuli, 2013; He *et al*., 2005; Belhumeur *et al*., 1997; Turk & Pentland, 1991), image histogram-based methods (Ahmadi *et al*., 2012; Malathi & Shanthi, 2010; Chapelle *et al*., 1999) and texture based methods (Kekre *et al*., 2010 (a); Kekre *et al*., 2010(b)). One of the major challenges in any of the applications that involve in image classification is to extract image features from a large collection of images. In geometric shape feature-based methods, usually, feature extraction is performed on binary images which are produced from a thresholding operation. The commonly extracted shape features include area, perimeter, center of mass, compactness, form factor, roundness, aspect ratio, elongation, curl, convexity, solidity and modification ratio. Template-based methods determine the image identity by measuring the correlation between the test image and some reference templates. Image textures can be artificially created or found in natural scenes captured in an image, and texture features gives us information about the spatial arrangement of colour or intensities in an image. Generally, artificially created textures are described with primitive texels (regular or repeated patterns) and natural textures are described as a quantitative measure of the arrangement of intensities.

Since the test objects in the present study are pixel sized nano-scale particles, it is impossible to extract geometric shape or texture features from test particles. Due to the same reason, creating reference templates for these particles is also impossible. Therefore, the present study uses colour and intensity histogram features. An image

histogram plots the number of pixels for each colour tone (histogram bin value) in the image and acts as a graphical representation of the tonal distribution in a digital image.

Histogram bin values have been extensively used in colour histogram based image classifications. Many of the well-known histogram comparison methods such as correlation, Chi-square, intersect and Bhattacharyya, are all based on histogram bin values. The probability mass density functions of image intensities, (1.1) and (1.2) below, respectively define the RGB (three colour channel) colour histogram and the intensity (single channel) histogram of an image with N pixels.

$$h_{R,G,B}(a,b,c) = N.prob(R = a, G = b, B = c) \quad 1.1$$

where *R*, *G* and *B* are the three colour (red, green and blue) channels.

$$h_A(a) = N.prob(A = a) \quad 1.2$$

where *A* is the selected colour (*R, G* or *B*) channel.

In both (1.1) and (1.2), a, b and c can get any integer value between 0 and 255.

The main difficulty with colour histogram based retrieval is histogram high dimensionality, even with drastic quantisation of the colour space. In contrast to colour histograms, the individual single channelled image histograms (e.g. R, G and B intensity histograms in RGB colour space) are computationally efficient to work with, even though they are less informative.

Normalised image histogram bin values can be considered as an image transform invariant feature of the objects which do not change the colours of its fragments irregularly with time.

In an intensity histogram, if

$h_A(X) = \max\{ h_A(a) / a \in [0,255]\}$, 1.3

then X can be defined as the Maximum Value Index (*MVI*) of the intensity histogram. In contrast to the singleton *MVI* of an intensity histogram, the *MVI* of a colour histogram is expressed by the triplet (X, Y, Z) where

$$h_{R,G,B}(X, Y, Z) = \max\{h_{R,G,B}(a,b,c) | \ a, b, c \ \epsilon \ [0,255]\}. \quad 1.4$$

With the images of small airborne particles, histogram bin values become quite ineffective for classification due to the high variability of particle density and the extensive overlapping of these pixel-sized objects in comparing images. By analysing the image histograms of consecutive video frames, it was discovered that the *MVI* of the histogram is a particle density independent feature and in this study six image signatures based on intensity and colour histogram *MVI*s are used for classification.

1.2 THE PROBLEM: PARTICLE DETECTION AND PARTICLE CLASSIFICATION IN HOUSEHOLD SMOKE DETECTORS

It was observed that the existing two types of household smoke detectors (photoelectric and ionization) response differently to different types of smoke. Photoelectric smoke detectors respond mostly to larger smoke particles (>1000 nm) and have a poor response to smaller smoke particles such as oil fires in kitchens. Even though, the other available type, radioactive smoke detectors can be used to detect such small smoke particles, they are not considered as environmentally friendly as photoelectric alarms and banned in some countries due to the presence of radioactive materials. On the other hand, both of these smoke detector types are prone to give off false positives for non-hazardous particles such as steam, which is a problem to both the fire services and to building occupants. Therefore, if the existing photoelectric alarm was modified to detect the smaller particles which can be detected by the ionization alarm, and modified to distinguish hazardous particles from non-hazardous particles, such a

smoke alarm would have the potential to replace both existing photoelectric and ionization alarms.

1.3 A SOLUTION: IMAGE HISTOGRAM BASED PARTICLE DETECTION AND CLASSIFICATION

The two terms, Image histogram based particle detection and image histogram based particle classification can be defined as follows.

Image histogram based particle detection: Use of image histograms features to classify images into two categories (images with particles and images without particles).

Image histogram based particle classification: Use of image histogram features to classify the images (with particles) into multi categories (steam, polyurethane, kerosene etc.)

Colour and intensity histogram features of Mie and Rayleigh scattered particle images were used to develop a new particle detection and classification algorithm for a photoelectric based smoke detector.

Particles were exposed to both white (wavelengths ranging from 400 nm to 800 nm) and red, green and blue lasers, where Rayleigh scattering can be observed with smaller particles and Mie scattering with larger particles. In the current study, seven different types of airborne particles (pinewood smoke, polyurethane smoke, steam, kerosene smoke, cotton wool smoke, cooking oil smoke and a test aerosol smoke (SD – 000) were tested. These smoke particle diameters ranged from 40 nm to 1000 nm).

1.4 MOTIVATION

All the existing classification methods (geometric feature-based methods, template-based methods, image histogram-based methods and texture based methods) deal with

larger objects with definite shape or texture or colour patterns and so are not useful for classifying nano-scale particles.

Since the test objects in the present study are the pixel sized nano-scale particles which represent as randomly moving single pixels in image frames, it is impossible to extract the geometric shape features, texture features or colour patterns from test particles and also due to the same reason, create reference templates for these particles are also unfeasible. Therefore, the present study tries to fills this gap by using particle density independent colour and intensity histogram feature, maximum value index, to classify these shapeless, textureless particles.

1.5 OBJECTIVES AND RESEARCH CONTRIBUTIONS

As mentioned above, the goal of this research is to develop an algorithm to detect and classify airborne nano-scale particles[1] with the aim of developing a new generation household smoke alarm using camera captured particle images, which prior detection and classification techniques has shown to be insufficient.

There are two main objectives.

1. Analysis of existing detection and classification techniques to identify the techniques and algorithms that can be used to detect and classify airborne nano-scale particles accurately.
2. Propose and develop a method to detect and classify airborne particles from camera captured images using image histogram features.

[1] Definition : Size range from approximately from 1 nm to 100 nm (ISO ISO/TS 27687:2008 Nanotechnologies - Terminology and definitions for nano objects - nanoparticle, nanofibre and nanoplate).

Research Contributions:

- Extensively evaluated:
    - the restrictions of double difference algorithm in background subtraction of nano-scale particle images
    - the limitations of filtering effects (median filter and Gaussian filter) on thresholded nano-scale particle images
    - the boundaries of bin value based histogram comparison methods (e.g. Chi-square, correlation, intersect and Bhattacharyya) in comparing the images with varying number of objects (particles)
- Developed an effective image histogram based airborne particle detection algorithm using Rayleigh scattered particle images in contrast to ineffectual traditional Mie scattering based photoelectric smoke detector (Instead of infrared light source which was used to capture the Mie scattered light in traditional smoke detectors, in the present study, we proposed a white light source or red, green and blue laser beams which can be used to capture both Mie and Rayleigh scattered light).
- Developed a histogram maximum value index (*MVI*) based particle image feature vector for classification. *MVI* is found as a particle density independent feature in nano-scale particle images.
- Extensively evaluated the efficiency of two of the well-known classification algorithms (k-nearest neighbour and multiple discriminant analysis) in classifying nano-scale particle images using *MVI* based feature vectors.

1.6 GUIDE TO THE THESIS

The background study of the current research consists of the three chapters; Chapter 2, Chapter 3 and Chapter 4. Chapter 2 provides the overall image of histogram based colour image retrieval systems with feature extraction techniques, light scattering theories behind the visibility of small nano-scale particles and classification algorithms. Previous studies on detection and classification of nano-scale airborne particles are described in Chapter 3. Chapter 4 explains how the traditional smoke detectors work, the reasons for failing in detection of certain kind of particles and other limitations of use of these commercially available smoke detectors. Experimental methodology is described in Chapter 5. The results which are obtained from a variety of techniques are analysed and discussed in detail in Chapter 6. Finally, Chapter 7 presents the conclusions and discusses future directions of this research.

2 – BACKGROUND

This chapter discusses the following topics; histogram based colour image retrieval systems (section 2.1), background subtraction methods (section 2.2), light scattering theories behind the visibility of small nano-scale particles (section 2.3) and classification algorithms (section 2.4) in detail. Under section 2.1, representation of digital colour images in different colour spaces, colour quantization methods and, histograms and image histogram comparison methods are discussed. In section 2.2, the relevance of different background subtraction methods to the current study is explained. Section 2.3 explains the different light scattering theories and particle size limitations for scattering, and, spectrums of artificial lighting systems. Under section 2.4 the relevant common classification algorithms available in the literature are described.

2.1 HISTOGRAM-BASED IMAGE RETRIEVAL AND CLASSIFICATION

Image classification is the problem of classifying images in a test set using a training set which is disjoint from the test set. The training data set consists of the data which can be used to construct or discover a predictive relationship. Generally, the term image retrieval is used to get the "closest" image (with respect to colour, shape, texture etc.) to the given query image from database. The major difference between image classification and image

retrieval is that classification needs labels for training data while retrieval does not. Retrieval is a purely a distance distance-based approach.

The present study proposes a new particle detection and classification algorithm based on image histogram features. In the past, Image histograms have been widely used in image processing for feature representation (colours, edges, etc.) (Dubuisson, 2010; Zhang *et al*. 2009; Bradski & Kaehler, 2008; Sergyan, 2008) and computer vision approaches such as image retrieval and object recognition (Bach *et al*., 1996; Flickner *et al*. 1995; Ogle, V. and Stonebraker, 1995). Many of these approaches require multiple comparisons of histograms for rectangular patches of an input image (Dubuisson, 2010; Laptev, 2010; Zhong & Defee, 2007). The dimensionality of the histogram depends on the number of colour channels used to construct the histogram. For example, histograms constructed with each of the single channel images of RGB colour space (intensity histograms) are two dimensional and histograms constructed with 3 colour channel images are 4 dimensional. The following section (2.1.1) explains the different colour models and representation of images with these models in detail.

2.1.1 COLOUR SPACES

Colour spaces (or colour models) are used to specify colours of image pixels uniquely. Various colour spaces have been defined depending on the application involved. For example, humans determine colours by parameters such as brightness, hue, and colourfulness (saturation). Most colour CRT monitors and colour raster graphics applications describe colours using three primary colours, red, green, and blue because colour generation for these applications are based on the additive red, green, and blue phosphors of a black computer monitor. The printing industry uses cyan, magenta, and yellow to specify subtractive colours because they are based on the reflectance and absorbance of inks by white paper. The most commonly used colour spaces in computer

vision applications are RGB (red, green, blue), HSL (hue, saturation, luminosity), and HSV (hue, saturation, value) colour spaces. An example of all the colours of a test colour image in its RGB, HSV and HSL colour spaces are shown in Figure 2.1. The test colour image (Figure 2.1(a)) has 160,000 pixels with 110,463 colours.

The RGB colour model and the HSV colour model (for comparison) are explained in detail in the following two sections.

2.1.1.1 RGB COLOUR MODEL

With the three additive primaries, red, green and blue, this model defines colours in a 3-dimensional cube in the Cartesian coordinate system. Figure 2.2(a) shows the RGB Cartesian coordinate system and Figure 2.2(b) shows the actual colours in the RGB colour model looking down from the "white" to origin.

2.1.1.2 HSV COLOUR MODEL

The HSV colour space forms a single cone (Figure 2.3) with the following parameters.

- Hue: The basic colour in the colour wheel, ranging from 0 to 360 degrees where both 0 and 360 degrees are red.
- Saturation: How pure the colour is, ranging from 0 to 100, where 100 is fully saturated and 0 is gray.
- Value: How bright the colour is, ranging from 0 to 100, where 100 is as bright as possible and 0 is as dark as possible (black).

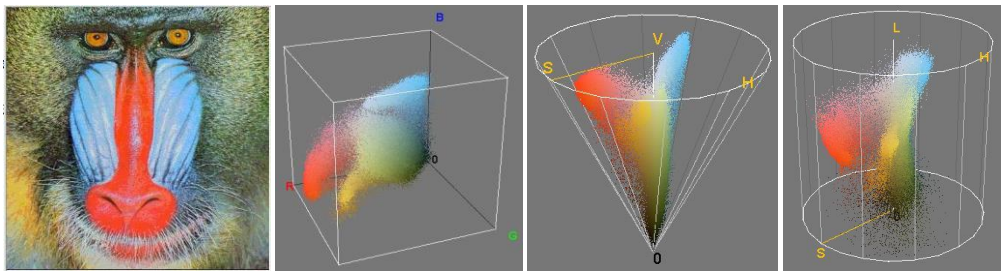

(a) (b) (c) (d)

Figure 2.1 All colours in RGB colour space (b), HSV colour space (c) and HSL colour space (d) of the test colour image (a)

2.1.1.3 HSL COLOUR MODEL

HSL colour model takes the following three values.

- Hue is a degree on the colour wheel; 0 (or 360) is red, 120 is green and 240 is blue. Numbers in between reflect different shades.
- Saturation is a percentage value; 100% is the full colour (this is an entirely different value from the saturation value of the HSV colour model).
- Lightness is also a percentage; 0% is dark (black), 100% is light (white), and 50% is the average.

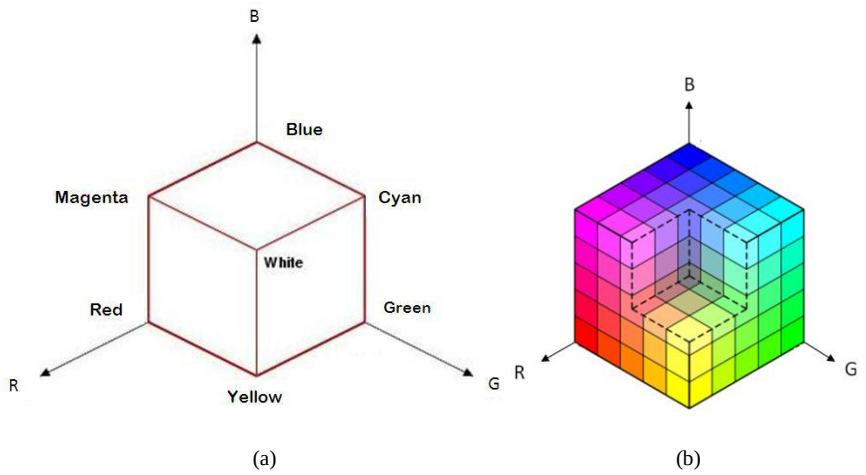

(a) (b)

Figure 2.2 (a) Cartesian coordinate system of RGB colour model, (b) The colours of the RGB colour model viewing through the direction of "white" to origin

Even though the HSL colour model is a cylindrical geometry (Figure 2.4(a)), often it is described as a biconel solid (Figure 2.4(b)) with the chroma dimension instead of saturation.

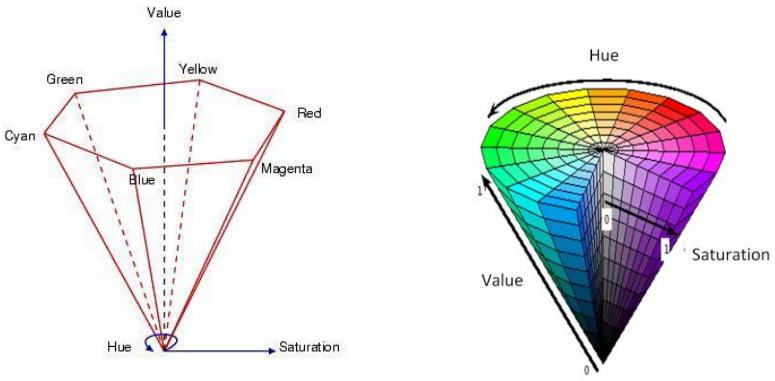

Figure 2.3 HSV colour model

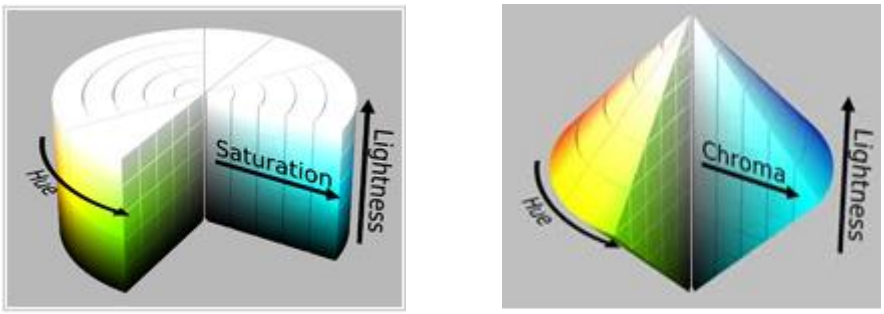

(a) (b)

Figure 2.4 Cylindrical (a) and biconel (b) representation of HSL colour model

The HSV, HSL and RGB colour models are compatible with each other, i.e. any colour of one model can be represented by a colour in the other model. For an example, following equations explains the colour conversion formulas between HSV and RGB colour models.

2.1.1.4 RGB TO HSV CONVERSION

$$H = cos^{-1}\left\{\frac{1/2[(R-G)+(R-B)}{\sqrt{(R-G)^2+(R-B)(G-B)}}\right\} \quad 2.1$$

$$S = 1 - \frac{3}{R+G+B}[\min(R,G,B)] \quad 2.2$$

$$V = \frac{1}{3}(R+G+B) \quad 2.3$$

2.1.1.5 HSV TO RGB CONVERSION

For 0º < H < 120º

$$b = \frac{1}{3}(1-S), \quad r = \frac{1}{3}\left[1+\frac{S\,cosH}{\cos(60^0-H)}\right], \quad g = 1-(r+b) \quad 2.4$$

For 120º < H < 240º

$$r = \frac{1}{3}(1-S), \quad g = \frac{1}{3}\left[1+\frac{S\,cosH}{\cos(60^0-H)}\right], \quad b = 1-(r+b) \quad 2.5$$

For 240º < H < 360º

$$g = \frac{1}{3}(1-S), \quad b = \frac{1}{3}\left[1+\frac{S\,cosH}{\cos(60^0-H)}\right], \quad r = 1-(r+b) \quad 2.6$$

The RGB colour model enables constructing numerous colours by varying its red, green and blue components separately. Today, most devices such as computer monitors, televisions, digital cameras and scanners use this colour model. On the other hand, unlike RGB, HSV colour model separates LUMA, or the image intensity, from CHROMA or the colour information. This feature is very useful in some computer vision applications where

it is necessary to not change the colour information while varying the intensity component (e.g. histogram equalization of a colour image). Therefore many computer vision researchers prefer to use HSV colour model rather than RGB colour model since it can sometimes be easier to research unwanted effects in images such as reflections, shadows and lighting changes.

As described in section 2.3, the separate red, green and blue colour components of Rayleigh scattered light can be used to analyse the image histograms features to build a successful classification algorithm, instead of HSV, the RGB colour model is sufficient enough to describe the images, if all the images were taken inside a closed chamber with minimal undesirable effects from shadowing, lighting changes and reflections.

2.1.1.6 RGB REPRESENTATION OF DIGITAL COLOUR IMAGES

Resolution: Pixels are the smallest image elements which are used to construct digital images. Image resolution is the number of pixels per specified area of the image and is written in the form width value x height value. Width and height are generally measured in pixels. Pixels are placed next to each other in a two dimensional grid to represent the image.

Bit depth: Another property of an image is the pixel bit depth. This is the number of bits that are used to store the colour information for each pixel. The number of unique colours that can be represented with the bit depth is explained in the following formula.

$$Number\ of\ unique\ colours = 2^{bit\ depth} \quad 2.7$$

For example, one bit can store only two colours because a single bit can only be 0 or 1 (2^1). If 24 bits are used 2^{24} or 16,777,216 unique colours can be represented. The following table shows different image types in terms of bit depth, total colours available, and their common names.

TABLE 2.1 TYPES OF IMAGES WITH DIFFERENT BIT DEPTHS

Bits Per Pixel	Number of Colours Available	Common Name(s)
1	2	Monochrome
2	4	CGA
4	16	EGA
8	256	VGA
16	65536	XGA, High Colour
24	16777216	SVGA, True Colour
32	16777216 + Transparency	
48	281 Trillion	

Colour Channel: An RGB image consists of three channels: red, green, and blue. If the image is 24-bit then each channel has 8 bits, for red, green, and blue. That is the image is composed of three images (one for each channel), where each image can store discrete pixels with conventional brightness intensities between 0 and 255. If the RGB image is 48-bit (very high resolution), each channel is made of 16-bit pixel images. Figure 2.5 shows a colour ape image and a RGB colour smoke image captured with laser beams (a) with its individual red (b), green (c) and blue (d) channel images. Note that even though, red, green and blue colours have been applied to the images in Figures 2.5(b), 2.5(c) and 2.5(d) to show the differences between the images clearly, they are single channel grayscale images (with no colour information).

2.1.2 IMAGE HISTOGRAM DEFINITION

Image histograms can be defined for images in any colour space. The image histograms of RGB, HSV and HSL colour spaces of the image in Figure. 2.1(a) are shown in Figure 2.6. The colour space can be partitioned into a minimal number of equally spaced cubes (colour bins). For every bin, the frequency within the bin is determined. In this example, each bin is represented by a sphere (ball) with a volume proportional to the frequency. Each of the histograms in these three colour spaces in Figure 2.6 has only 271 colour bins (after partition). Such quantization of colour spaces is explained below.

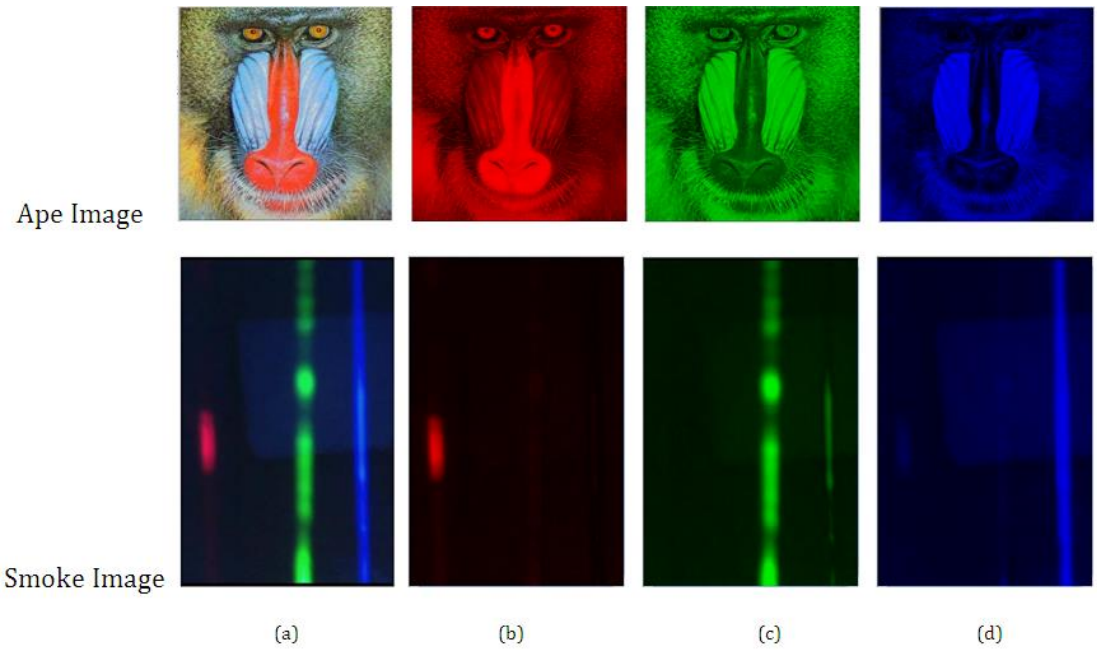

Figure 2.5 A colour ape image and a RGB colour smoke image (a) with their individual red (b), green (c) and blue (d) channel images

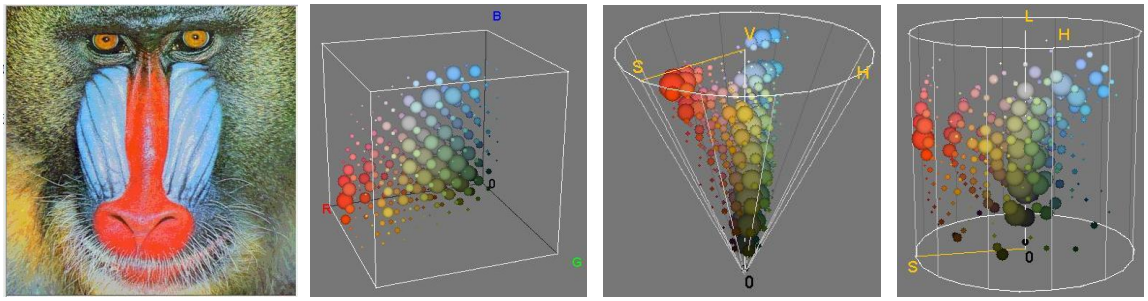

Figure 2.6 271 colour bin histograms in RGB colour space (b), HSV colour space (c) and HSL colour space (d) of the colour image (a)

The RGB colour histogram of an image with N pixels is defined by the following probability mass density function of the image intensities.

$$h_{R,G,B}(a,b,c)=N.\text{Prob}(R=a, G=b, B=c) \quad 2.8$$

where R, G and B are the three colour (red, green and blue) channels.

The histogram of a single channelled image (or intensity histogram) is defined as

$$h_A(a)=N.\text{Prob}(A=a) \quad 2.9$$

where A is the selected colour (R, G or B) channel. For an example, in a 24 bit colour image, a, b and c can get any integer value between 0 and 255 in both (2.8) and (2.9).

Since image histograms do not reveal spatial information of the pixels of a given colour, they are invariant to rotation and translation. Additionally, Image histograms are robust against occlusion and changes in camera viewpoint. In the present study, both colour and intensity histograms have been tested for their efficiency in classifying particles.

2.1.2.1 COLOUR QUANTIZATION

The principle challenge of using RGB colour histogram based retrieval is the high dimensionality of a histogram (For an example, a 24 bit RGB colour image histogram contains 16777216 (=256 x 256 x 256) bins). Therefore, in computer graphics, colour quantization or colour image quantization is used to reduce the number of distinct colours used in an image while keeping the new image as visually similar as possible to the original image. Figure 2.7 shows the resultant images with their histograms of an image (polyurethane smoke with laser lights) used in the current study with different quantization levels.

Uniform[2], Popularity (Clark, 1995; Heckbert, 1982), Median Cut (Heckbert, 1982; Kruger, 1994) and Octree (Gervautz & Purgathofer, 1988; Bloomberg, 2008; Clark, 1996) are some of the popular colour quantization algorithms available in the literature. For example, Figure 2.7 shows a smoke image (captured with laser beams) and its different

[2] http://www-scf.usc.edu/~csci576b/Slides/Lecture4_ColorQuantization.pdf (visited on 03/03/2014)

quantized images, quantized with to Popularity algorithm which constructs a histogram of equal-sized ranges and assigns colours to the ranges containing the most points.

In contrast to colour histograms, it is computationally inexpensive to work with the three single red, green and blue channelled image histograms even though they are less informative. Figure 2.8 shows the histograms (after quantized to 12 colours) of single red (a), green (b) and blue (c) channelled images which is shown in Figures 2.5 (b), 2.5 (c) and 2.5 (d) respectively.

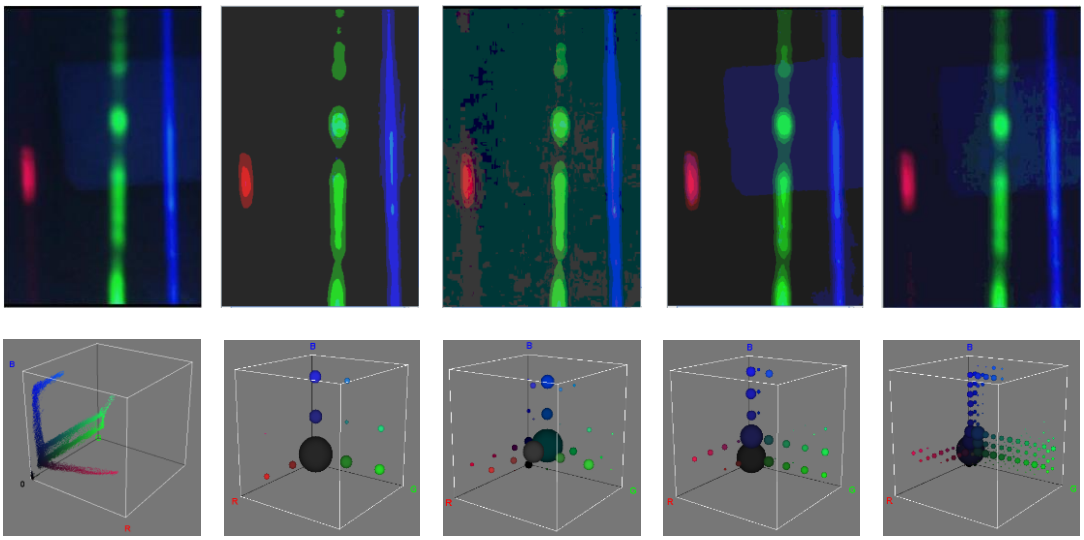

(a) (b) (c) (d) (e)

Figure 2.7 A smoke image (captured with laser beams) with 19989 colours and representation of its all colours in RGB colour space (a), and the images and histograms after quantization to 11 colours (b), 27 colours (c), 38 colours (d) and 153 colours (e)

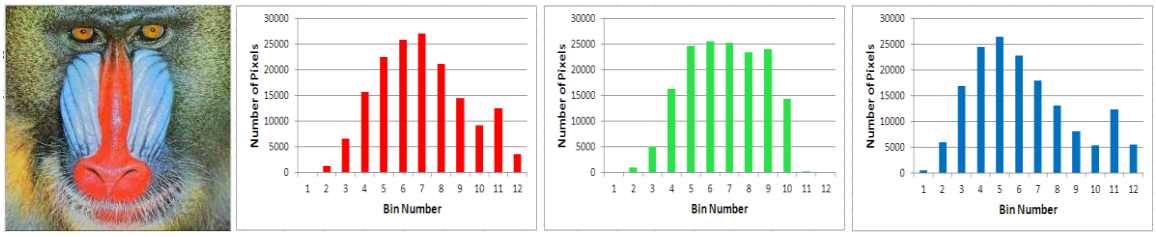

(a) (b) (c) (d)

Figure 2.8 Histograms of single red (b), green (c) and blue (d) channel images of figures 5 (b), 5 (c) and 5 (d) respectively, after quantized to 12 colours. (a) is the original RGB colour image

2.1.2.2 HISTOGRAM COMPARISON:

Of the histogram comparison methods available in the literature, the most commonly used four histogram comparison methods (correlation method, Chi-square method, intersection method and Bhattacharyya distance) are discussed here (Dubuisson, 2010; Bradski and Kaehler, 2008). All these methods compare the bin values of each bin in the comparing histograms. All these four methods will be discussed here in detail and the notation $H_i(j)$ in all these methods, is the value of j^{th} bin of the i^{th} histogram *Hi*.

Correlation method

In statistics, the correlation coefficient *r* measures the strength and direction of a linear relationship between two variables on a scatter plot. The value of *r* is always between +1 and –1.

The value of *r* can be calculated using the equation,

$$r_{xy} = \frac{\sum XY - \frac{(\sum X)(\sum Y)}{n}}{\sqrt{(SS_x)(SS_y)}} \text{ or } r_{xy} = \frac{\sum XY - \frac{(\sum X)(\sum Y)}{n}}{\sqrt{\left(\sum X^2 - \frac{(\sum X)^2}{n_x}\right)\left(\sum Y^2 - \frac{(\sum Y)^2}{n_y}\right)}} \quad 2.10$$

If *N* is the number of bins in each of the histograms (H_1 and H_2) of two images, the correlation comparison parameter between the two histograms can be defined as

$$d_{correl}(H_1, H_2) = \frac{\sum_i H_1'(i).H_2'(i)}{\sqrt{\sum_i H_1'^2(i).H_2'^2(i)}} \quad 2.11$$

where $H_k'(i) = H_k(i) - \left(\frac{1}{N}\right)(\sum_j H_k(j))$.

For the correlation method, a high score represents a better match than a low score. A perfect match is 1 and a maximal mismatch is –1; a value of 0 indicates no correlation (random association).

Chi-square method

Chi-square method is first suggested by Pearson to ... and the parameter χ2 is defined as

$$\chi 2 = \sum \frac{(Observed\ value - Expected\ value)^2}{Expected\ value} \quad 2.12$$

If $H_1(i)$ and $H_2(i)$ are the number of pixels in the i^{th} bin in the first and second histogram respectively and r is the number of bins in each of the histograms, the Chi-square comparison coefficient between the two histograms, H_1 and H_2, can be defined as

$$d_{chi-square}(H_1, H_2) = \frac{1}{MN} \sum_{i=1}^{r} \frac{(MH_1(i) - NH_2(i))^2}{H_1(i) + H_2(i)} \quad 2.13$$

where, $M = \sum_{i=1}^{r} H_1(i)$ and $N = \sum_{i=1}^{r} H_2(i)$.

If both images have same number of pixels (i.e. $M=N$), then

$$d_{chi-square}(H_1, H_2) = \sum_{i=1}^{r} \frac{(H_1(i) - H_2(i))^2}{H_1(i) + H_2(i)} \quad 2.14$$

For chi-square method, a low score represents a better match than a high score. A perfect match is 0 and a total mismatch is unbounded (depending on the size of the histogram).

Intersection method

Swain and Ballard (1990 and 1991) proposed a straightforward method to calculate the matching rate between two histograms; histogram intersection method. Assuming the histograms of a model image and a target image are H_1 and H_2 respectively, and each contains n bins, Swain and Ballard (1991) defined the intersection $d_{intersection}\ (H_1,H_2)$ of two histograms as:

$$d_{intersection}(H_1, H_2) = \sum_{i=1}^{n} min(H_1(i), H_2(i)) \quad 2.15$$

For histogram intersection, high scores indicate good matches and low scores indicate bad matches. If both histograms are normalized to 1,

i.e., $\sum_{i=1}^{n} H_1(i) = 1$ and $\sum_{i=1}^{n} H_2(i) = 1$,

then a perfect match is 1 and a total mismatch is 0. The resultant fractional matching value between 0 and 1 is actually the proportion of pixels from the model image that have corresponding pixels of the same colour in the target image.

Histogram intersection method is graphically illustrated in Figure 2.9. NH_1, NH_2 and IH_1H_2 are a normalized histogram of H_1, normalized histogram of H_2 and intersection of NH_1 and NH_2 respectively (histogram data, H_1 and H_2 were obtained from the two histograms in Figures 2.8(c) and 2.8(d) respectively).

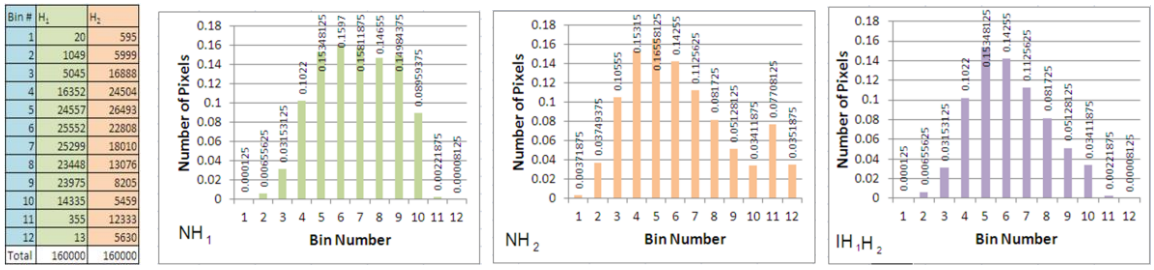

$$NH_1(i) = \frac{H_1(i)}{\sum_{i=1}^{n} H_1(i)} \qquad NH_2(i) = \frac{H_2(i)}{\sum_{i=1}^{n} H_2(i)} \qquad IH_1H_2(i) = \min(H_1(i), H_2(i))$$

$$\sum_{i=1}^{n} NH_1(i) = 1 \qquad \sum_{i=1}^{n} NH_2(i) = 1 \qquad \sum_{i=1}^{n} IH_1H_2(i) = 0.7184$$

Figure 2.9 Histogram Intersection Method

This histogram intersection method is robust to four important problems that hinder the recognition: distractions in the background of the object, viewing the object from a variety of viewpoints, occlusion and varying image resolutions (Swain and Ballard, 1991).

Bhattacharyya distance

In the context of histogram comparison, the Bhattacharyya distance $d_{Bhattacharyya}(H_1,H_2)$ is expressed as

$$d_{Bhattacharyya}(H_1, H_2) = \sqrt{1 - \sum_i \frac{\sqrt{H_1(i).H_2(i)}}{\sqrt{\sum_i H_1(i) \,.\, \sum_i H_2(i)}}} \qquad 2.16$$

If both histograms are normalized to 1, then

$$d_{Bhattacharyya}(H_1, H_2) = \sqrt{1 - \sum_i \sqrt{H_1(i).H_2(i)}} \qquad 2.17$$

Bhattacharyya histogram comparison method is graphically illustrated in Figure 2.10. NH_1, NH_2 are the normalized histogram of H_1 and the normalized histogram of H_2 respectively (again, histogram data, H_1 and H_2 were obtained from the two histograms in Figures 2.8(c) and 2.8(d) respectively).

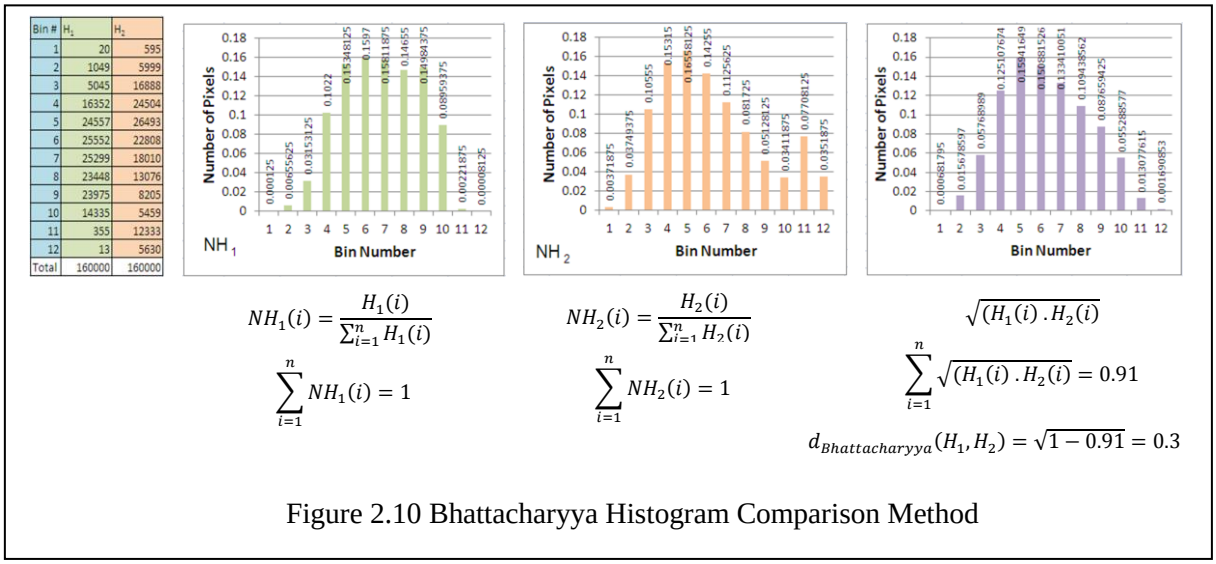

Figure 2.10 Bhattacharyya Histogram Comparison Method

For Bhattacharyya matching, low scores indicate good matches and high scores indicate bad matches. A perfect match is 0 and a total mismatch is 1.

For an example, Figure 2.11 shows a steam image and a polyurethane smoke image captured with laser lights (a) with their colour information in RGB colour space (b), 92 colour quantised image (c) and RGB colour histogram with 92 colours (D). The results obtained after comparing the images of three smoke types (polyurethane, kerosene and pinewood) with the above mentioned histogram comparison methods are shown in Table 2.2 for illustration purposes.

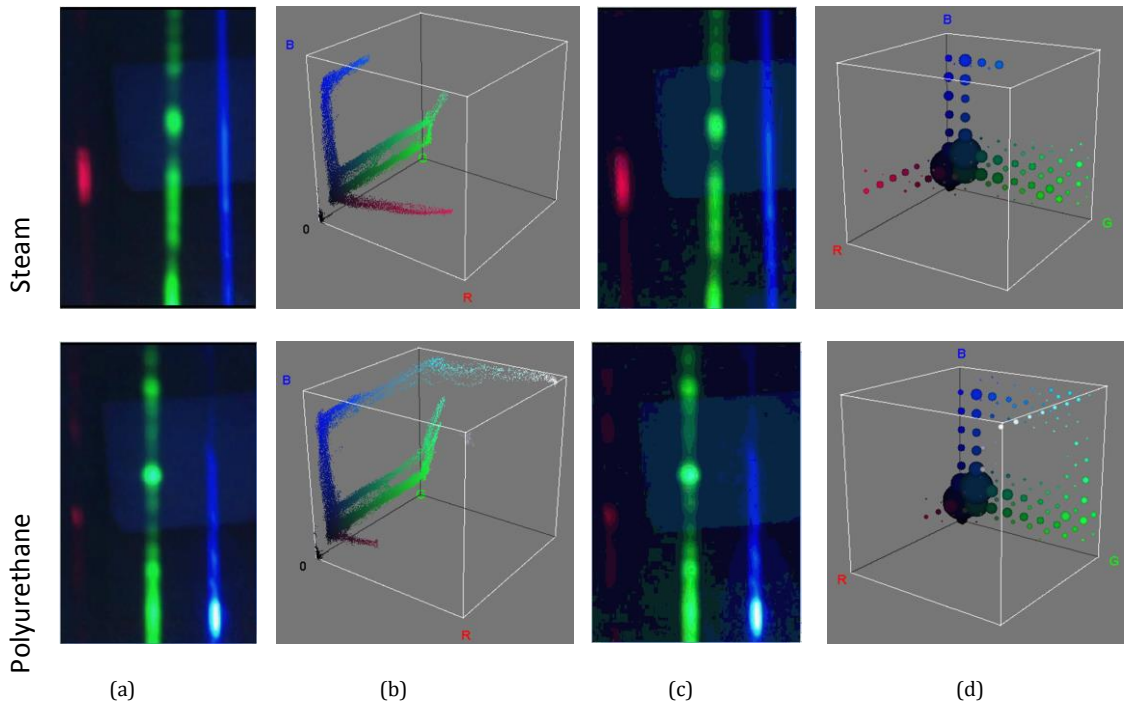

Figure 2.11 Particle image (a), all colours in RGB colour space (b), Quantized image (92 colours)(c) and Histogram (d)

Because all these histogram comparison methods are based on the bin values of the comparing histograms, the efficiency of these methods are limited to comparing the images of the objects which doesn't change with the bin values in their image histograms over time.

TABLE 2.2 HISTOGRAM COMPARISON PARAMETERS USING DIFFERENT HISTOGRAM COMPARISON METHODS

Image	Bhattacharyya	Intersect	Correlation	Chi square
Polyurethane	0.12	0.32	0.78	0.92
Kerosene	0.89	0.11	0.21	1.2
Pinewood	0.67	0.91	0.01	1.23

2.1.2.3 MAXIMUM VALUE INDEX

In an intensity histogram, if

$$h_A(X) = \max\{ h_A(a) | \, a \in [0,255]\}, \quad 2.18$$

X can be defined as the Maximum Value Index (*MVI*) of the intensity histogram. In contrast to the singleton *MVI* of an intensity histogram, the *MVI* of a colour histogram is expressed by the triplet (*X, Y, Z*) where

$$h_{R,G,B}(X, Y, Z) = \max\{h_{R,G,B}(a,b.c) | \, a, b, c \in [0,255]\}. \quad 2.19$$

In the literature published, comparisons of histogram bin values were extensively used in colour histogram based image classifications (Zhang *et al*. 2009; Bradski & Kaehler, 2008; Sergyan, 2008). In the case of images of airborne nano-scale particles, this signature becomes quite ineffective due to the high variability of particle density and the overlapping of these pixel sized objects in comparing images. For an example, Figure 2.12 shows grayscale difference image histograms of four selected frames in a test image sequence (first kerosene sequence) with the thresholded difference images.

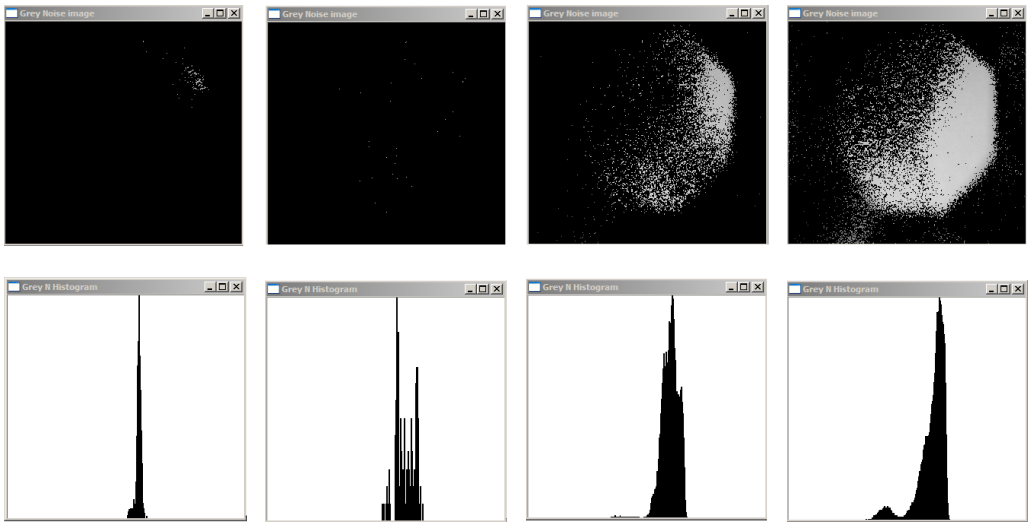

(a) (b) (c) (d)

Figure 2.12 Histograms of 50th (a), 100th (b), 150th (c) and 200th (d) frames of first Kerosene sequence (captured with digital microscope) with the thresholded difference images

2.2 BACKGROUND SUBTRACTION

The main goal of background subtraction is to distinguish all the objects of interest from a given frame sequence recorded using a fixed camera. Theoretically, this can be done by detecting all the foreground objects as a difference between the current frame and its static background.

$$| frame_i – background_i | > Threshold$$

With this approach, the first problem that one faces is a way to obtain a static background. In common open environments, the backgrounds are often not fixed due to the three common factors (Grimson *et al.*, 1998; Stauffer & Grimson, 1999)).

- Changes in Illumination: This can either be gradual change (e.g. changes in day light) or a sudden change (e.g. clouds).
- Changes in Motion: Camera oscillations, tree branches, sea waves etc.
- Changes in background geometry: Parked cars

The following section describes some common background subtraction methods.

2.2.1 FRAME DIFFERENCE ALGORITHM

If the background is fixed and static (i.e. no changes due to any of the factors mentioned above), the frame difference method is very effective in isolating foreground moving objects. Difference pictures are constructed by comparing the corresponding pixels of the two frames involved. In general, the differences between the corresponding pixels of the comparing two frames are grouped and for each group, all the corresponding pixels in the difference picture will get a same unique value (Jain *et al.*, 1995; Xia, *et al.*, 2009). For an example, the pixel value at the pixel (x, y) of the simplest form of a binary difference picture DP_{jk} between the j^{th} frame F_j and k^{th} frame F_k , $DP_{jk}(x, y)$, is expressed by the following formula 2.20.

$$DP_{jk}(x,y) = \begin{cases} 1, & if\ \left|F_J(x,y) - F_K(x,y)\right| > \tau \\ 0, & Otherwise \end{cases} \qquad 2.20$$

where τ is a predefined threshold, $Fi(x, y)$ is the pixel value at the pixel (x, y) of i^{th} frame.

The pixels which have the value 1 in a binary difference picture expressed by the above formula represent the changed (modified) pixels in the second frame of the comparing two frames. Difference pictures are highly sensitive to the value of the threshold and strongly dependant on the object's speed and the frame rate. For an example, Figure 2.13(c) shows the difference picture between the two frames in Figures 2.13(a) and 2.13(b). Figures 2.13(d), 2.13(e) and 2.13(f) are the thresholded difference pictures of the same two frames (Figures 2.13(a) and 2.13(b)) constructed with different thresholds (τ). Images in Figures 2.13(a) and 2.13(b) are the 110th frame and the first frame (before introduction of particles) of the first captured steam image sequence respectively.

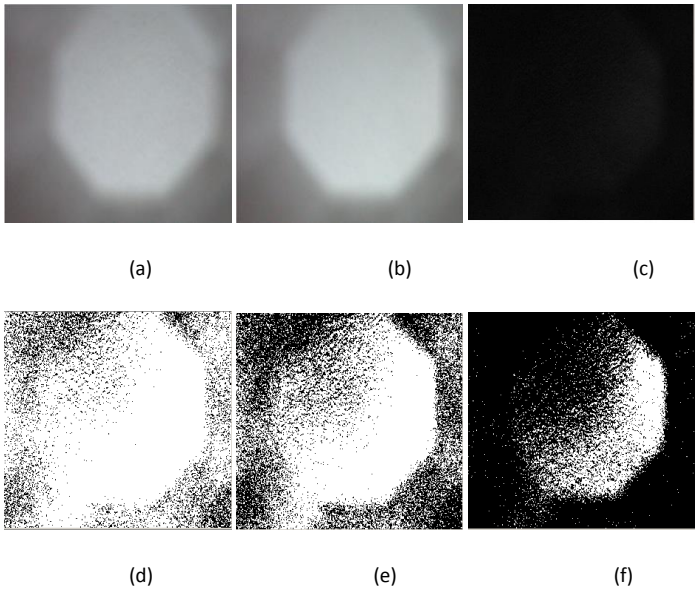

Figure 2.13 Captured images of without smoke (a) and with smoke (b), with the difference picture (c) and thresholded difference images with thresholds τ = 8 (d), τ = 10 (e) and τ = 15 (f)

2.2.2 DOUBLE DIFFERENCE ALGORITHM

Generally, the double difference image *(DDn)* of the nth frame *(Fn)* is constructed with the use of three consecutive frames, previous frame *(Fn-1), current frame (Fn)* and the next frame *(Fn+1)* and it is defined as

$$DD_n(x,y) = \begin{cases} 1, & if\ flag = 1 \\ 0, & otherwise \end{cases} \qquad 2.21$$

where

$flag = (DP_{n-1,n} = 1) \wedge (DP_{n,n+1} = 1)$ and

$DD_n(x, y)$ is the pixel value at the pixel (x, y) of the double difference picture DD_n (Xia *et al.*, 2009).

For example, Figure 2.14(c) shows a double difference picture (*DDn*) constructed with two difference pictures, Figure 2.14(a) ($DP_{n-1,n}$) and Figure 2.14(b) ($DP_{n,n+1}$). Difference images were constructed with the consecutive frames, 117, 118 and 119, of the first captured steam image sequence.

(a) (b) (c)

Figure 2.14 Double difference picture (c) constructed with the difference pictures $DP_{n-1,n}$ (a) and $DP_{n,n+1}$ (b)

The logical AND operation of the equation 2.21 gives a pixel in the double difference image with the value of 1 only when the corresponding pixels of both consecutive difference images have the value of 1. Double difference image is much better in suppressing noise than the simple frame difference method because it is less likely to trace noise as a change in both difference images.

Nano-scale particles (used in the current study) appear as single individual pixels or irregular shaped cluster of pixels in the captured images. Furthermore, there are many new pixels appearing (images of new particles) and also existing old pixels are disappearing in the consecutive images. Due to these behaviours of the used particles, double difference method filters out a vast number of image pixels as noise pixels. Therefore, the double difference method cannot be considered as an appropriate method to construct the difference images in small sized particle images.

2.2.3 PFINDER:

Pfinder (Wren *et al*., 1997) uses a simple multi-class statistical model, where background pixels are modelled by a single Gaussian, and updated by the adaptive filter

$$\mu_t = (1 - \alpha)\mu_{t-1} + \alpha I_t , \qquad 2.22$$

where μ_t is the 2D spatial means of the Clusters of 2D points

and foreground pixels are explicitly modelled by a mean and covariance, which are updated recursively. *Pfinder* requires an empty scene at the start-up and clusters the object pixels using image properties such as colour and spatial similarity and combines them to form coherent connected regions called "blobs" in which all the pixels have similar image properties (Figure 2.15).

(a) (b) (c)

Figure 2.15 Pfinder blob construction (Video input (a), Segmented image (b)and 2D blob representation (c))(adopted from Wren *et al*. 1997)

Even though, originally *Pfinder* has been designed to detect features in video images in order to recognize human figures, later improvements of *Pfinder* can also track body parts of a person (e.g. head and hands) and can recognize the poses and the body gestures. However, *Pfinder* does not cope with multi-modal backgrounds, in which a histogram of the pixel intensity contains more than one distinct peak and also multiple objects (people) in

the same image. Therefore, with the images of nano-scale particles, *Pfinder* becomes inoperative because it attempts to analyse the multiple pixel sized objects in the image as one distinct object due to the failure of forming "blobs" for individual pixels. Also, there have been no reports on the success of *Pfinder* in outdoor scenes (Stuffer & Grimson, 1999; Wren *et al*., 1997).

2.2.4 FOREGROUND DETECTION WITH KALMAN FILTERING:

When a state of a linear system is assumed to be distributed by a Gaussian, Kalman filter technique is used to estimate the state. R.E. Kalman (1960) published a paper describing a recursive solution to the discrete-data linear filtering problem. The Kalman filter is a set of mathematical equations that provides an efficient computational (recursive) means to estimate the state of a process in several aspects: it supports estimations of past, present, and even future states, and it can do the same even when the precise nature of the modelled system is unknown (Patel & Thakore, 2013).

To overcome the influences of illumination changes in the background, Koller *et al*. (1994), Ridder *et al*. (1995) employed a model with Kalman filtering. It made their system more robust to illumination changes in a scene. They modelled each pixel with a Kalman filter and used a pixel-wise automatic threshold.

2.2.5 MIXTURE OF ADAPTIVE GAUSSIANS:

If only lighting changed over time, a single, adaptive Gaussian per pixel would be sufficient.

In practice, multiple surfaces often appear in the view frustum of a particular pixel with the changes in lighting conditions. In many instances, multiple, adaptive Gaussians has been used to deal with these conditions (Grimson *et al*., 1998; Ivanov *et al*. 1999; Stauffer &

Grimson, 1999). In this approach each pixel is modelled separately by a mixture of K Gaussians

$$P(I_t) = \sum_{i=1}^{K} \omega_{i,t}\eta(I_t; \mu_{i,t}) \quad 2.23$$

If all the images were captured in a closed chamber, illumination/lighting changes or movements of the objects in the background cannot be expected. Therefore, both of the latter mentioned two background subtraction models (Kalman Filtering or Mixture of adaptive Gaussians) become futile.

2.3 LIGHT SCATTERING EFFECT BY SMOKE PARTICLES ON R, G AND B CHANNEL HISTOGRAMS OF SMOKE IMAGES

There are two principle types of Scattering, non-selective scattering and selective scattering. When all wavelengths of the incident light are equally scattered then it is called non-selective scattering. This type of scattering is caused by particles which are much larger than the wavelength of the incident light. Because all wavelengths are equally scattered, the scatters (particles) collectively appear as white colour.

According to the theory of light scattering, the visibility of small particles mainly depends on two types of selective scattering, Mie and Rayleigh. If the size of the scatters is less than one tenth of the incident wavelength, Rayleigh scattering occurs[3] (Kopeika, 1989; Li *et al*., 2001) and these scatters are called Rayleigh scatters. Intensity of the Rayleigh scattered light is inversely proportional to the fourth power of the wavelength of the incident light (Equation 2.24). Therefore, Rayleigh scattering is strongly dependant on the wavelength (selective scattering). Waves with shorter wavelength are scattered more than the waves with longer wavelengths. This type of scattering is more severe towards the ultraviolet and blue end of the visible spectrum and is negligible at wavelengths beyond

[3] Wikipedia, http://en.wikipedia.org/wiki/Rayleigh_scattering (visited on 12/08/2013).

1000 nm. For example, blue light is scattered around four times as much as red light, and UV light is scattered about 16 times as much as red light by Rayleigh scatters.

Rayleigh scattered light intensity by a single particle is given by the following equation (2.24).

$$I(\theta) = I_0 \frac{1 + cos^2\theta}{2R^2} \left(\frac{2\pi}{\lambda}\right)^4 \left(\frac{n^2 - 1}{n^2 + 2}\right)^2 \left(\frac{d}{2}\right)^6 \quad 2.24$$

Where $I(\theta)$ is the scattered light intensity by the particle at angle θ,

θ is the scattering angle

I_0 is the intensity of incident light

R is the distance to the particle

λ is the wavelength of incident light

n is the refractive index of the particle and

d is the diameter of the particle.

According to the equation 2.24, if we keep I_0 and θ constant, then the different scattering intensities can be obtained for different incident wavelengths according to the diameter and the refractive index of the particle. Because the intensity of Rayleigh scattered light depends on the size of the particle (proportional to the sixth power of the particle size) and the wavelength of the incident light, the shorter-wavelength-light such as violet and blue will scatter more than the longer-wavelength-light such as green and red in the visible spectrum for a particle of the same size (Figure. 2.16(a)). The incident light with same wavelength will be scattered in different intensities by different sized particles (Figure. 2.16(b)).

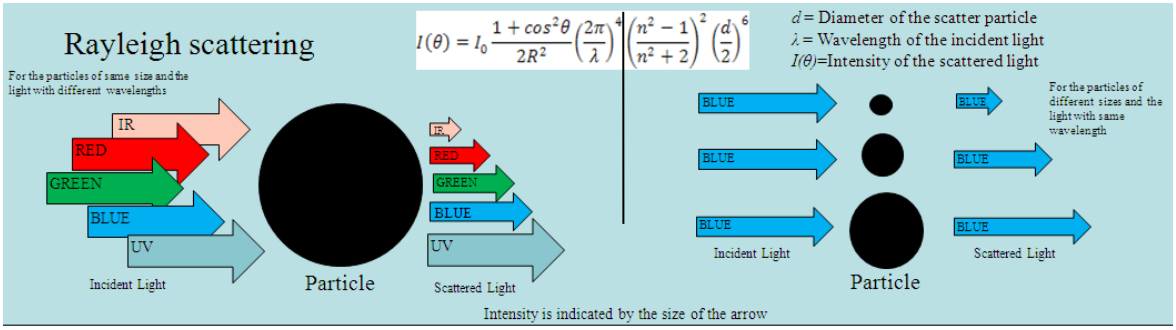

(a) (b)

Figure 2.16 Rayleigh Scattering (the amount of scattering intensity depends on wavelength of the incident light and the size of the scatter)

Using the equation 2.24 the relative figures for Rayleigh scattered light intensities of incident lights of different wavelengths (380 nm – 750 nm of visible light, 340 nm ultraviolet light and 800 nm infrared light) were calculated by a particle of the same size (Figure 2.17).

If the particle size is greater than the incident wavelength then Mie scattering is predominant[4] (Kopeika, 1989; Li *et al*., 2001). This type of scattering has a greater effect on the larger wavelengths than Rayleigh scattering. It depends on various factors such as the ratio of the size of scatter particle to the incident wavelength, the refractive index of the object and the angle of incidence.

[4] Wikipedia, The free encyclopaedia, http://en.wikipedia.org/wiki/Rayleigh_scattering (visited on 12/08/2013).

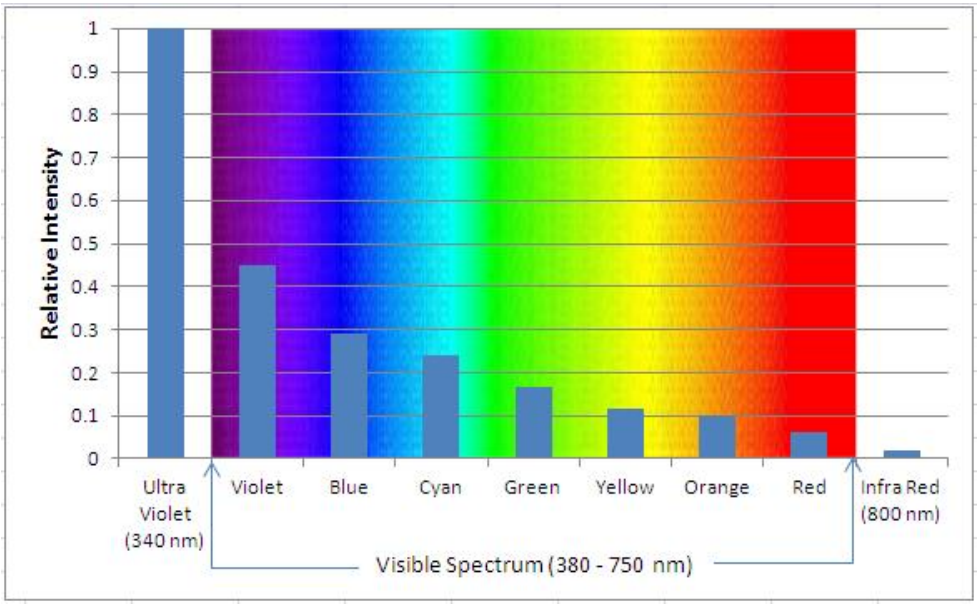

Figure 2.17 Relative intensities of Rayleigh scattered light for different incident lights of different wavelengths by the same size of particles (for comparison, relative scattered light intensities of ultraviolet light of wavelength 340 nm and infrared light of wavelength 800 nm are also shown)

Mie scattered light intensity by a single particle is given by the following equation (2.25).

$$I(\theta) = I_0 \frac{\lambda^2}{8\pi^2} [i_1(\alpha, n, \theta) + i_2(\alpha, n, \theta)] \qquad 2.25$$

where $I(\theta)$ is the Mie scattered light intensity by the particle at angle θ,

θ is the scattering angle

I_0 is the intensity of incident light

λ is the wavelength of incident light

n is the refractive index of the particle and

$\alpha = 2\pi r / \lambda$

where r is the radius of spherical particle.

Mie scattering is non-selective.

Figure 2.18 shows the place of the test particles in the electromagnetic spectrum.

As shown in Figure 2.17, Rayleigh scattering is negligible at the wavelengths below 1000 nm. This theory clearly explains the failure of detecting smaller sized particles by common household photoelectric smoke detectors. In general, the photodiodes of these common household smoke detectors are able to detect only the MIE scattered infrared (IR) light (wavelength ≈ 900 nm) scattered by the smoke particles because they use an IR light emitting diode as the light source (for smaller sized particles with this wave length, Rayleigh light scattering is impossible and for larger particles (> 900 nm), the only possible scattering is Mie scattering) (Figure 2.19(a)). According to these scattering theories, the expected size ranges of Rayleigh and MIE scatters for the IR light (900 nm = the infrared wavelength of the existing smoke alarm) and UV light 370 nm = the minimum wavelength of the available UV LEDs) are shown in Figures 2.19(b) and 2.19(c) respectively.

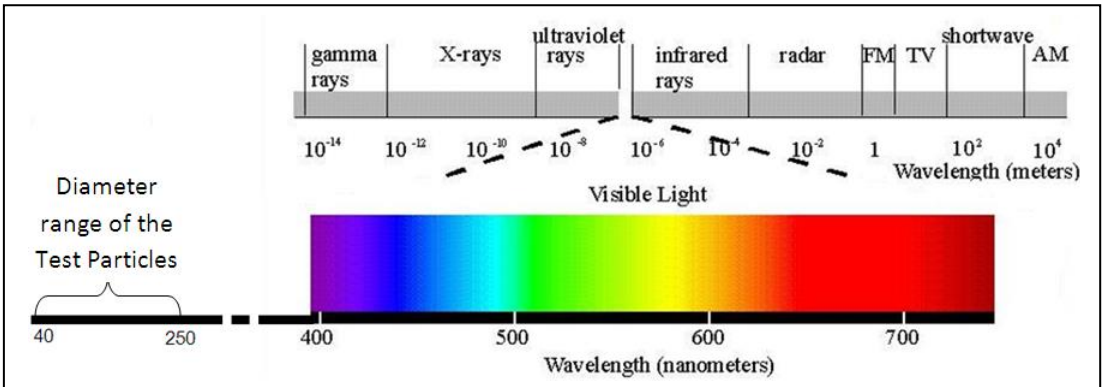

Figure 2.18 Place of the test particles in the in the electromagnetic spectrum

White LEDs were found to cover a wide spectrum ((~400 nm to ~800 nm) with higher intensities at the low end of spectrum. Therefore, in the present study, a phosphor-based white LED (MC20358, SPC Technology) was used to illuminate the chamber. The spectrum (relative luminous intensity vs. wavelength) of this white LED is shown in Figure 2.20 (a)

and spectrums of several other available light sources are shown in Figure 2.20(b) for comparison.

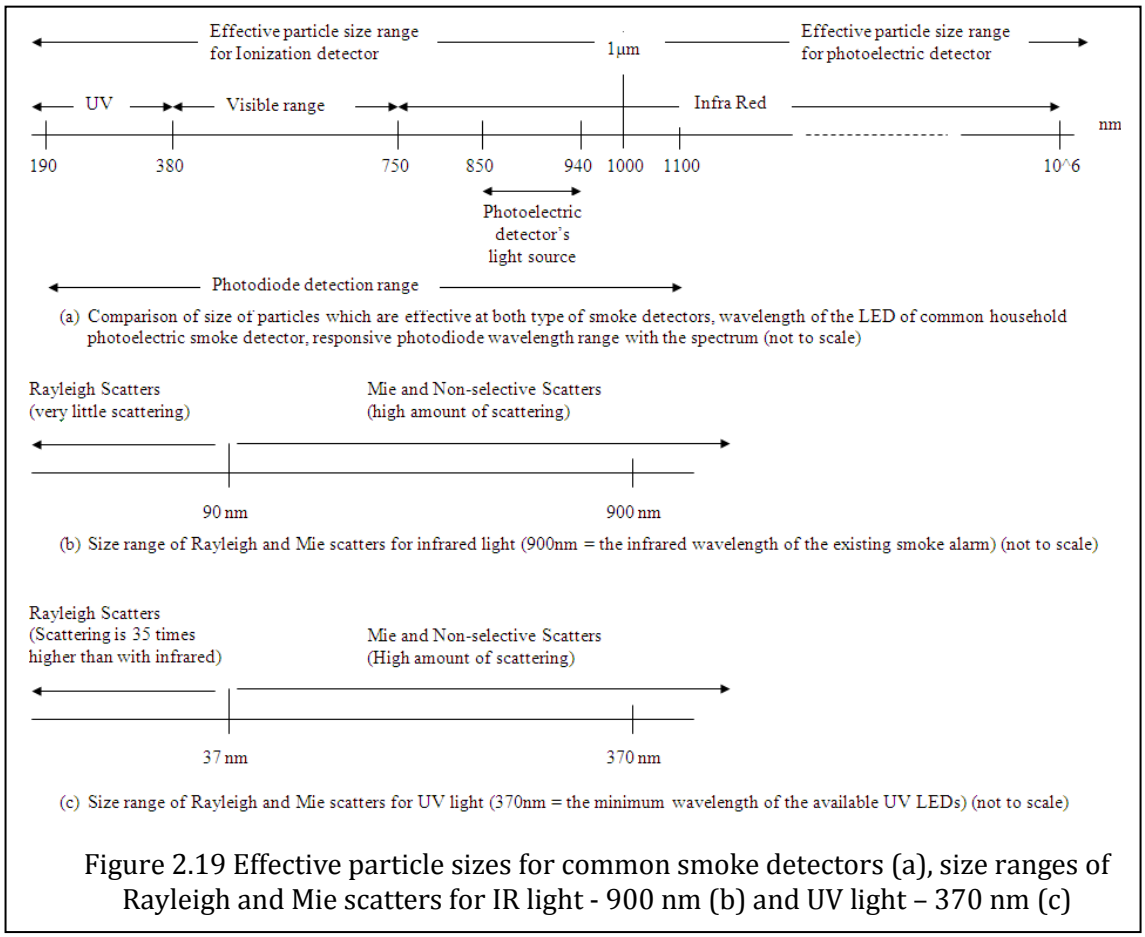

Figure 2.19 Effective particle sizes for common smoke detectors (a), size ranges of Rayleigh and Mie scatters for IR light - 900 nm (b) and UV light – 370 nm (c)

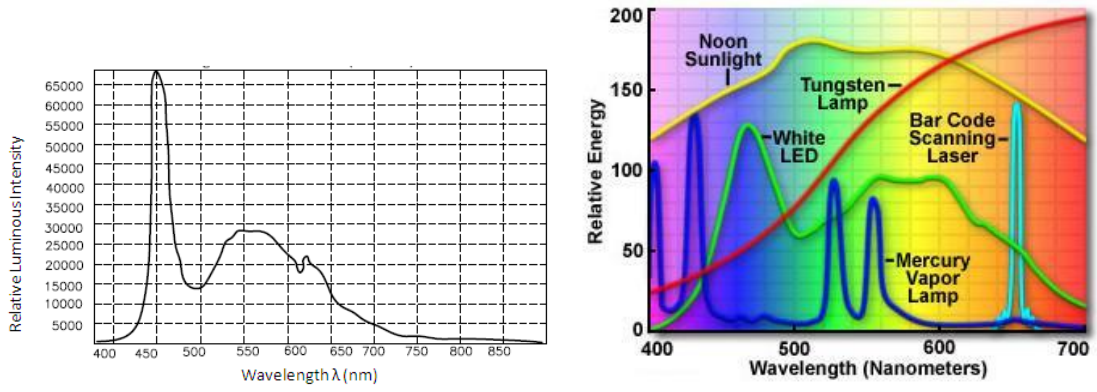

Figure 2.20 Spectrum of phosphor based white LED (a) (adopted from the technical datasheet of SPC Technology, MC20358) and Comparison of spectrums of commonly available light sources (b) (adopted from http://www.olympusmicro.com/primer/lightandcolor/lightsourcesintro.html, retrived 08/05/2014)

2.4 CLASSIFICATION ALGORITHMS

Image classification algorithm is used to classify images into classes according to its visual content. Image retrieval is an important application of image classification, which searches through an image dataset to retrieve the images with particular visual content. Three of the most popular classification algorithms (Linear Discriminant Analysis, K-nearest neighbourhood, and Support Vector Machines) are described in the following sections.

2.4.1 LINEAR DISCRIMINANT ANALYSIS (LDA)

Based on the observations made on the object, Linear Discriminant Analysis classifies objects into a number of predetermined groups. Here, it is assumed that the groups are known or predetermined and they are in a nominal scale (do not have order). With a given set of objects and a set of measured features from those objects, Linear Discriminant Analysis determines

1. Which set of features can best describe the group membership of the object?
2. What is the classification *rule* or *model* to best separate those groups?

Linear Discriminant Analysis assumes that the groups can be separated by a linear combination of chosen features (i.e. independent variables) that describe the objects. For example, if only two features were chosen, then the groups will be separated by lines and if there are three features, the separator will be a plane. If the number of chosen features is more than three, then the groups are separated by a hyper-plane (Tang &Tao, 2006; Hamsici & Martinez, 2008; Cazzanti & Gupta, 2007).

Construction of Linear Discriminant Analysis (LDA) formula

The following table (Table 2.3) illustrates the construction of LDA with a sample data set which only belongs to two groups (five feature vectors from each group) for clarity.

TABLE 2.3 CONSTRUCTION OF LDA

Formulate the data sets and the test sets. x_i= feature vectors of group *i*. Each row represent feature vector of one object and each column represents one feature of the feature vector. $x_i = \begin{bmatrix} a_{11} & \cdots & a_{1n} \\ \vdots & \ddots & \vdots \\ a_{n_i 1} & \cdots & a_{n_i n} \end{bmatrix}$	$x_1 = \begin{bmatrix} 131 & 136 & 136 \\ 129 & 134 & 133 \\ 130 & 135 & 134 \\ 130 & 133 & 134 \\ 132 & 133 & 135 \end{bmatrix}$ $x_2 = \begin{bmatrix} 135 & 142 & 140 \\ 134 & 141 & 140 \\ 135 & 142 & 140 \\ 136 & 141 & 141 \\ 135 & 142 & 140 \end{bmatrix}$
Compute the mean of each data set (μ_1, -, -, -, μ_n) and mean of entire data set (μ). $\mu = p_1 \times \mu_1 + - - - - + p_n \times \mu_n$ Where p_1 and p_2 are the apriori probabilities of the groups.	$\mu_1 = [130.4 \quad 134.2 \quad 134.4]$ $\mu_2 = [135 \quad 141.6 \quad 140.2]$ $\mu = [132.7 \quad 137.9 \quad 137.3]$
Calculate the mean corrected data (x_i^o) and covariance matrix (Cov_i) of each group. $x_i^o = x_i - \mu$ $Cov_i = \frac{(x_i^0)^T x_i^0}{n_i}$	$x_1 = \begin{bmatrix} -1.7 & -1.9 & -1.3 \\ -3.7 & -3.9 & -4.3 \\ -2.7 & -2.9 & -3.3 \\ -2.7 & -4.9 & -3.3 \\ -0.7 & -4.9 & -2.3 \end{bmatrix}$ $x_2 = \begin{bmatrix} 2.3 & 4.1 & 2.7 \\ 1.3 & 3.1 & 2.7 \\ 2.3 & 4.1 & 2.7 \\ 3.3 & 3.1 & 3.7 \\ 2.3 & 4.1 & 2.7 \end{bmatrix}$ $Cov_1 = \begin{bmatrix} 6.33 & 8.43 & 7.51 \\ 8.43 & 15.05 & 11.25 \\ 7.51 & 11.25 & 9.45 \end{bmatrix}$ $Cov_1 = \begin{bmatrix} 5.69 & 8.51 & 6.87 \\ 8.51 & 13.93 & 10.61 \\ 6.87 & 10.61 & 8.57 \end{bmatrix}$
Calculate the pooled within group covariance matrix and inverse of the pooled covariance matrix. $C = \frac{1}{n}\sum_{i=1}^{g} n_i . Cov_i(r,s)$	$\frac{5}{10} \times 6.33 + \frac{5}{10} \times 5.69 = 6.01$ ------- $\frac{5}{10} \times 9.45 + \frac{5}{10} \times 8.57 = 9.01$ $C = \begin{bmatrix} 6.01 & 8.47 & 7.19 \\ 8.47 & 14.49 & 10.93 \\ 7.19 & 10.93 & 9.01 \end{bmatrix}$ $C^{-1} = \begin{bmatrix} 4.53 & 0.93 & -4.74 \\ 0.93 & 1.00 & -1.96 \\ -4.74 & -1.96 & 6.27 \end{bmatrix}$
Calculate the prior probability vector *p* (each row represents the prior probability of group *i*).	$p = \begin{bmatrix} 5/10 \\ 5/10 \end{bmatrix}$
Assign the object *k* to group *i* that has the maximum f_i. X_k is the feature vector of the object *k*.	$f_i = \mu_i C^{-1} x_k^T - \frac{1}{2}\mu_i C^{-1} \mu_i^T + \ln(p_i)$

2.4.2 K-NEAREST NEIGHBOURS (KNN)

KNN is a supervised learning algorithm (Hastie *et al.* 2001; Chen *et al.* 2010; Yu & Yu, 2007) that has been successfully used in many applications such as statistical pattern recognition (e.g. recognition of hand writing (Zanchettin *et al*. 2012)) and image classification (e.g. classification of satellite images (Shixin *et al.* 2000)). This classifier does not construct any model to fit new instances. Instead, it calculates the minimum distance from the query instance to the training samples to determine the K-nearest neighbours and takes simple majority of these K-nearest neighbours to be the prediction of the query instance.

KNN is robust to noisy training data (especially if we use inverse square of weighted distance as the "distance") and it is accurate if the training data is large. However, because it computes distance of each query instance to all training samples, the computation cost is very high. Again, in contrast to linear discriminant analysis, this method doesn't discriminate the non-significant attributes and the parameter K (number of nearest neighbours) should be pre-determined.

For a two dimensional space, if a prototype object (model object that has the ideal feature values to represent all the reference images of a particular class) is used, the situation is illustrated in Figure 2.21.

The Euclidean distance d between the feature vectors of the test image and a reference image can be calculated using the following formula.

$$d = \left(\sum_{i=0}^{Nc} \left| f_p^i - f_o^i \right|^2\right)^{1/2} \qquad 2.26$$

Where f_p is the feature vector for test image and f_o is the feature vector for a reference image. Nc is the number of harmonics needed to index the shape. If d_i is the distance

between the test image and the i^{th} reference image then the test image can be assigned to the reference image R where

$$d_R = \min_{i=1}^{M}[d_i].$$

M is the number of reference images

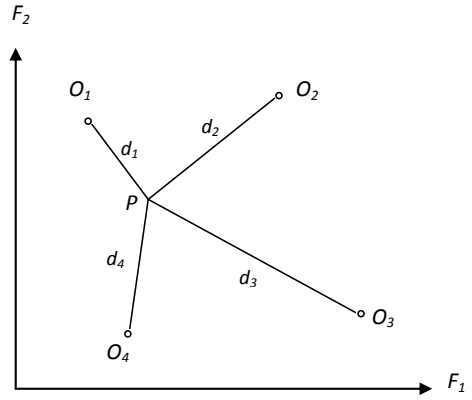

Figure 2.21 Nearest Neighbourhood Classifier. Point *P* represents the test image. Points O_1, O_2, O_3 and O_4 are the Prototypes of reference images. d_1, d_2, d_3 *and* d_4 are the Euclidean distances between the feature vectors of point *P* and the points O_1, O_2, O_3 and O_4 respectively (adopted from Jain *et al.*, 1995)

Figure 2.22 illustrates the situation where no prototype object is found. Here, each class represents a cluster of points in the feature space. Therefore, either the distance to the closest point or the distance to the centroid of the cluster of points of each class from the test image can be considered.

Table 2.4 further illustrates the classification with KNN with the same sample data which was used in the above LDA example (from polyurethane and Kerosene particle sequences).

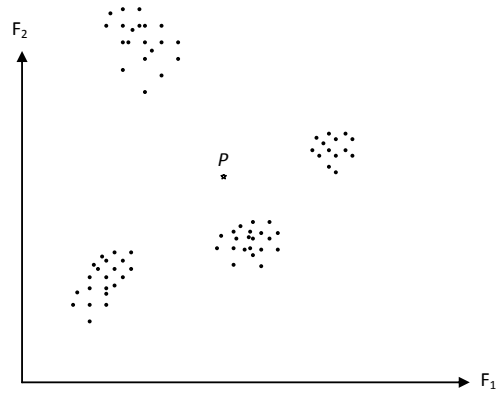

Figure 2.22 Feature space where no prototype species can be found. All reference images of a particular species are represented as a cluster of points in the feature space. Point *P* represents the test image (adopted from Jain *et al.*, 1995)

2.4.3 SUPPORT VECTOR MACHINES

A Support Vector Machine (SVM) is a statistical learning theory based discriminative classifier formally defined by a separating hyperplane. In other words, given labelled training data (supervised learning), the algorithm outputs an optimal hyperplane which categorizes new examples (OpenCV, 2013). This method has successfully been applied in many classification methods such as handwritten digits recognition (Bottou *et al.,* 1994), finger movement detection (Darmakusuma *et al*., 2012), histogram-based image classification (Chapelle *et al*., 1999) and also in many biomedical image classifications (Georgara, *et al*., 2012; Furay *et al*., 2000).

The aim of the SVM algorithm is based on finding the discriminant that gives the largest minimum distance to the training examples. Therefore, the optimal separating discriminant function maximizes the margin (twice the distance to the training examples from hyperplane) (Figure 2.23).

TABLE 2.4 CLASSIFICATION WITH KNN

<table>
<tr>
<td>1. Formulate the data sets and the test sets. Determine the parameter K (= number of nearest neighbours)</td>
<td>K=3 (predetermined)
<table>
<tr><th></th><th>Feature 1</th><th>Feature 2</th><th>Feature 3</th><th>Group</th></tr>
<tr><td rowspan="10">Training Data</td><td>131</td><td>136</td><td>136</td><td rowspan="5">Group 1</td></tr>
<tr><td>129</td><td>134</td><td>133</td></tr>
<tr><td>130</td><td>135</td><td>134</td></tr>
<tr><td>130</td><td>133</td><td>134</td></tr>
<tr><td>132</td><td>133</td><td>135</td></tr>
<tr><td>135</td><td>142</td><td>140</td><td rowspan="5">Group 2</td></tr>
<tr><td>134</td><td>141</td><td>140</td></tr>
<tr><td>135</td><td>142</td><td>140</td></tr>
<tr><td>136</td><td>141</td><td>141</td></tr>
<tr><td>135</td><td>142</td><td>140</td></tr>
<tr><td>Test Data</td><td>133</td><td>136</td><td>141</td><td>?</td></tr>
</table>
</td>
</tr>
<tr>
<td>2. Calculate the distance between the query-instance and each of the training samples
$d = (\sum_{i=0}^{Nc} \left| f_p^i - f_o^i \right|^2)^{1/2}$</td>
<td>
<table>
<tr><th>d_i</th><th>Group</th></tr>
<tr><td>5.385164807</td><td>1</td></tr>
<tr><td>9.16515139</td><td>1</td></tr>
<tr><td>7.681145748</td><td>1</td></tr>
<tr><td>8.185352772</td><td>1</td></tr>
<tr><td>6.782329983</td><td>1</td></tr>
<tr><td>6.403124237</td><td>2</td></tr>
<tr><td>5.196152423</td><td>2</td></tr>
<tr><td>6.403124237</td><td>2</td></tr>
<tr><td>5.830951895</td><td>2</td></tr>
<tr><td>6.403124237</td><td>2</td></tr>
</table>
</td>
</tr>
<tr>
<td>3. Sort the distance and determine nearest neighbours based on the Kth minimum distance

4. Gather the category Y of the nearest neighbours</td>
<td>
<table>
<tr><th>di</th><th>Group</th></tr>
<tr><td>5.196152423</td><td>2</td></tr>
<tr><td>5.385164807</td><td>1</td></tr>
<tr><td>5.830951895</td><td>2</td></tr>
<tr><td>6.403124237</td><td>2</td></tr>
<tr><td>6.403124237</td><td>2</td></tr>
<tr><td>6.403124237</td><td>2</td></tr>
<tr><td>6.782329983</td><td>1</td></tr>
<tr><td>7.681145748</td><td>1</td></tr>
<tr><td>8.185352772</td><td>1</td></tr>
<tr><td>9.16515139</td><td>1</td></tr>
</table>

<table>
<tr><th>di</th><th>Group</th></tr>
<tr><td>5.196152423</td><td>2</td></tr>
<tr><td>5.385164807</td><td>1</td></tr>
<tr><td>5.830951895</td><td>2</td></tr>
</table>
3 Nearest neighbours
</td>
</tr>
<tr>
<td>5. Use simple majority of the category of nearest neighbours as the prediction value of the query instance

$d_R = \min_{i=1}^{M}[d_i].$</td>
<td>
<table>
<tr><td>Test Data</td><td>133</td><td>136</td><td>141</td><td>2</td></tr>
</table>
</td>
</tr>
</table>

The discriminant has the form

$$f(x) = b + w^T x \qquad 2.27$$

where w is known as the weight vector and b as the bias.

In 2D the discriminant is a line, in 3D it is a plane, and in nD it is a hyperplane. Learning the SVM can be formulated as an optimization of

$$max \frac{2}{\|w\|} \text{ subject to } w^T x_i + b \begin{cases} \geq 1 \; if \; y_i = +1 \\ \leq -1 \; if \; y_i = -1 \end{cases} for \; i = 1, 2, 3, \ldots . . N \qquad 2.28$$

or equivalently

$$min\|w\|^2 \text{ subject to } y_i(w^T x_i + b) \geq 1 \text{ for } i = 1, 2, 3, \ldots \ldots N \qquad 2.29$$

where x symbolizes the training examples closest to the hyperplane. In general, the training examples that are closest to the hyperplane are called support vectors.

With K-NN classifier, although, it was necessary to `carry' the training data for classifying new data, with SVM the training data is used to learn w and then discarded. Only w is needed for classifying new data.

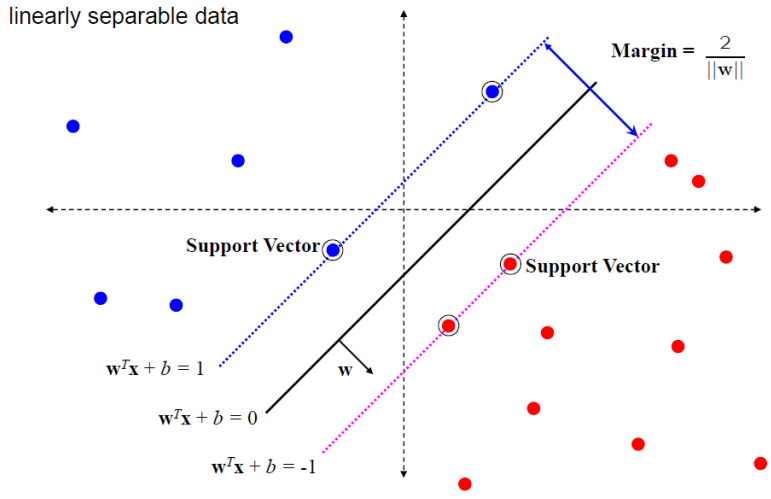

Figure 2.23 Optimal hyperplane with linearly separable data (adopted from Zisserman, 2014. http://www.robots.ox.ac.uk/~az/lectures/ml/lect2.pdf, visited on 14/02/2014)

3 –SMOKE DETECTION AND CLASSIFICATION

Generally, **smoke detection** can be defined as the detection of smoke within a predetermined threshold in a certain environment (e.g. a closed chamber or in an open space) and **smoke classification** can be defined as the categorisation of the detected smoke into known classes (e.g. wood smoke or kerosene smoke).

3.1 SMOKE CLASSIFICATION

The following sections describe three smoke classification studies found in the literature along with the instruments used by the researchers.

3.1.1 SMOKE CLASSIFICATION USING THE SIGNAL ACQUISITION AND PROCESSING UNIT

By analysing the output signal of a silicon photodiode to measure the intensity of the Mie scattered light by the particles, Li *et al.* (2001) have attempted to discriminate three different types of particles: kerosene smoke, cigarette smoke and water vapour. A semiconductor infrared laser of wavelength λ=780 nm was used as the light source. This method successfully discriminated the above three types of particles with a discrimination rate of more than 95%.

According to Mie scattering theory, different size particles have different scattering light intensities at the same scattering angle. In their experiment, Li *et al*. (2001) have tried to measure the scattering light intensities of the particular particles they used by utilising four

highly sensitive avalanche photodiodes (APDs) placed at four different angles. The signal acquisition and processing unit of the particle discriminating system of their study is shown in Figure 3.1. The four avalanche photodiodes (APD1, APD2, APD3 and APD4) in the signal acquisition and processing unit were fixed in the positions of 90˚, 30˚, 120˚ and 60˚ with reference to the direction of the laser beam.

All the particles used by Li *et al.* (2001) in this study were larger sized particles (> 1 μm) (Fabian, 2007). Figure 3.2 compares the sizes of different particles that activate both types of detectors (ionization and photoelectric) with the wavelengths of the electromagnetic spectrum. A photodiode can detect wavelengths between 190 nm and 1100 nm. Even though a photodiode can respond to such a large band of the electromagnetic spectrum, the peak spectral responsivity of a typical common silicon or pin photodiode lies around 900 nm. For example, Figure 3.3 shows the variation of detector sensitivity to wavelength of a photodiode. [Photodiode, Wikipedia]. Common household photoelectric detectors use an LED which emits near infrared (NIR) (wavelength between 850 nm – 940 nm) radiations. Since Rayleigh scattering is nearly negligible with infrared light (according to Eq. 2.24 in Chapter 2) with larger particles, in this study, the resulted scattering can be considered mainly from the Mie scattering (Li *et al*., 2001).

The major shortcoming of Li *et al*.'s (2001) experiment for discriminating particles in common household smoke alarms is that it cannot be used to discriminate small particles (< 1 μm) because with the infrared light source (λ=780), Mie scattering is negligible for such small particles (Figure 3.2). Therefore, to identify small particles (which cannot be detected by photoelectric detectors), a different technique should be developed.

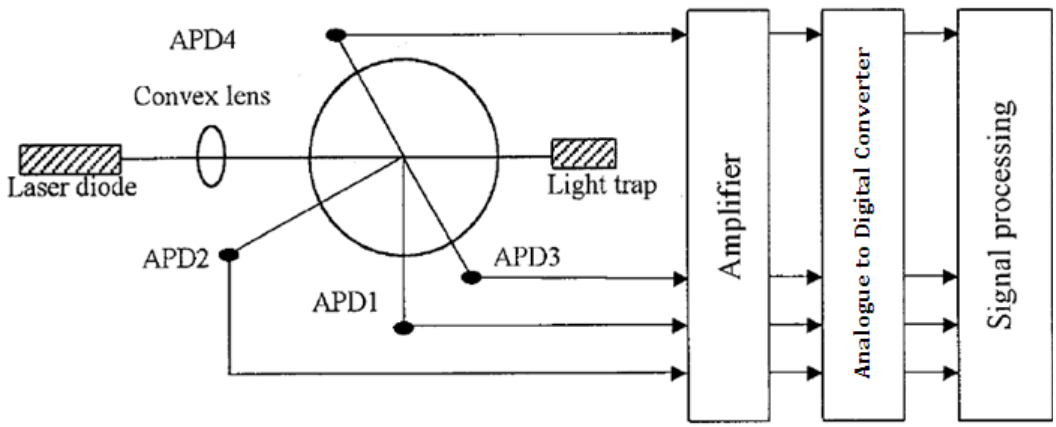

Figure 3.1 Signal acquisition and processing unit (adopted from Li *et al.*, 2001)

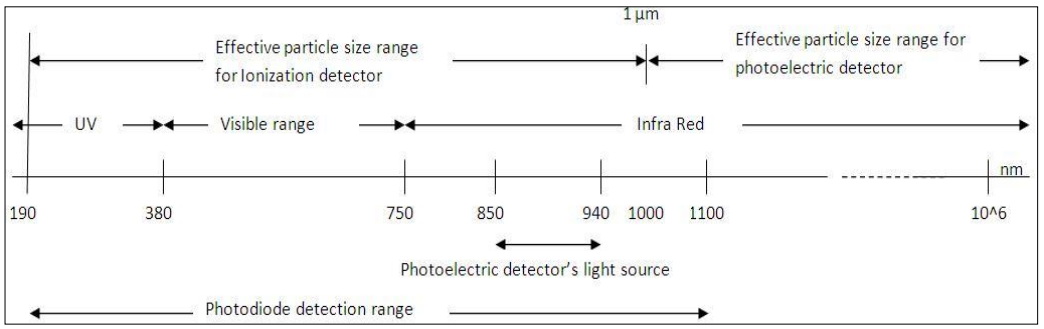

Figure 3.2 Comparing the particle size detected by ionisation and IR smoke detectors, with wavelengths of the IR LED and photodiode

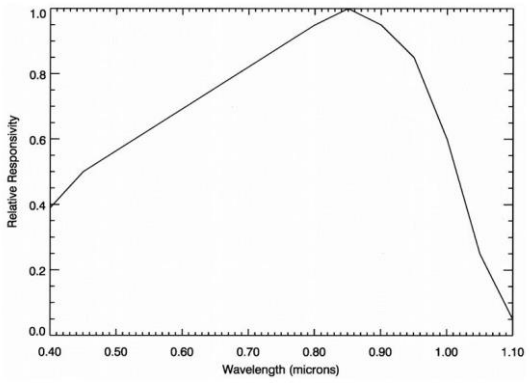

Figure 3.3 Photodiode detector responsivity versus wavelength

3.1.2 SMOKE CLASIIFICATION WITH "LARGE AGGLOMERATE OPTICAL FACILITY"

Using the Large Agglomerate Optical Facility (Figure 3.4), Weinert *et al.* (2003) measured the differential mass scattering cross section of various non-flaming and flaming fire-generated smoke aerosols and nuisance aerosols (beech wood, cotton lamp wick, toast, cooking oil, dust, polyurethane, propylene, heptanes, acetylene, ethylene) created in the Fire Emulator/Detector Evaluator. Analysis of Weinert *et al.*'s data showed that the differential mass scattering cross section can be used effectively to distinguish the smoke aerosol generated by a flaming fire from that of a non-flaming fire or nuisance aerosol.

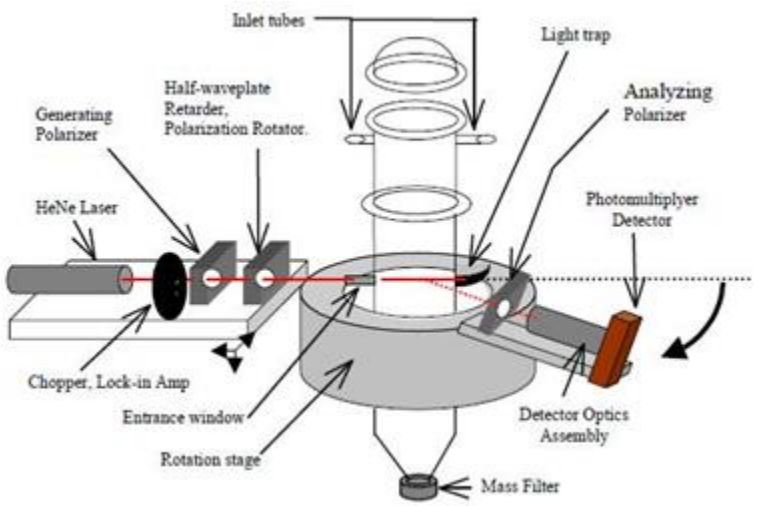

Figure 3.4 The "Large Agglomerate Optical Facility" light scattering apparatus used to measure the differential mass scattering cross section (adopted from Weinert *et al.*, 2003)

The differential mass scattering cross section is defined as

$$\sigma(\theta) = \frac{u(\theta)}{MK} \qquad 3.1$$

where $u(\theta)$ is the volume corrected detector signal, K is the calibration constant and M is the aerosol mass concentration.

Figure 3.5 shows the variation of polarization ratio, which is a widely used parameter for characterizing aerosol polarization, with the scattering angle of all the aerosol sources of their study.

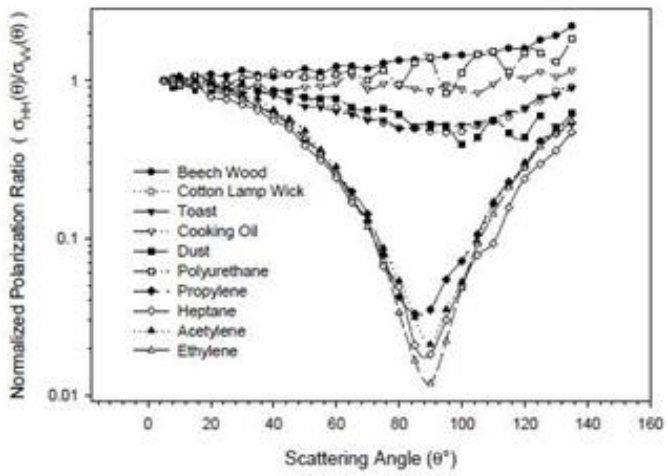

Figure 3.5 Variation of polarization ratio (normalized to 1 at θ=5°) with scattering angle for different aerosols (adopted from Weinert *et al.*, 2003)

The polarization ratio is defined as

$$\rho(\theta) = \frac{\sigma_{HH}(\theta)}{\sigma_{VV}(\theta)}. \tag{3.2}$$

where

$$\sigma_{VV}(\theta) = \frac{1}{\rho_p V_p k^2}\left|\sum_n \frac{2n+1}{n(n+1)}(a_n\pi_n + b_n\tau_n)\right|^2 \tag{3.3}$$

and

$$\sigma_{HH}(\theta) = \frac{1}{\rho_p V_p k^2}\left|\sum_n \frac{2n+1}{n(n+1)}(a_n\tau_n + b_n\pi_n)\right|^2. \tag{3.4}$$

Here, a_n and b_n are the Mie scattering coefficients of scattering particles, π_n and τ_n are the angular functions, k is the wave number, λ is the wavelength ρ_p is the particle bulk density and V_p is the particle volume.

Even though, the differential mass scattering cross section can be used to assess the response of a light scattering smoke detector, Weinert *et al*. (2003) have concluded that the light scattering results in their study are not adequate by themselves to make definitive separation of the examined non-flaming and nuisance aerosols. Conversely, the Large Agglomerate Optical Facility is a room sized apparatus (Mulholland & Choi, 1998), and therefore, is not a practical solution for discriminating nuisance and hazardous particles in households.

3.1.3 SMOKE CLASSIFICATION WITH MASS SPECTROMETER

According to Science Magazine [Science Magazine, 2013], a recent advancement in medical science related to cancer detection was observed with the smoke from cauterizing tissues. A new smart knife, also known as the "iKnife (intelligent knife), sucks up the smoke as it cuts flesh and pipes the smoke to a refrigerator-sized mass spectrometer (Figure 3.6) which compares the patient sample (i.e., the smoke from the patient tissue) with a library of smoke “signatures” from cancerous and non-cancerous tissues. iKnife categorizes the patient samples into three categories (healthy, cancerous or unidentifiable) and gives an instant feedback to surgeons rather than them having to wait on sample analysis by a pathology lab.

Mass spectrometers are good at detecting and classifying different sized particles and can be recommended for centralized places such as medical laboratories and research institutes. However, mass spectrometers are not practical for detecting smoke and fires in non-centralised residential, commercial and industrial spaces, because of their large size and very high cost

Figure 3.6 Mass spectrometer

3.2 SMOKE DETECTION

Andrew *et al.* (2014) detected ten different particles of commonly available domestic odour sources, including candle, joss sticks, air freshener, mosquito coil, newspaper, card board, plastic materials, styrofoam and wood with the maximum accuracy of 99.68%. To get this accuracy they have fed the modified recorded signals which were recorded with signal measuring device called Portable Electronic Nose (PEN3) into covariance k-nearest neighbour algorithm.

Other than this work, a large number of studies have been carried out to detect airborne particles in open environments like forests and tunnels using surveillance cameras with extensive use of noise filters to eliminate the unnecessary environmental noise (Töreyin & Cetin, 2007; Töreyin *at el*., 2006; Dedeoglu *et al*. 2005). All of this prior research is based on the extraction and analysis of behavioural characteristics and features of smoke clouds, but none of them addressed the issue of classifying individual particles by extracting the individual particle characteristics. Motion and moving direction (Narwade & Chakkarwar, 2013, Lee & Han, 2007; Capitan *et al*., 2007; Xu & Xu, 2007; Han & Lee, 2006), texture (Lee

& Han, 2007), edge detection [Lee & Han, 2007; Han & Lee, 2006; Cappellini *et al*. 1989), region analysis (Narwade & Chakkarwar, 2013, Truong & Kim, 2011, Lee & Han, 2007), colour information (Narwade & Chakkarwar, 2013, Truong & Kim, 2011, Lee & Han, 2007; Capitan *et al*., 2007; Xu & Xu, 2007; Han & Lee, 2006; Chen *et al*., 2006), disorder (Narwade & Chakkarwar, 2013, Xu & Xu, 2007), frequent flicker in boundaries, self-similarity and local wavelet energy (Xu & Xu, 2007), shape variation or growth [Chen *et al*., 2006; Xu & Xu, 2007) are some of the extracted features and behavioural characters of smoke clouds in these studies. These classifications were carried out merely for distinguishing the smoke clouds from other non-hazardous image features such as changing background lighting and moving vehicles and not for classifying types of hazardous smoke from non-hazardous air-borne particles. None of this prior research computed a clear quantifiable measure to enable comparing the classification efficiency and the accuracy of their work with other studies.

Since all of the input images of these studies have been taken in open environments, these studies have used noise filters to highlight various types of noise caused by the surrounding environment to isolate the smoke cloud. Although these studies have successfully distinguished smoke particles from other non-hazardous image features such as variations in ambient illumination and moving vehicles, none of them have addressed the issue of recognising hazardous smoke from non-hazardous air-borne particles.

3.2.1 SMOKE PIXEL ISOLATION IN OPEN ENVIRONMENTS

The following section describes some of the selected smoke pixel isolation methods in previous studies.

In the fire and smoke detection study by Lee & Han (2007) and Han & Lee (2006), two different algorithms have been used to obtain the difference images of fire and smoke. For

fire images they have used a model image of a normal state (without fire) and affected images (input images with fire).

The binary images of the normal state image *F(x,y)* and the input images *N(x,y)* were calculated as

$$F_b(x,y) = \begin{cases} 1 & R \geq T_R,\ G \geq T_{G,} \quad B \geq T_B \\ 0 & otherwise \end{cases} \quad 3.5$$

$$N_b(x,y) = \begin{cases} 1 & R \geq T_R,\ G \geq T_{G,} \quad B \geq T_B \\ 0 & otherwise \end{cases} \quad 3.6$$

T_x is the threshold value of the colour channel x ($x\epsilon\{R,G,B\}$).

Then the thresholded difference was defined as

$$D_T(x,y) = N_b(x,y) - F_b(x,y)\ , \quad 3.7$$

and the difference image has been obtained from the following equation.

$$if\ D_T(x,y) < 0\ then\ D(x,y) = 0\ else\ D(x,y) = D_T(x,y) \quad 3.8$$

In the smoke detection algorithm, at first gray image *G(x,y)* has been obtained with

$$G(x,y) = \begin{cases} F_{input}(x,y) & T_1 < F_{input}(x,y) < T_2 \\ 0 & otherwise \end{cases} \quad 3.9$$

and the absolute value of the difference image *D(x,y)* from two consecutive gray images,

$$D_i(x,y) = |G_i(x,y) - G_{i-1}(x,y)| \qquad i=1,2,.....N \quad 3.10$$

In the equation 3.9, T_1 and $T2$ has been used to remove the too bright or too dark regions such as ceiling region or light in tunnel since their main objective was to detect fires and smoke in tunnel environments. We have omitted this constraint because all the images have been taken in a closed smoke chamber in this study. However, similar to the fire detection algorithm (equations 3.5 and 3.6) of Lee & Han (2006, 2007), we also used normal state (without smoke) images and the affected images (input images with fire) to develop the background subtraction method.

Xiong *et al.* (2007), used an adaptive Gaussian Mixture Model (GMM) to approximate the background modelling process in their video based smoke detection study. All the images have been taken in an open environment. GMM has been used mainly because of the changing lighting conditions of their images. Again, this difficulty has been removed in this study (all the images were taken in a closed environment).

A different approach to isolate smoke pixels has been used by Çelik *et al*. (2007) in the process of detecting fire and smoke without sensors. The smoke pixels do not show chrominance characteristics like fire pixels and the colour of the smoke ranges from white-bluish to white (at the beginning) and black-grayish to black (towards the start of the fire). Therefore, he formulated the smoke pixels as

$$|R(x,y) - G(x,y)| \leq Th$$

$$|G(x,y) - B(x,y)| \leq Th \tag{3.11}$$

$$|R(x,y) - B(x,y)| \leq Th$$

where Th is a global threshold ranging from 15 to 25.

Using the equation defined in 3.11, Figure 3.7 shows some example smoke-pixel segmentations from smoke images. In addition, using the idea that the saturation (S) of the colour of the smoke should be as low as possible (at the early stages), a new rule (equation 3.12) has been defined on top of the equation 3.11 using HSV colour space.

$$S(x,y) \leq 0.1 \tag{3.12}$$

Figure 3.8 shows an example smoke segmentation with this new rule.

(a) (b)

Figure 3.7 Smoke segmentation from RGB input image using equation (7), smoke image (a), segmented image (b) (adopted from Çelik *et al*. (2007))

(a) (b)

Figure 3.8 Smoke segmentation from RGB input image using equations (7) and (8). smoke image (a), segmented image (b) (adopted from Çelik *et al.* (2007))

By analysing static and dynamic features of smoke Chen *et al*. (2006) have proposed two sets of decision rules for extracting smoke pixels from an image.

- Static analysis

  The grayish colour of the smoke has been classified into two gray levels: light-gray and dark-gray. Since the R, G, B components of smoke pixels are almost equal and the intensities of light-gray and dark-gray smoke regions range from gray levels L_1 to L_2 and D_1 to D_2 respectively,

$$rule\ 1: R \mp \alpha = G \mp \alpha = B \mp \alpha \qquad \alpha \in [15,20]$$

$$rule\ 2: L_1 \leq I \leq L_2 \qquad L_1 \in [80,150]$$

$$rule\ 3: D_1 \leq I \leq D_2 \qquad D_1 \in [150,220]$$

  where the values of α, L_1, L_2, D_1 and D_2 are all obtained from data experiments.

  The decision rule for extracting smoke pixels is

  If (rule 1) AND [(rule 2) OR (rule 3)] = TRUE Then Smoke-pixel

  Else not Smoke-pixel

  Figure 3.9 shows the isolated smoke pixels from two types of smoke images; burning papers (a) burning wood (b) from the above decision rules.

Figure 3.9 Smoke pixel isolation with decision rules, smoke from burning papers (a), smoke from burning wood (b) (adopted from Chen *et al*. (2006))

- Dynamic analysis

  Here, disorder of smoke cloud has been considered to separate smoke pixels from the other objects. Disorder has been measured as the ratio of circumference to the area of the smoke region. The decision rule is expressed as

  If (SEP / STP) ≥ STD Then smoke-pixels

  Else not smoke-pixels

  Here, *SEP* is the sum of circumferences of smoke regions segmented, *STP* is the number of smoke pixels extracted, and *STD* is the disorder threshold which is used to distinguish smoke pixels from other smoke-like objects. *STD* was obtained from statistical experiments. In addition, to enhance the reliability of smoke detection the growth rate of the smoke cloud has also been considered in this study. The growth rate is defined by the area (A_i) increment over a given time which is same as the

ratio of pixel quantity (P_i) obtained by the frame-difference between frame *i* and *i+k* to the frame number (equation 3.13).

$$\Delta A_{d_i} = \frac{dA}{dt} = \frac{A_{i+k} - A_i}{t_{i+k} - t_i} = \frac{P_{i+k} - P_i}{(i+k) - i} \quad 3.13$$

As Rayleigh theory suggested, the *R*, *G* and *B* components of the scattered light cannot be considered to be equal as in the study of Chen *et al*. (2006) and the intensity variation of *R*, *G* and *B* components of the scattered light can be analysed separately to build the unique feature vectors. Furthermore, if all the images have been taken in a small closed smoke chamber with randomly distributed individual smoke particles, it is impracticable to measure a growth rate of the smoke cloud.

4 – PARTICLE DETECTION WITH TRADITIONAL SMOKE DETECTORS

A smoke detector or a smoke alarm is a device that detects smoke and issues an alarm to alert nearby people that there is a potential fire. A household smoke detector will typically be mounted in a disk shaped plastic enclosure about 150 mm in diameter and 25 mm thick, but the shape can vary according to the manufacturer.

Because smoke rises, most detectors are mounted on the ceiling or on a wall near the ceiling. Therefore to avoid the nuisance of false alarms, most smoke detectors are placed away from kitchens. Most homes have at least one smoke detector near bedrooms to wake up the sleeping occupants; ideally in the hallway as well as in the bedroom.

Smoke detectors are usually powered by one or more batteries but some are connected directly to household wiring. Often smoke detectors that are directly connected to household wiring have a battery as a power supply backup in case of electricity failure[5].

[5] http://en.wikipedia.org/wiki/Smoke_detector

4.1 TYPES OF SMOKE DETECTORS

Followings are the commonly available smoke detector types[6].

- Thermal type detectors: Detect heat from a fire causing a bimetallic strip to flip over or a pneumatic chamber to expand.
- Photoelectric type detectors: Detect light scattered by smoke.
- Ionization type detectors: Detect changes in ionization current caused by smoke.
- Beam light obscuration type detectors: Detect the presence of smoke between a separately arranged light transmitter and receiver.
- Light obscuration type detectors: Detect reductions in light permeability due to the presence of smoke (both light transmitter and receiver are in the detector's smoke chamber).
- Heat radiation type detectors: Like infrared detectors which identify a fire outbreak by detecting infrared radiation levels of a flame

Out of these types, most of the household smoke detectors are based on the two techniques: Photoelectric Detection and Ionization Detection. Most of the commercially available household smoke detectors use only one of these techniques but some of them include both techniques to increase sensitivity to smoke. However, it is advisable to have both of these types of smoke detectors simultaneously in a household because the sensitivity of these two smoke detectors depends on the type of the smoke.

4.1.1 PHOTOELECTRIC DETECTORS

Most photoelectric smoke detectors use a near-infrared (IR) light-emitting diode (LED) as a light source that emits invisible near-IR light having a wavelength of 880 nm

[6] http://www.electronics-manufacturers.com/info/sensors-and-detectors/smoke-detectors.html

or 940 nm. Silicon photodiodes respond very well to these wavelengths and often serve as photosensors in photoelectric smoke detectors. Photoelectric detectors are again in two types: light sensing (scattering) type and light obscuring (blocking) type.

- Light scattering smoke detectors

This is the most common type of household photoelectric smoke detector. The technology behind these detectors is based on the light scattering effect of small airborne particles. Figure 4.1 illustrates the behaviour of this type of detectors.

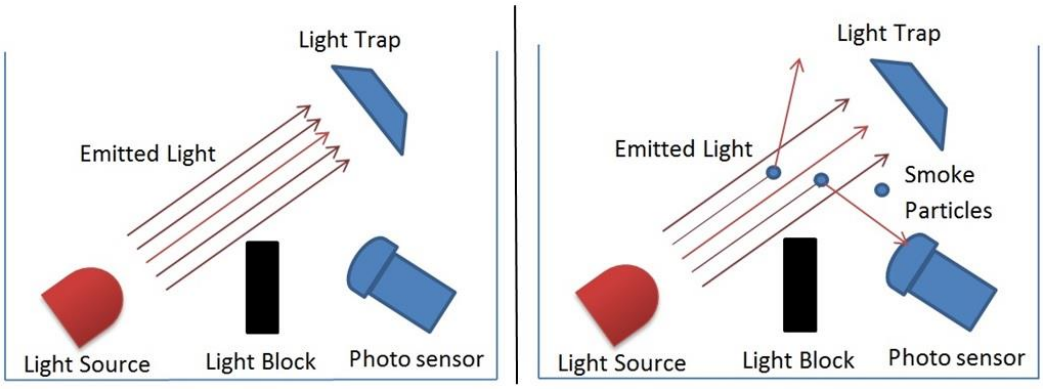

Figure 4.1 Detection of smoke by scattered light. No smoke is present in the left panel. The smoke in the right panel scatters some of the light from the source toward the photo-sensor

Inside a light scattering smoke detector there is a light source and a photosensor, but they are positioned at 90-degree angles to one another as in Figure 4.2. When no obstacle is present, the light from the light source on the left shoots straight across and no light is detected by the photosensor. When smoke enters the chamber, the smoke particles scatter the light and some scattered light hits the sensor. When the amount of incident light reaches a predetermined threshold of the sensor, the sensor sets off an alarm in the smoke detector.

- Light obscuring smoke detectors:

These types of smoke detectors rely on the blocking of the light beam between a light emitter and a sensor by an obstacle. When the smoke is present, it acts as an obstacle and will reduce the amount of incident light on the sensor. If the incident light is diminished to a threshold value, an alarm is sounded (Figure 4.2). The obscuration sensors in general measure the obscuration or cloudiness of the air.

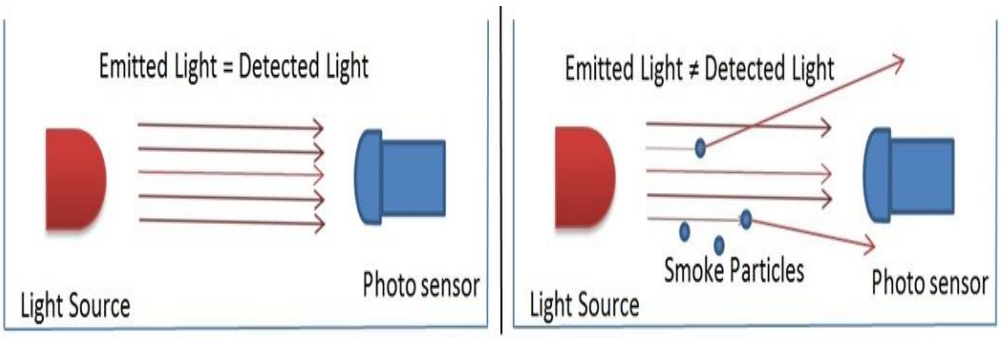

Figure 4.2 Detection of smoke by attenuated light. No smoke is present in the left panel. The smoke in the right panel blocks some of the light arriving at the photo-sensor

4.1.2 IONIZATION DETECTORS

Compared to photoelectric detectors, Ionization smoke detectors are less expensive and more sensitive to smaller sized particles. These detectors consist of an ionization chamber and a source radiation (radioactive material). Normally, americium-241 is used as the radioactive material (typical detector contains 1/5000th of a gram or 0.9 microcurie of americium-241). Americium has a half-life of 432 years and is a good source of alpha particles. Figure 4.3 demonstrates the behaviour of ionization chamber.

The alpha particles generated by the americium ionize oxygen and nitrogen atoms of air in the chamber by releasing an electron off an atom. As the electrons and positive ions move towards the positively charged plate and negatively charged plate respectively, the sensor in the smoke detector can sense resulting current. When smoke is present they neutralize the ions in the ionization chamber, resulting a drop in the current which sets off the alarm.

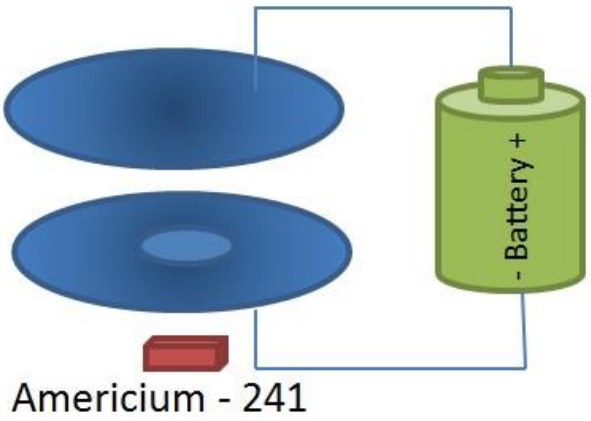

Figure 4.3 Ionization Chamber

4.2 LIGHT SCATTERING BEHAVIOUR BY SMOKE PARTICLES

A photoelectric smoke alarm activates when its photodiode receives some light which is scattered by the smoke particles inside the smoke chamber. Smoke particle sizes of different materials were obtained from the small-scale tests and intermediate-scale tests by Fabian & Gandhi (2007) to study the light scattering behaviour of smoke particles. The test materials were sorted according to the mean smoke particle diameter in an ascending order and graphically displayed in the Figures 4.4 to 4.7.

The particles that act as Mie scatters for the infrared light with wavelength 900 nm (which is the peak wavelength of the existing photoelectric smoke detector's light source) can be considered as the particles which have the diameter greater than 90 nm

(one tenth value of the incident wavelength). The particles which have the diameter less than 90 nm can be considered as Rayleigh scatters. Therefore, in the Figures from 4.4 to 4.7, the smoke particles of the materials in which the mean particle diameter falls under the dotted horizontal line (which represents the size of 90 nm) can be considered as Rayleigh scatters and others can be considered as Mie scatters.

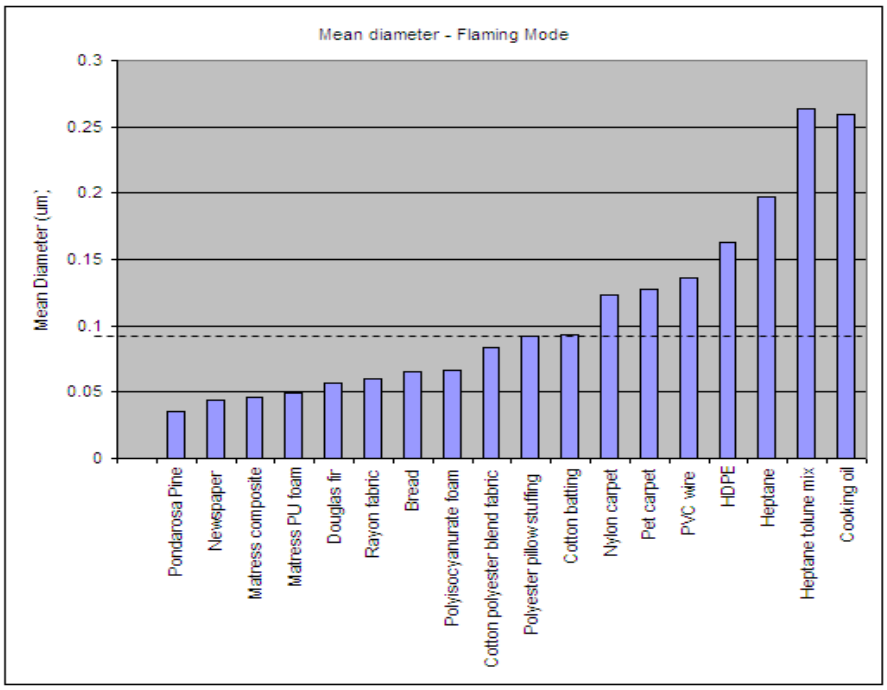

Figure 4.4 Mean particle diameter in non-flaming mode from small scale tests. The dashed line represents the size of the one tenth of the wavelength of the incident light of the photoelectric smoke alarm

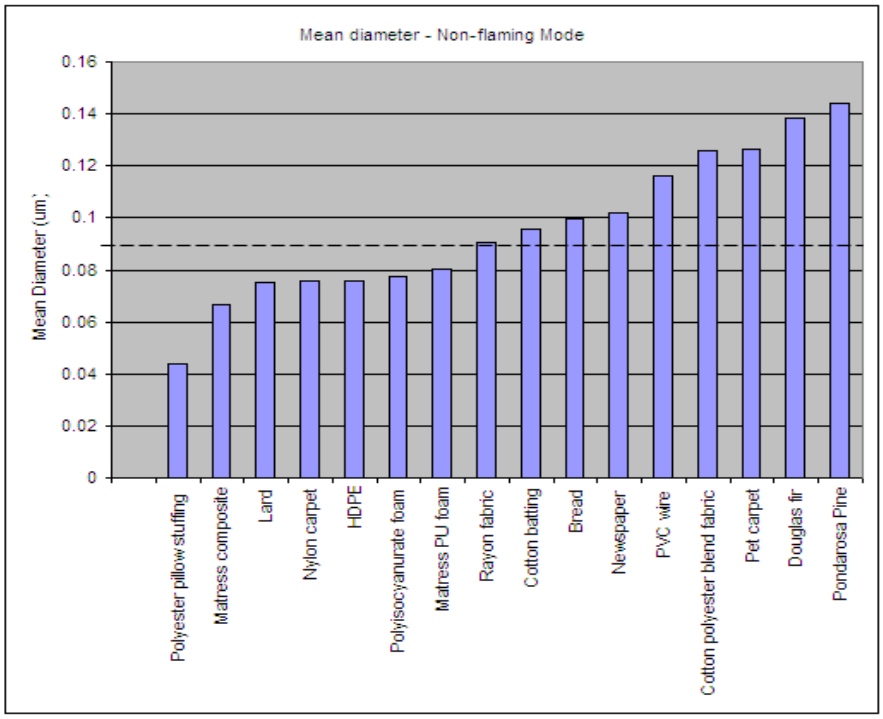

Figure 4.5 Mean particle diameter in flaming mode from small scale tests. The dashed line represents the size of the one tenth of the wavelength of the incident light of the photoelectric smoke alarm

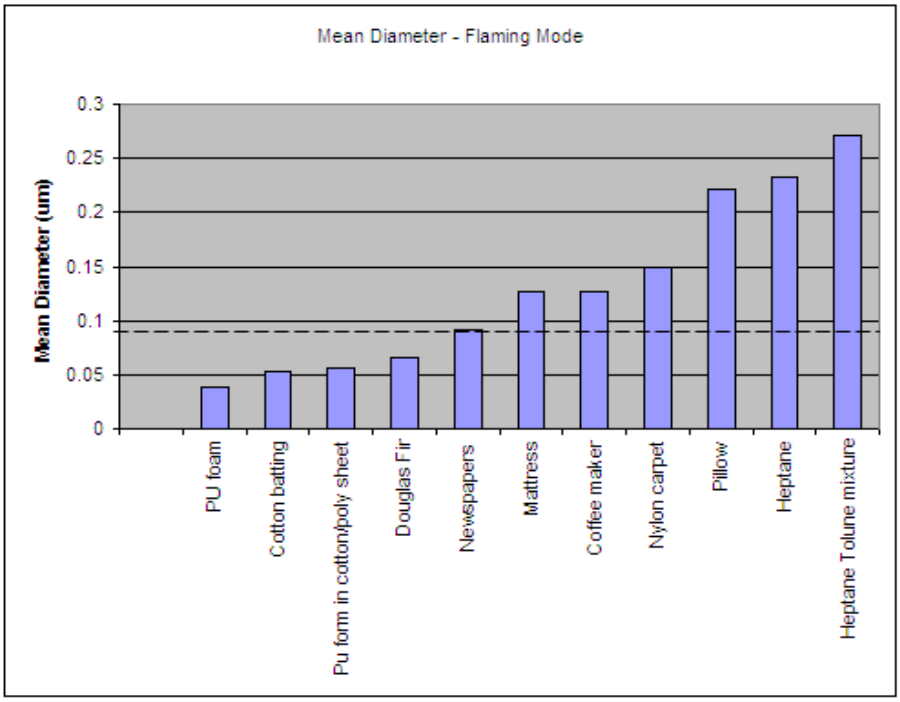

Figure 4.6 Mean particle diameter in flaming mode from intermediate scale tests. The dashed line represents the size of the one tenth of the wavelength of the incident light of the photoelectric smoke alarm

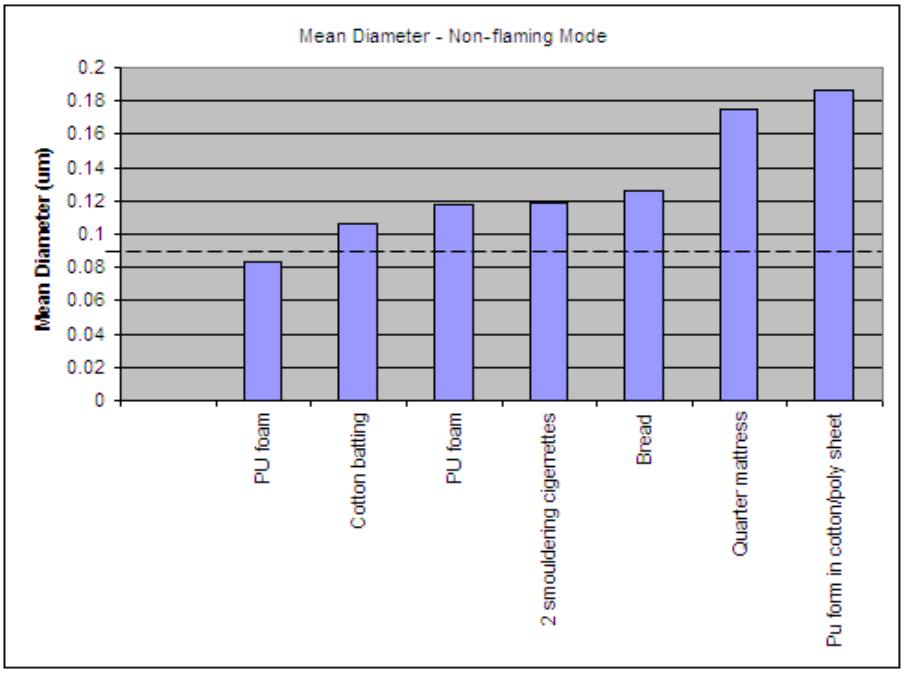

Figure 4.7 Mean particle diameter in non-flaming mode from intermediate scale tests. The dashed line represents the size of the one tenth of the wavelength of the incident light of the photoelectric smoke alarm

According to the behavioural observations of different smoke alarms to different types of smoke, it is apparent that photoelectric smoke alarms detects most of the light scattered from Mie scattering or non-selective scattering. For example, the responses of photoelectric smoke alarm for different types of smoke was obtained from the task 3 of the study by Fabian and Gandhi (2007). Table 4.1 shows the response of the photoelectric smoke alarm to flaming fires and Table 4.2 shows the same for non-flaming fires.

TABLE 4.1 RESPONSE OF THE PHOTOELECTRIC ALARM FOR DIFFERENT TYPES OF SMOKE WITH FLAMING FIRES (DT = DID TRIGGER; DNT = DID NOT TRIGGER)

Sample	Number of tests	Response	Mean Trigger Time(s)
UL 217 Douglas fir	3	DT	172
UL 217 Shredded newspaper	4	DT	150
UL 217 3:1 Heptane/Toluene mixture	4	DT	70
Coffee maker – 12 cup, no carafe	2	DT	386
Mattress PU foam- wrapped in CA TB 117 50:50 cotton/poly sheet –100x100x100 mm foam	1	DNT	--
Mattress PU foam- wrapped in CA TB 117 50:50 cotton/poly sheet –150x150x150 mm foam	1	DNT	--
	1	DT	171
Nylon carpet – 100x100 mm sample	1	DNT	--
	2	DT	272

The mean smoke particle diameter of polyisocyanurate in both flaming and non-flaming modes is less 90 nm. For the alarm trigger time, polyisocyanurate was only tested with non-flaming fires and the photoelectric alarm did not trigger for this fire.

TABLE 4.2 RESPONSE OF THE PHOTOELECTRIC ALARM FOR DIFFERENT TYPES OF SMOKE WITH NON-FLAMING FIRES (DT = DID TRIGGER; DNT = DID NOT TRIGGER)

Sample	Number of tests	Response	Mean Trigger Time(s)
Ponderosa pine	5	DT	3314
Bread – 4 slices	3	DT	394
Polyisocyanurate insulation – 150 x150x200 mm piece	1	DNT	--
Mattress PU foam – 150x150x50 mm foam	2	DNT	--
Mattress PU foam – 100x125x100 mm foam with a 25x150x150 mm piece on two opposing sides	2	DT	3090
Mattress PU foam – wrapped in CA TB 117 cotton sheet – 100x150x200 mm foam	1	DT	3530
Mattress PU foam – wrapped in CA TB 117 cotton sheet – 125x125x300 mm foam	1	DT	4207
Mattress PU foam – wrapped in polyester microfiber sheet – 125x125x300 mm foam	2	DT	4741
Nylon carpet – 150x150 mm sample	1	DT	5727
Polystyrene pellets – 69.8 g	1	DT	5546

In the test with nylon carpet, a photoelectric alarm was triggered for the non-flaming fire but did not trigger for the flaming fire. In the flaming mode, the mean diameter of the smoke particles of the nylon carpet was less than 90 nm (75 nm) and it was greater than 90 nm for the non-flaming fires (125 nm).

Even though, in both flaming and non-flaming modes of the small scale tests and in the flaming mode of intermediate scale tests, the mean smoke particle diameter of PU foam falls under the dotted line, in non-flaming mode of intermediate scale tests, it falls above the dotted line. For PU foam, the photoelectric alarm was triggered only for non-flaming fires.

Although, the smoke particle size for polystyrene pellets is not available from the small scale or intermediate scale tests, the mean smoke particle diameter of polystyrene pellets have been measured at 0.5% /ft obscuration level and is recorded as the 220 nm (table 26 of task 3 in Fabian and Gandhi, 2007). The photoelectric alarm also triggered for non-flaming fires of polystyrene pellets.

4.3 LIMITATIONS OF EXISTING HOUSEHOLD SMOKE DETECTORS

4.3.1 SENSITIVITY

Extensive prior research[7],[8] (Ahrens, 1998; Fabian & Gandhi, 2007, Qualey *et al*., 2001) suggest that no sensor type (photoelectric or ionization) is universally better at detecting all type of fires since each sensor operates on a different principle and therefore may respond differently to various conditions. Ionization detectors are recommended for areas containing highly combustible materials such as flaming liquids, newspapers, and paint cleaning solutions, which create flaming fires. On the other hand, photoelectric detectors are recommended for areas which contain furniture such as sofas, chairs, mattresses etc. which burn slowly and create smouldering fires.

Ionization smoke detectors are more sensitive than the photoelectric type detectors in detecting smaller particles of combustion, i.e. generally smaller than one micron (considered generally invisible to the human observer). They are predominately created by fast flaming fires. Alternatively, photoelectric smoke detectors are more sensitive than ionization detectors in detecting large combustion particulate, i.e. generally larger than one micron (considered to be visible to the human observer). They are created by smouldering fires (Ahrens, 1998; Fabian & Gandhi, 2007, Qualey *et al*., 2001).

[7] www.firesafetycouncil.com/pdf/review_on_best_sensor_type_for_kitchens.pdf

[8] http://www.electronics-manufacturers.com/info/sensors-and-detectors/smoke-detectors.html

Smoke is generally classified as black or gray. Obscuration detectors typically work well for black smoke but are less sensitive to gray smoke. The colour of the smoke greatly affects the amount of light that is scattered. Gray smoke particles are generally much easier to detect as they tend to scatter the light from the photo-emitting diode[9]. Therefore, light scattering detectors generally work well for gray smoke but have a decreased sensitivity to black smoke (Qualey *et al.*, 2001).

Ionization smoke detectors are prone to nuisance alarms frequently as they wrongly identify other polar molecules including water vapour, moisture, and humidity as smoke (Ahrens, 1998).

4.3.2 ACTIVATION TIME

Early detection of fires is very crucial because the time to tenable conditions in residences can be as little as 3 minutes for typical flaming fire scenarios[10]. Even though both ionization and photoelectric detectors quickly alert occupants in most fire scenarios, in controlled experiments ionization detectors react earlier than photoelectric detectors in fast flaming fires, such as those involving paper or flammable liquids. On the other hand, photoelectric detectors react substantially earlier than ionization detectors in smouldering fires (Brammer, 2002; Fabian & Gandhi, 2007; Qualey *et al.*, 2001).

Brammer (2002) compared the activation times of both ionization and photoelectric type smoke detectors for two test fires (Test A and Test B) and the results are shown in Figures 4.8 (a) and 4.8(b). Both tests were performed on single chairs with timber frames, upholstered with "combustion modified high-resilient foam" with a fire retardant cotton cover. The fires took place in the lounge.

[9] http://www.electronics-manufacturers.com/info/sensors-and-detectors/smoke-detectors.html

[10] http://www.nist.gov/public_affairs/releases/smoke_detectors.htm

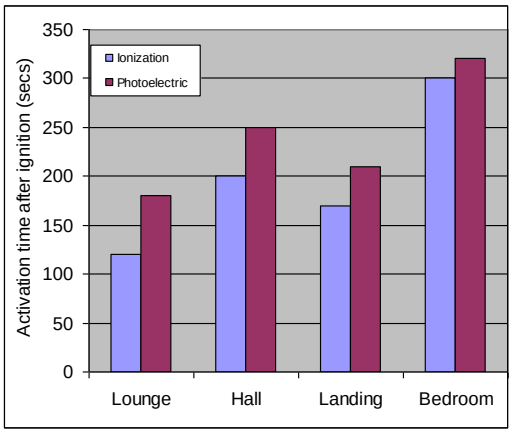

(a) Test A

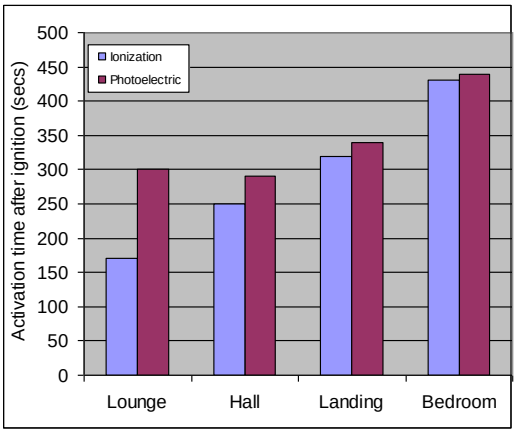

(b) Test B

Figure 4.8 Comparison of activation times of both ionization detector and photoelectric detector for two test fires (adopted from Brammer, 2002)

"Combustion modified high-resilient foam" is a kind of polyurethane foam. According to Fabian & Gandhi (2007), polyurethane based materials give the smallest size particles in both flaming and non-flaming combustions and small size particles activate the ionization detectors first. This clearly explains the results of the Brammer (2002) study.

According Fabian & Gandhi (2007), for all but one flaming fires ionization detector activated first. For some flaming fires involving polyurethane foam with cotton/poly fabric (which gives smaller size particles), the photoelectric detector did not activate. And for a flaming test with PU foam with cotton/poly fabric using a smaller sample size, neither alarm types activated. For most of the non-flaming fires, the photoelectric alarm activated first, but for many of the materials, the ionization detector did not work at all.

4.3.3 FALSE POSITIVES

False alarms and nuisance activations are problems to the fire services and building occupants. They interrupt other activities and may lead people to ignore the warnings of

smoke alarms. In New Zealand, false alarms accounted for almost 40% of the fire call responses in 1998. About half of all false alarms were from fire alarm systems (Ahrens, 2004). Steam and normal cooking activities can also cause false positives.

Cooking smoke tends to contain a lot of smaller particles (less than one micron) that can activate an ionization detector rather than larger particles that can activate a photoelectric detector (Ahrens, 1998). In the study of Ahrens (1998), it is found that 97% of the devices tested for nuisance alarms were ionization detectors. However, according to an information report from Applied Research Office of the Fire Marshal, Ontario (2005), normal cooking activities can cause nuisance alarms in photoelectric and ionization type alarms and neither type of detector was demonstrably better in reducing nuisance alarms.

Mainly there are three suggestions to avoid the nuisance alarms.

- Reduce the sensitivity of the smoke alarm.

  Even though, reducing the sensitivity of smoke alarms can reduce the likelihood of nuisance alarms, it was found that the detectors involved in nuisance alarms were more sensitive to fires than those were not (Smith, 1993).

- Install photoelectric detectors in kitchen area.

  Photoelectric detectors are less prone to nuisance alarms in kitchen area than ionization detectors. The problem arises with this option is most of the fires involved in cooking activities are flaming fires which release much smaller size particles. These particles are less sensitive to photoelectric detectors.

- Relocate the smoke alarm

  Install the smoke alarm away from cooking appliances.

4.4 ADVANTAGES AND DISADVANTAGES OF HAVING IR LEDS IN PHOTOELECTRIC SMOKE ALARMS

Even though a photodiode could detect radiations with wavelengths between 190 nm to 1100nm, the peak spectral responsivity of typical silicon photodiode (of existing photoelectric smoke alarms) lies around 900 nm. Therefore, for the optimal response from these photodiodes, the ideal light source is the IR LED with the wavelength of 900nm. On the other hand, with infrared light, the smoke particles with less than 90 nm diameters can be considered as the Rayleigh scatters. Since the Rayleigh scattering is strongly wavelength dependant, the amount of light scattered by Rayleigh scattering is very little. Therefore the photo receiver receives only the light scattered by Mie and non-selective scattering. These types of scattering can occur only by the smoke particles with diameters greater than 90 nm. Therefore, photoelectric alarms with IR LEDs cannot detect any particles with less than 90 nm diameters (Figure 4.9).

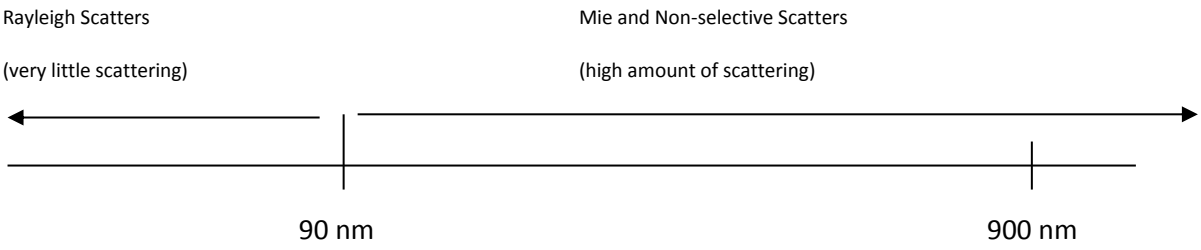

Figure 4.9 Size range of Rayleigh and Mie scatters for infrared light (900nm = the infrared wavelength of the existing smoke alarm)

4.5 ADVANTAGES OF REPLACING IR LED OF THE PHOTOELECTRIC ALARM WITH A UV LED

Compared to Rayleigh scattering with infrared light, Rayleigh scattering with UV light scatters 35 (=900^4/370^4) times as much as UV radiation. On the other hand, UV light can be scattered by the smoke particles having a diameter more than 37 nm with Mie

and non-selective scattering (Figure 4.10). Therefore, a photoelectric alarm with a UV LED and a compatible photo-receiver (UV photodiode, CCD array or UV camera) detects much smaller smoke particles than an existing photoelectric alarm.

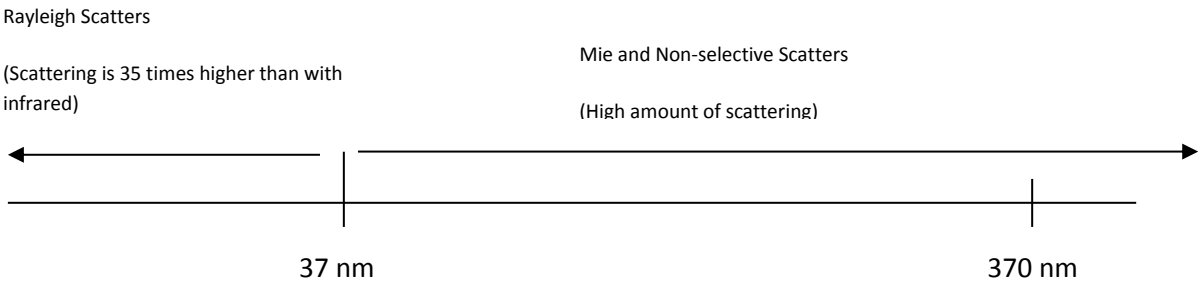

Figure 4.10 Size range of Rayleigh and Mie scatters for UV light (370nm = the minimum wavelength of the available UV LEDs)

4.6 NECESSITY FOR A NEW TYPE OF SMOKE DETECTOR

The existing two types of household smoke detectors (photoelectric and ionization) respond differently to different types of smoke. Photoelectric smoke detectors respond mostly to large smoke particles while ionization detectors respond mostly to small size smoke particles. Ionization alarms contain a tiny amount of radioactive material and are not considered as environmentally friendly as photoelectric alarms.

By considering the pros and cons of these existing smoke detectors, it is obvious that there is a necessity for a new type of smoke detector which can work well in a whole range of smoke-particle-sizes. The new detector should be able to distinguish the differences between the smoke caused by day to day cooking activities resulting in nuisance alarms from the smoke caused by actual hazardous events.

4.7 CHALLENGES FOR VIDEO-BASED SMOKE DETECTION SYSTEMS

According to Xiong *et al*. (2007), the performance of video-based smoke detection is still inferior to those of traditional particle-sampling based detectors in terms of detection rate and false alarm rate. They have identified the following challenges for video based smoke recognition.

- Video smoke signal can vary with smoke density, different lighting conditions, diverse backgrounds and interfering non-rigid objects etc.
- Due to the behaviour of smoke, it cannot be characterised well with the primitive image features such as intensity, motion, edge, and obscuration
- It is very difficult to model the visual patterns of smoke

5 – PROPOSED METHODOLOGY

5.1 PROPOSED IMAGE HISTOGRAM BASED SOLUTION FOR SMOKE DETECTION AND CLASSIFICATION

Smoke detectors based on computer vision techniques using open space surveillance cameras to detect smoke clouds are not useful solution to detect common household fires since they require external ambient light at all times to function. However, in those studies, the techniques used to characterise the smoke can be adopted to develop a smoke classification algorithm based on image histogram features. The proposed algorithm characterizes the smoke not in the open space but in the smoke chamber of the detector. The proposed smoke detector encompasses many features of an existing photoelectric smoke detector, with the photodiode replaced by a CCD array. The images (of the scattered light) captured by the CCD array will be fed into an embedded signal processor to support the histogram feature classification algorithms.

Figure 5.1 compares the sizes of different particles that activate both types of detectors with wavelengths of the spectrum. A photodiode can detect wavelengths between 190 nm to 1100 nm[11]. Even though, a photodiode can respond to such a large band of spectrum, the peak spectral responsivity of typical low cost silicon or pin

[11] http://en.wikipedia.org/wiki/Phototransistor#Other_modes_of_operation

photodiode lies around 900 nm[12]. For example, Figure 5.2 shows the variation of detector sensitivity to wavelengths of a photodiode in an optical lighting system[13]. To get the maximum response from the photodiode (since the final value is entirely depend on the single output of the photodiode, i.e. the output voltage), common household photoelectric detectors use an LED which emits near infrared (NIR) (wavelength between 850 nm – 940 nm) radiations[14].

A CCD array is sensitive to a broader spectrum of light (from UV to IR) than the photodiode response graphed above. Since smaller particles are more effective at scattering shorter wavelengths of light, by replacing the single conventional IR LED with a set of LEDs producing a broader spectrum of light, a more effective photoelectric smoke detector can be introduced which detects both smaller and larger particles (for the relative sizes of particles, see the table 5.1). This solution is only now possible with recent breakthroughs in LED's shorter wavelength transmission and CCD array's shorter wavelength sensitivity. Significant recent cost reductions of such CCD arrays and signal processors now enable manufactures to manufacture a low cost smoke sensor encompassing smoke particle sizes detected by both traditional optical and ionisation smoke detectors.

Another advantage of this proposed approach is that it is possible to analyse various smoke image characteristics such as colour and intensity histograms (comparing two or more video frames) which is not possible with photodiodes. For example, this proposed approach may enable smoke detectors to differentiate between smoke from a hazardous fire and steam causing nuisance alarms.

---

[12] http://sales.hamamatsu.com/en/products/solid-state-division/si-photodiode-series.php

[13] http://en.wikipedia.org/wiki/Photodiode

[14] http://www.sas.org/tcs/weeklyIssues/2004-07-16/feature1/

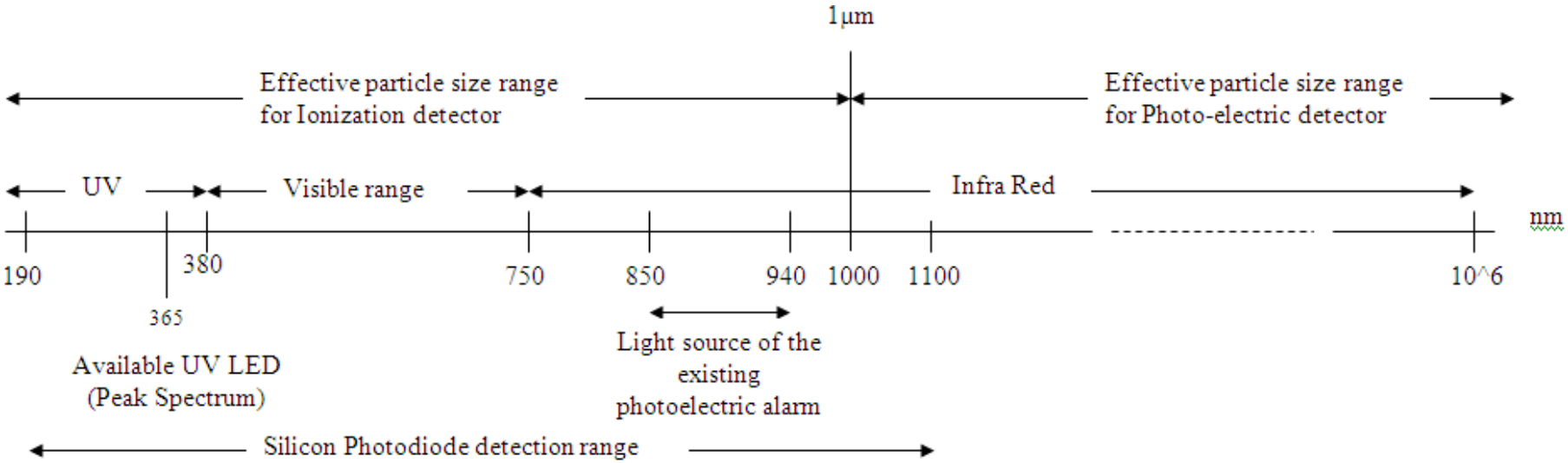

Figure 5.1 Comparison of size of particles which are effective at both type of smoke detectors, wavelength of the LED of common household photoelectric smoke detector, responsive photodiode wavelength range with the spectrum (not into scale)

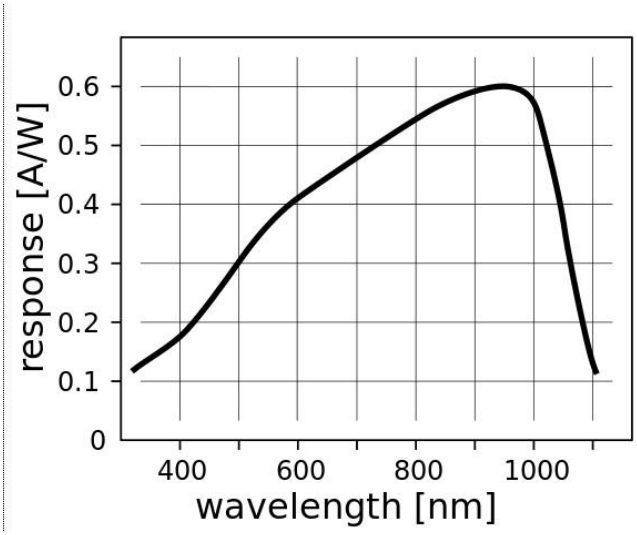

Figure 5.2 Silicon photodiode detector responsivity (ratio of the generated photocurrent to incident light power) versus wavelength

TABLE 5.1 RELATIVE SIZES OF DIFFERENT SMOKE PARTICLES

Smoke type	**Mean Particle diameter (µm)**	
	Flaming Mode	**Non-Flaming Mode**
Polyester pillow	0.091	0.041
Cotton Batting	0.095	0.086
Ponderosa pine	0.037	0.156
PU Foam	0.048	0.085
Heptane	0.195	Not found
Cooking Oil	0.226 – 0.293	0.077
News Paper	0.041	0.101
Fly ash	1-300	1 - 300
Nylon Carpet	0.112	0.072

5.2 EXPERIMENTAL SETUP

The present study consists of three experiments. This chapter describes the methods used for each experiment. The three experiments conducted in the present study were:

- Particle detection with white LED
- Particle detection and classification with red, green and blue laser beams
- Particle classification with white LED

The purpose of the experiment, setting up the instruments and method of evaluation of each experiment are discussed under each section.

5.3 PROPOSED PARTICLE DETECTION WITH WHITE LED

5.3.1 AIM

As described in the chapter 4, the detection of the full range of particles (from 40 nm to 1 μm in diameter) with the commercially available photoelectric type smoke detectors is limited. Therefore, instead of the IR (Infrared) LED which is commonly use in the commercially available photoelectric type smoke detectors, a white LED was tested to investigate the possibility of detecting the full range of particles by capturing both Mie and Rayleigh scattered light (see chapter 2.3).

5.3.2 INSTRUMENT SETUP AND IMAGE CAPTURING

To avoid the intensity changes in the background by outside light sources, all the images were captured in a shoebox size (30 mm x 15 mm x 10 mm) closed particle chamber. Four different backgrounds (white, black, checkerboard and grayscale) were tested inside the chamber.

A phosphor-based white LED (MC20358, SPC Technology) which covers a wide range of the spectrum (~400 nm to ~800 nm) was used to illuminate the chamber. The spectrum (relative luminous intensity vs. wavelength) of this LED is shown in Figure 5.3.

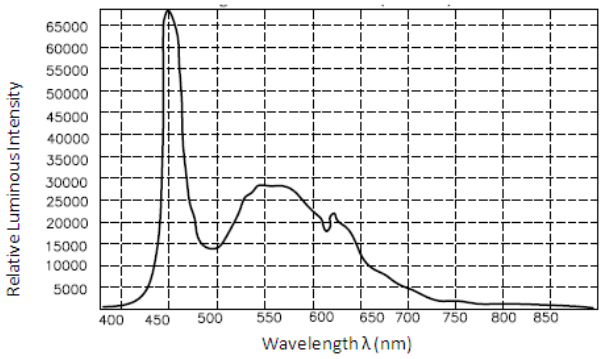

Figure 5.3 Spectrum of phosphor based white LED (adopted from the technical datasheet of SPC Technology, MC20358)

Three image capturing devices (USB digital microscope, simple web camera and a cyber-shot camera) were used inside the chamber to capture the colour video frames.

For each particle type, separate frame sequences were captured before and after the introduction of particles.

5.3.3 METHOD OF EVALUATION

Comparison of image histograms between the images before and after the introduction of particles was used to detect the presence of particles in the images. Four popular histogram comparison methods (correlation, Chi-square, intersect and Bhattacharyya method) were used to compare the histograms. With each of the histogram comparison method, each frame of the frame sequence was compared with

1. one of the randomly selected frame which was not affected by the particles (i.e. with a frame before the particle introduction) of the same sequence and,
2. the previous frame of the same sequence (except the first frame).

When the histogram comparison parameter exceeded a predefined threshold, the compared frame was selected as an affected frame and the particles were considered as "detected". Obtained results were compared with the smoke detection results of Fabian and Gandhi (2007).

5.4 PROPOSED PARTICLE DETECTION AND CLASSIFICATION WITH RED, GREEN AND BLUE LASER BEAMS

5.4.1 AIM

As Rayleigh theory suggested, a particle can scatter light with lower wavelengths in the electromagnetic spectrum in high intensities and higher wavelengths in less intensities (see section 2.3). Rayleigh scattering of incident light with wavelength λ by a single particle is explained by the following equation.

$$I(\theta)_\lambda = I_0 \frac{1+\cos^2\theta}{2R^2}\left(\frac{2\pi}{\lambda}\right)^4\left(\frac{n^2-1}{n^2+2}\right)^2\left(\frac{d}{2}\right)^6 \qquad 5.1$$

The intensity of Rayleigh scattered light depends on the size of the particle (proportional to the sixth power of the particle size) and the wavelength of the incident light (inversely proportional to the fourth power of the wavelength). Assuming that θ, I_0 and R are constant, for a particle with refractive index n and diameter d, the ratio between the scattered intensities of different incident lights with wavelength λ_1 and λ_2 , $R_{\lambda1,\lambda2}$, can be expressed by the equation 4.2.

$$R_{\lambda1,\lambda2} = \frac{I(\theta)_{\lambda1}}{I(\theta)_{\lambda2}} = \left(\frac{\lambda_2}{\lambda_1}\right)^4 \qquad 5.2$$

Again, since $I(\theta)_\lambda \propto d^6$ (where d is the diameter of the particle),

a unique $R_{\lambda 1, \lambda 2}$ can be obtained for different wavelengths λ_1 and λ_2 according to the size (diameter) of the particle.

Each type of test particles (approximately with the same diameter) were exposed to three separate light with different wavelengths (red, green and blue) simultaneously with the aid of three laser pointers. Scattered light was captured using a 3 megapixel cybershot camera with 30 frames per second.

5.4.2 INSTRUMENT SETUP AND IMAGE CAPTURING

As in experiment 5.3, all the images were captured in a shoebox size (30 mm x 15 mm x 10 mm) closed particle chamber. Three laser pointers (red, green and blue) which were placed in 3 cm apart were used in the chamber to illuminate the particles. The scattered light of all the three laser beams were captured simultaneously before and after the introduction of the particles.

Specifications of those laser pointers used in experiments are in table 5.2. Intensity diagrams of these laser pointers were not available in the manufacturer's instruction manual. The characteristic spectrums of typical laser pointers are shown in Figure 5.4.

TABLE 5.2 SPECIFICATIONS OF USED LASER POINTERS

Red Laser	Green Laser	Blue Laser
Max Output: 5 mW Wave Length: 650 +/-10 nm Output wave: Continuous wave Power: 2 x AAA battery	Max Output: 5 – 6 mW Wave Length: 532 nm Output wave: Continuous wave Power: 2 x AAA battery	Max Output: 5 mW Wave Length: 405 nm Output wave: Continuous wave Power: 2 x AAA battery

5.4.3 METHOD OF EVALUATION

As in experiment 5.3, a comparison of image histograms between the images before and after the introduction of particles will be used to detect the presence of particles in the images. Again, the four histogram comparison methods (correlation, Chi-square, intersect and Bhattacharyya method) which were used in the experiment 5.2 were also used to compare the histograms. All the colour images were converted into their single channel red, green and blue images and comparisons were made to find out the uniquely identifiable features (as described in section 5.3.1) for classification.

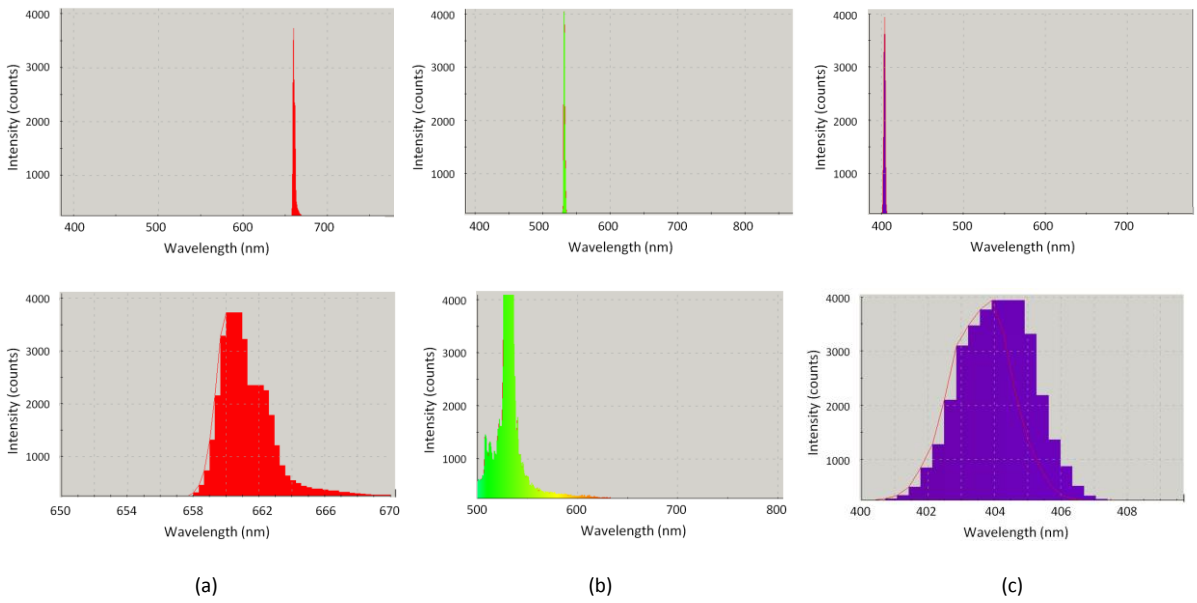

Figure 5.4 Relative positions of the Red (a), green (b) and blue (c) laser spectrums in the electromagnetic range (above) with detailed spectrums (below) (http://ledmuseum.candlepower.us/led/spectra3.htm, visited on 8/12/2014)

5.5 PROPOSED PARTICLE CLASSIFICATION WITH WHITE LED

5.5.1 AIM

This experiment was designed to overcome the poor results from experiment 5.3. The variation of image particle density independent feature; histogram maximum value index (*MVI*) was tested for particle classification. Instead of the single scattered red, green and blue wavelengths which were captured in the experiment 5.3, scattered light from a continuous spectrum of light was captured and analysed for unique features.

5.5.2 INSTRUMENT SETUP AND IMAGE CAPTURING

A white background in a closed particle chamber (to avoid the intensity changes in the background by outside light sources) was used. All the images were captured inside the chamber. A small electric fan was continuously operated inside the chamber to maintain the particle density evenly inside the chamber (to achieve a reasonably evenly distributed noise in video frames).

A phosphor-based white LED (MC20358, SPC Technology) which covers a wide range of spectrum (~400 nm to ~800 nm) was used to illuminate the chamber. The spectrum (relative luminous intensity vs. wavelength) of this LED is shown in Figure 5.3.

A USB digital microscope was used to capture the colour video frames. Depending on the distance, it can magnify objects up to a maximum of 200X with resolution 640 x 480 pixels. For each particle type, separate frame sequences were captured before and after the noise which was introduced by the particles.

5.5.3 METHOD OF EVALUATION

This section describes the following steps in detail; particle isolation with a frame difference algorithm, feature extraction, feature representation and classification.

5.5.3.1 PARTICLE ISOLATION WITH MODIFIED FRAME-DIFFERENCE ALGORITHM

If I_{t_n} is an image of the frame *n* which is taken at time t_n, the pixel value *s* located at *x* at time t_n in the difference image is defined as

$$\boldsymbol{s}(t_n, \mathbf{x}) = |p(\mathrm{I}_{t_n}, \mathbf{x}) - p(\mathrm{I}_{t_{n-1}}, \mathbf{x})| \tag{5.3}$$

where $p(\mathrm{I}_t, \mathrm{x})$ is the pixel value at x in the image $\mathrm{I_t}$.

Let k is the number of frames before the particle cloud was introduced. Then the noise pixels in the n^{th} (n>k) affected image can be identified by the difference image between $\mathrm{I_{t_n}}$ $(\mathrm{n} > k)$ and one of the non-affected images $\mathrm{I_{t_m}}$ $(\mathrm{m} \geq \mathrm{k})$. By modifying the equation 1, the pixel value d located at x at time $\mathrm{t_n}$ in the difference image of these affected and non-affected images can be defined as

$$\mathbf{d}(t_n, \mathbf{x}) = |p(\mathrm{I}_{t_n}, \mathbf{x}) - p(\mathrm{I}_{t_m}, \mathbf{x})| \tag{5.4}$$

where $m \in [1, k]$ and $n \in] k, N]$, *N* is the total number of frames.

The thresholded difference image was used to construct the "noise-only image" and the pixel value **n** located at **x** at time t_n in the noise-only image was calculated as

$$\mathbf{n}(t_n, \mathbf{x}) = \begin{cases} p(\mathrm{I}_{t_n}, \mathbf{x}) \; for \;\; \mathbf{d}(t_n, \mathbf{x}) \geq T \\ 0 \qquad for \;\; \mathbf{d}(t_n, \mathbf{x}) < T \end{cases} \tag{5.5}$$

(See chapter 6, section 6.3.2 for an example of a smoke image with the thresholded (black and white) difference image constructed using equation 5.3, the image isolated smoke pixels using equation 5.5 and the corresponding noise histogram of smoke pixels).

5.5.3.2 FEATURE EXTRACTION WITH RGB LAYER HISTOGRAMS

After isolating the objects from the images using equation (5.5), red, green and blue single channelled object images were obtained by dividing the frames of each captured frame sequence (3-channel arrays) into their red, green and blue (RGB) planes. Histograms of both colour and single channel object images were constructed.

As described in section 2.1.2.3, it was discovered that the *MVI* of the histogram is a particle density independent feature. In this proposed method, six image signatures based on intensity and colour histogram *MVI*s were used for classification. For clarity, the notation $MVI_{k,l}$ was used to identify these signatures. In this notation k is the histogram type (either intensity or colour) and l is the selected channel (R, G or B). For example, $MVI_{Intensity,\ G}$ is the histogram *MVI* of the constructed "green" channel image. $MVI_{Colour,\ G}$ is the green value of the colour histogram *MVI* of the colour image (value of the second element of the tuple).

Moving windows of a fixed number of frames (number of frames = N) were used to calculate the running mode, mean and standard deviation of *MVI*s (the mode, mean and standard deviation of *MVI*s inside the moving window) of the constructed histograms.

Two mutually independent feature vector sets (one with running means and standard deviations and the other with running modes) were constructed for both single channel and colour images.

5.5.3.3 FEATURE REPRESENTATION

Mode, mean and standard deviation of maximum value index were calculated for each RGB layer sequence of each particle type using a moving window of N (N=50, 100, 150 and

200) frames. The six dimensional feature vector $F_{x,i}$, shown below, was created with the means and the standard deviations of each window.

$F_{x,i} = (x_1, x_2, x_3, x_4, x_5, x_6)$

where x_1, x_2 and x_3 are the means of maximum value indexes of the frames of the moving windows over red, green and blue sequences and, x_4, x_5 and x_6 are the standard deviations of those frames in red green and blue sequences respectively. i is the window number and x is the particle type.

Similarly a three dimensional feature vector, shown below, was constructed using the running modes.

$F_{x,i} = (x_1, x_2, x_3)$

where, x_1, x_2 and x_3 are the running modes of maximum value indexes of the frames of the moving windows over red, green and blue sequences.

5.5.3.4 CLASSIFICATION

Feature vectors were classified using two widely used supervised classification algorithms: linear discriminant analysis (LDA) and K-nearest neighbour algorithm (KNN). The classification algorithms were tested for their efficiency.

The linear discriminant analysis formula is defined as

$$f_i = \mu_i C^{-1} x_k^T - \frac{1}{2} \mu_i C^{-1} \mu_i^T + \ln(p_i) \qquad 4.6$$

where $\mu_i C^{-1} \mu_i^T$ is the Mahalanobis distance, which is the distance to measure dissimilarity between several groups. The object k with the feature vector x is assigned to the group i if it has the maximum f_i.

With KNN, if d_i is the distance between the test image and the i^{th} reference image then the test image can be assigned to the reference image R where

$$d_R = \min_{i=1}^{M}[d_i].$$

M is the number of reference images

(See section 2.4 for more details on classifications with linear discriminant analysis and K-nearest neighbour algorithm).

In each particle frame sequence, half of the total number of windows was used as the training data and the other half were used as the test data. For example, when the moving window size (N) is 100, 1000 training instances and 1000 test instances were used.

6 - RESULTS AND DISCUSSION

Results of both experiments; smoke detection and smoke classification, which are described in Chapter 5 –Proposed Methodology, are shown and discussed in this chapter. Description of the test particles and the reasons for selecting them are explained in section 6.1. Results of the smoke detection experiment with histogram comparisons are shown in section 6.2. Section 6.3 shows the results of particle classification with colour laser beams (6.3.1) and particle classification with white LED light (6.3.2).

6.1 TEST SAMPLES

The selected test samples are presented in table 6.1 and included both natural and synthetic materials with different chemical structures. Test samples were selected after a lengthy review of common smoke types found in contemporary household fires (Fabian & Gandhi, 2007; Australian Standard™, Fire detection and alarm systems—Smoke alarms (ISO 12239:2003, MOD), 2003; Ahrens, 2004).

TABLE 6.1 SELECTED TEST PARTICLES

Test Sample	Comment
Pinewood smoke	Natural material, commonly found in building structures
Polyurethane smoke	Synthetic, flexible, open cell structure, commonly found in home furnishing
Steam	Common particle type which gives false positives in household smoke alarms
Kerosene smoke	Hydrocarbon liquid, Short straight chain hydrocarbon
Cotton wool smoke	Natural material, commonly found in home furnishing
Cooking oil smoke	Hydrocarbon liquid, "intermediate" length hydrocarbon
Test Smoke	SD 000 (Test Smoke Aerosol Spray)

According to the Australian Standard™, Fire detection and alarm systems—Smoke alarms (ISO 12239:2003, MOD), the four types of test materials that use in testing smoke alarms are "beech" wood smoke, polyurethane smoke, cotton wool smoke and heptane/toluene mix smoke. Due to the unavailability of the used heptane/toluene mixture in the market and the failure of finding the exact name of the used beech wood species in the Australian standards, in the current experiment, a commonly available wood type (pinewood) and kerosene (another short-chained hydrocarbon) was used. Kerosene fires are one of the most common causes for household fires in developing countries because kerosene is widely used in lighting material in rural areas of these countries where electricity is not available or too costly for widespread use[15]. Radiata Pine is the main tree species in New Zealand plantation forests and widely used as a building material (building structures, plywood, medium density fibreboards (MDF) and laminated veneer lumber)

[15] http://en.wikipedia.org/wiki/Kerosene, retrieved 13 February 2013.

and in furniture[16]. With these two types of particles (kerosene smoke and pinewood smoke), two hazardous smoke particle types (polyurethane smoke, cotton wool smoke which are common in typical household fires), two common non-hazardous particles that gives false positives in traditional smoke detectors (steam and cooking oil smoke) and one other test smoke (SD 000, Test Smoke Aerosol Spray) which is commonly used in testing household smoke detectors were also tested in the current study. Out of these seven test particles, all the particles except wood smoke are monotype particles. Wood smoke consists of many different types of particles such as steam, resins and different types of hydrocarbon particles.

6.2 SMOKE DETECTION

All the seven particle types that were listed in table 6.1 were used in the smoke detection experiment. A total 42,000 images (image sequence of 500 frames from each seven particle types, captured with three types of cameras in four backgrounds) were tested in this smoke detection experiment.

Image sequences were captured using three types of cameras; a simple web camera (1.3 Megapixel, 10 frames per second), a cyber-shot camera (3 Megapixel, 30 frames per second) and a digital microscope (1.3 Megapixel, 10 frames per second). A phosphor-based white LED, which covers the spectrum from 400 nm to 800 nm, was used as the light source to illuminate the background. The spectrum of the white LED is shown in Figure 6.1[17].

[16] http://www.nzwood.co.nz/species/radiata-pine, retrieved 13 February 2013.

[17] http://newzealand.rs-online.com/web/p/visible-leds/7134015/

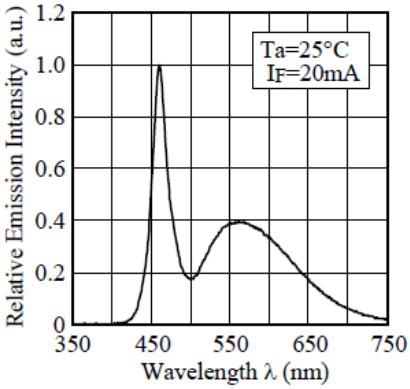

Figure 6.1 The spectrum of the white LED for ambient temperature 25°C and forward current 20 mA

Four types of backgrounds; black, white, checkerboard and gray-scale, were used. Gray-scale background image was created by assigning each pixel of the image with a random gray value between 0 and 255. Figure 6.2 shows the computer generated images of the four backgrounds used. Computed intensity histograms of these computer generated images are shown in Figure 6.3.

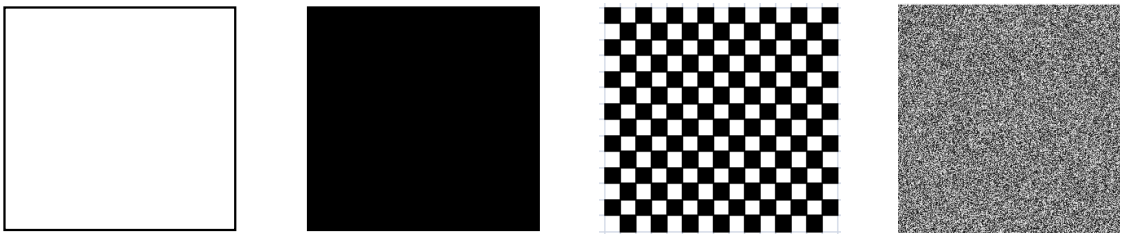

(a) White (b) Black (c) Checker Board (d) Gray-scale

Figure 6.2 Four types of computer generated backgrounds used in smoke detection

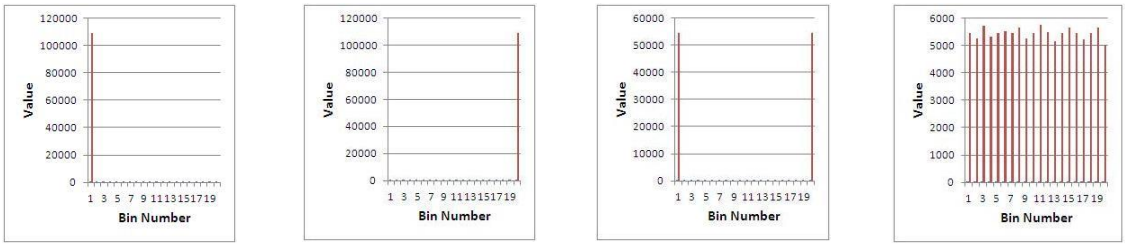

(a) White (b) Black (c) Checker Board (d) Gray-scale

Figure 6.3 Theoretical histograms of the computer generated backgrounds in Fig. 6.2

These images were printed using a laser printer on a white paper to use as the backgrounds in the smoke chamber. Inside the smoke chamber, images were captured with a white LED light source before and after the introduction of smoke. All images were converted into their three single channel colour images (red, green and blue) as well as into gray scale images. Intensity histograms were then calculated for single channel and gray scale images of printed backgrounds.

The histograms of images of printed backgrounds vary slightly from theoretical histograms of the computer generated images (fig 6.2 and 6.3) owing to the applied lighting conditions, printer properties and the properties of the used camera . For example, Figure 6.4 shows the white, black and gray-scale background images before the introduction of particle (wood smoke) ("*Before*") and the images of same backgrounds after the introduction of smoke ("*After*") captured by the digital microscope. It also shows the gray-scale histograms of these images compared with the theoretical histograms in Figure

6.3. Red, green and blue single channel image histograms were also calculated to observe the behaviour of histogram comparison parameters in each colour channel (red, green and blue) image. The histograms of each of these single channel images of smoke were compared with a histogram of an image with no smoke (usually, the first frame of an image sequence) using four different common histogram comparison methods (correlation, Chi-square, intersect and Bhattacharyya method). The variation of the comparison parameter of each method with different backgrounds and each particle type for each colour channel was observed. For example, Figure 6.5 shows the variation of the comparison parameters of each comparison method with white background for kerosene smoke in each colour channel of the first 500 frames in the image sequence. To observe the histogram variation between the consecutive frames, histograms of each image were also compared with the previous image of the image sequence instead of the reference image and the results are shown in Figure 6.6 (for clarity only blue channel image histogram comparisons are shown here).

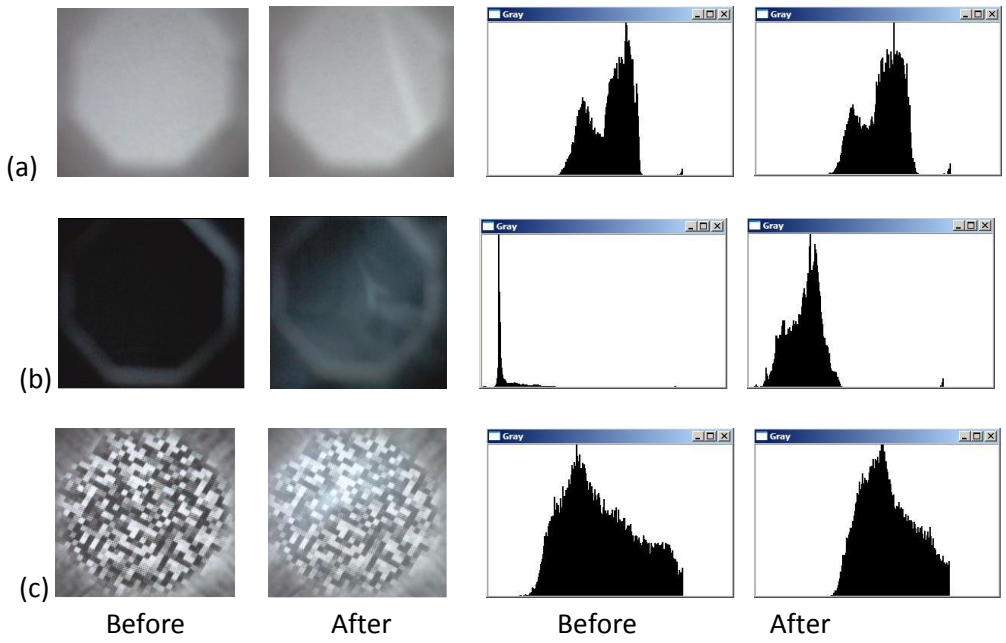

Figure 6.4 White (a), Black (b) and Grayscale (c) background images before and after introduction of smoke particles with image histograms (before and after)

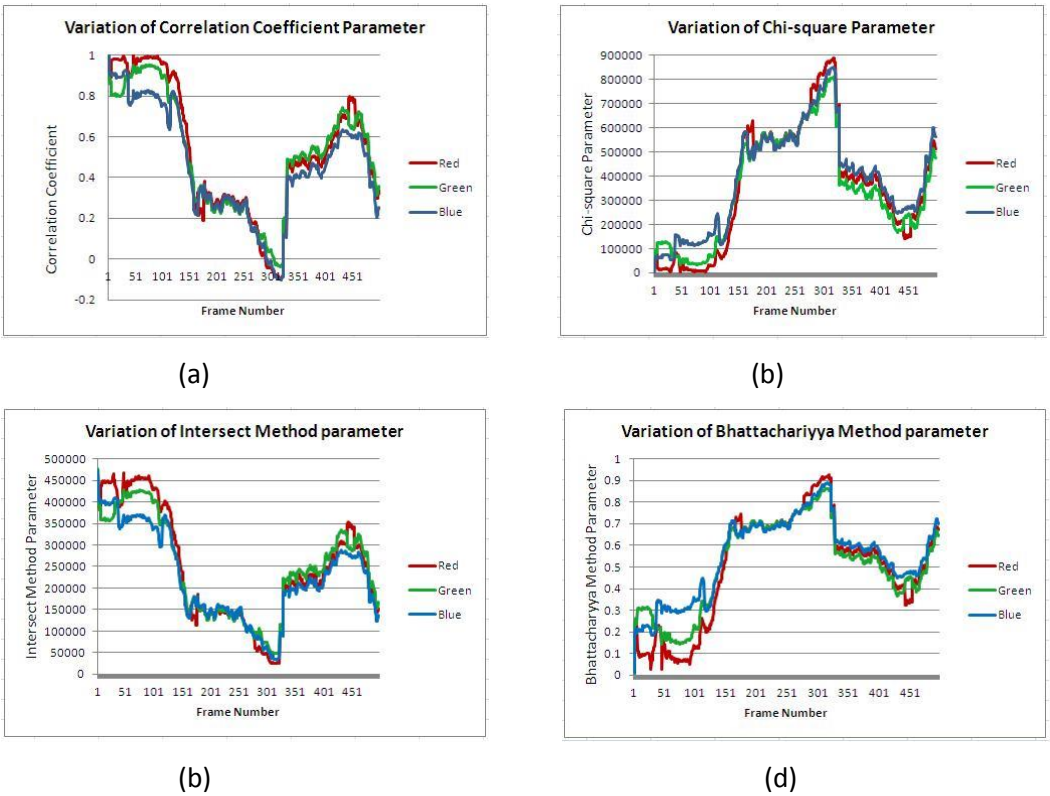

Figure 6.5 Variation of histogram comparison parameters; Correlation method (a), Chi-square method (b), Intersect method (c) and Bhattacharyya method (d) of red, green and blue channel image histograms with polyurethane smoke and white background. Each smoke image is compared with the first image of the image sequence (image without smoke)

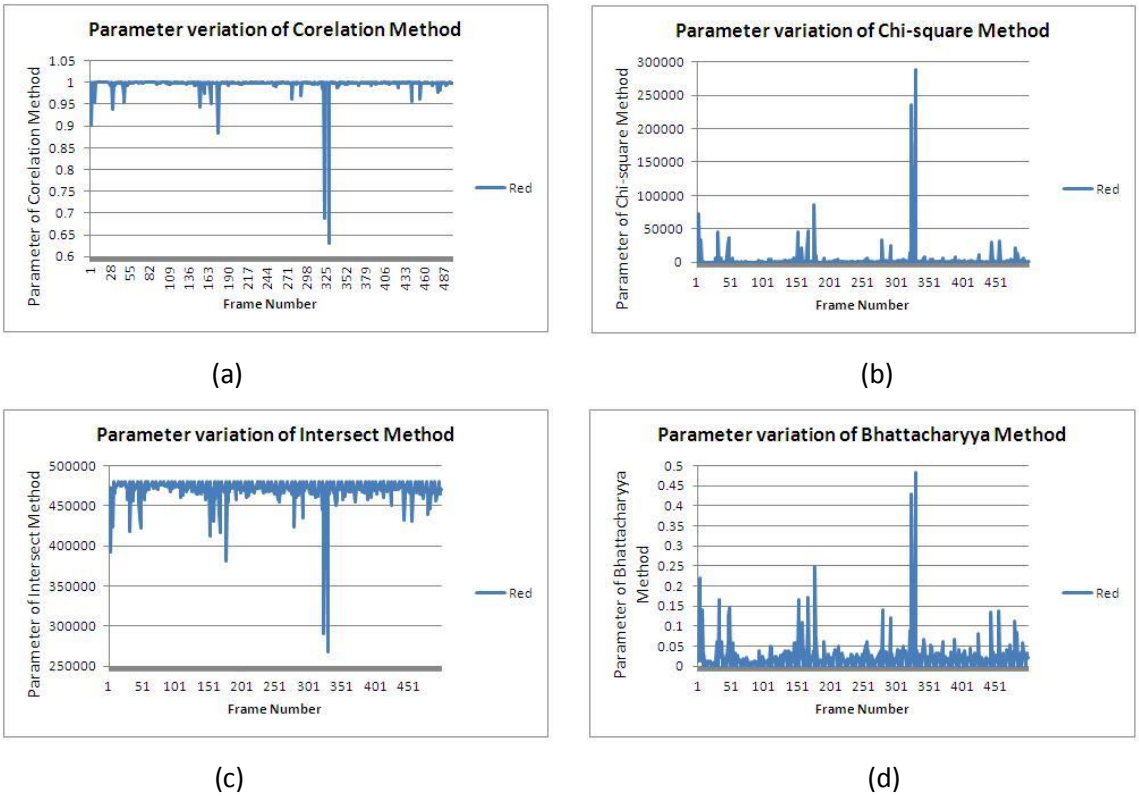

Figure 6.6 Variation of histogram comparison parameters; Correlation method (a), Chi-square method (b), Intersect method (c) and Bhattacharyya method (d) of blue channel image histograms with polyurethane smoke and white background. Each image is compared with the previous image of the image sequence

Discussion:

Histogram comparison parameters in Figure 6.5 shows that image histograms of any of the single channel (red, green, blue or gray-scale) images of all test particles captured with white LED light can effectively be used to recognise the presence of that particular particle. For example, as shown in to Figure 6.5 (d), the Bhattacharyya comparison parameter is greater than 0.3 for all the images with kerosene smoke in the sequence. Figure 6.5 also shows that any of the four histogram comparison methods used here can be effectively used to separate images with smoke from those without smoke. Compared to the effectiveness of detecting smaller smoke particles by common photoelectric smoke alarms, this can be considered as a significant achievement since common photoelectric smoke

alarms do not respond to particles less than approximately 100 nm diameter (see Chapter 4).

Figure 6.6 shows the sudden variations of image histograms between consecutive frames. Of the four comparison methods used here, Bhattacharyya is the best since it accounts for smaller variations between frames (fig. 6.6 (d)). For example, compared to the Bhattacharyya method, correlation method values from consecutive frames after a sudden change are almost same (which is not valid) (fig. 6.6 (a)).

Parameter variations of Bhattacharyya method for all test particles are shown in Figure 6.7 (for clarity, histograms of only green channel images are shown here).

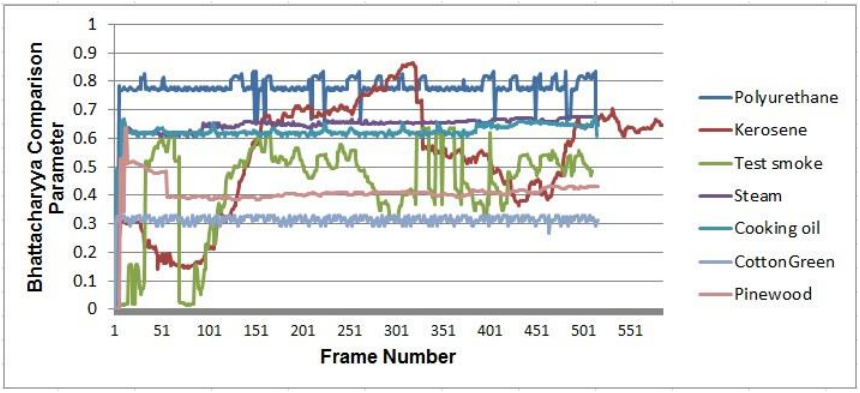

Figure 6.7 Parameter variations of Bhattacharyya method for all the test particles

The uneven variation of the histogram comparison parameters in Figures 6.5 and 6.6 depicts the dissimilarity even between the histograms of the images of the same particle sequence. In a same particle sequence, all the particles are similar in size and, therefore, each particle scatters the same intensities of light according to the wavelength. But different particle densities of each image results in the values of the bins being different in comparing histograms. Therefore, it is very unlikely that it can extract comparable features which are unique to individual smoke types from these image histogram bin values. Also,

compared to the images of single solid objects, in these particle images, histogram bin values do not give much comparable information even with the normalised values.

6.3 SMOKE CLASSIFICATION

Out of the seven test particle types in table 6.1, polyurethane smoke, cooking oil smoke, cotton wool smoke, steam, kerosene smoke and test smoke are all monotype particles. Pinewood smoke, which is another common hazardous smoke type in common household fires and consists of mixture of different sized particles (mostly steam, ash and resin smoke), was used in both classification experiments to compare its behaviour with other monotype particles.

6.3.1 RESULTS WITH DIGITAL MICROSCOPE AND COLOUR LASER BEAMS

As explained by the Rayleigh scattering theory, incident light is scattered in different intensities, according to its wavelength, by the same size of particles. With each test particle type, a sequence of 500 images of scattered light of red, green and blue laser beams were captured using a cyber-shot camera (3 Megapixel, 30 frames per second). All images were captured in a closed particle chamber.

As an example, three captured images of scattered light by three test particle types: kerosene smoke, polyurethane smoke and steam, are shown in Figure 6.8 (a), 6.8(b) and 6.8(c) respectively.

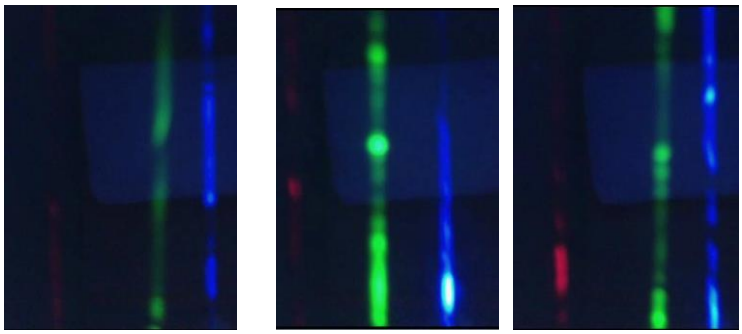

(a) (b) (c)

Figure 6.8 Images of scattered laser light beams by Polyurethane smoke (a), Kerosene smoke (b) and steam (c) particles

Ten sample images (starting with the 300th frame and then every 10th frame) of the scattered laser light image sequence with polyurethane smoke particles are shown in Figure 6.9. The red, green and blue channel image histograms of the laser images in Figure 6.9 are shown in Figure 6.10.

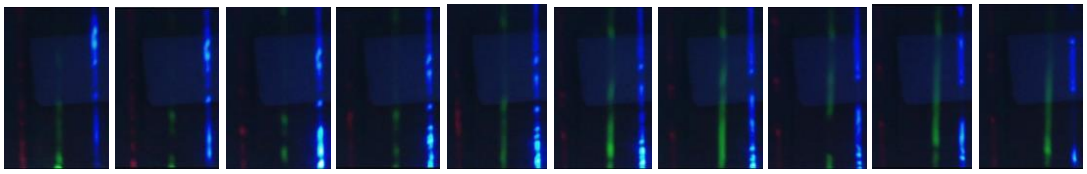

300th 310th 320th 330th 340th 350th 360th 370th 380th 390th

Figure 6.9 Scattered lights of red, green and blue laser images of the polyurethane smoke sequence, starting with the 300th frame and then every 10th frame (from left to right)

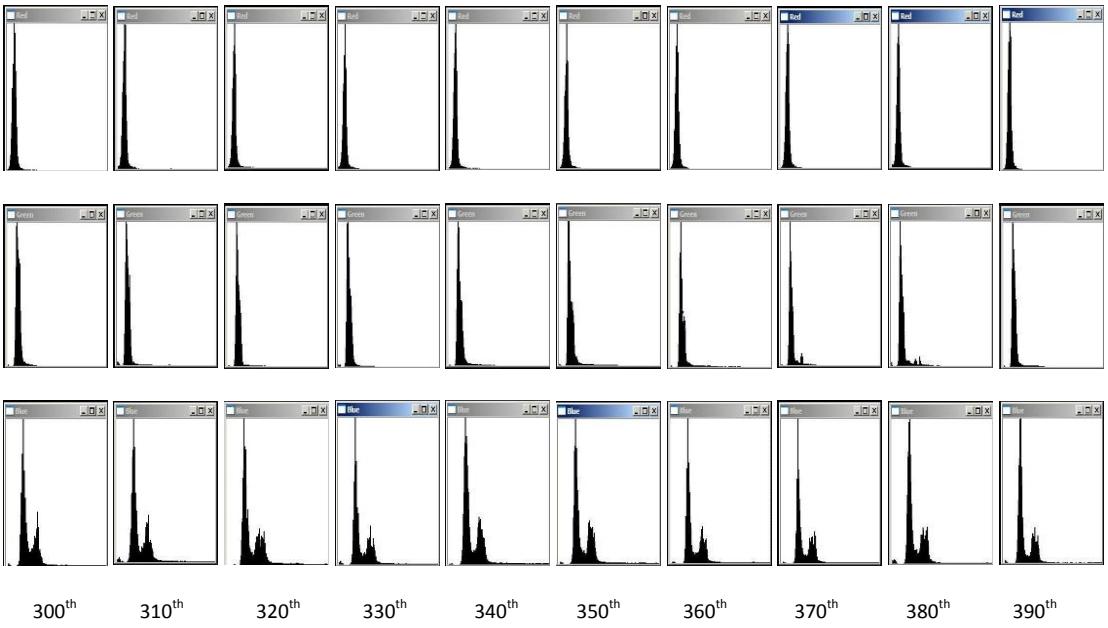

Figure 6.10 Red, green and blue Histograms (respectively top to bottom) of the laser images (figure 6.9) of the polyurethane smoke sequence, starting with the 300th frame and then every 10th frame (left to right)

Figure 6.11 shows the variation of red, green and blue colour histogram comparison parameter with Bhattacharyya method between first frame and the consecutive frames of polyurethane smoke sequence. Variation of the red, green and blue colour histogram comparison parameter with Bhattacharyya method between randomly selected reference frame of the polyurethane smoke sequence and the frames of the kerosene smoke sequence with laser beams is shown in Figure 6.12.

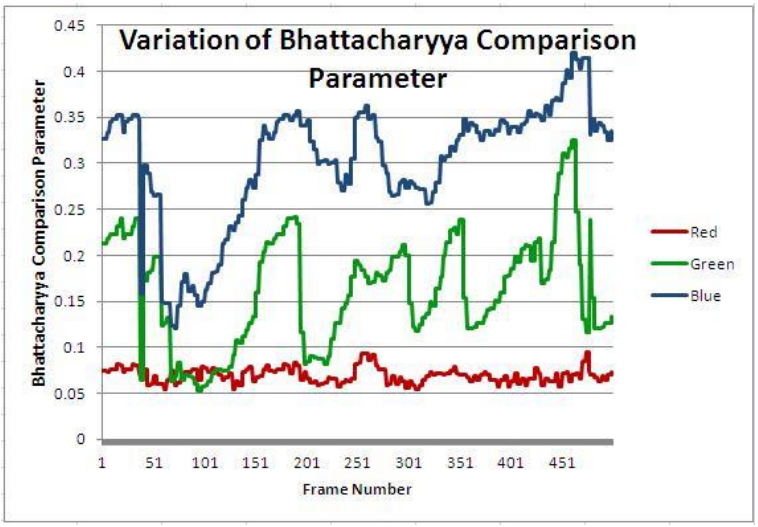

Figure. 6.11 variation of Bhattacharyya red, green and blue colour histogram comparison parameters between first frame and the consecutive frames of polyurethane smoke sequence

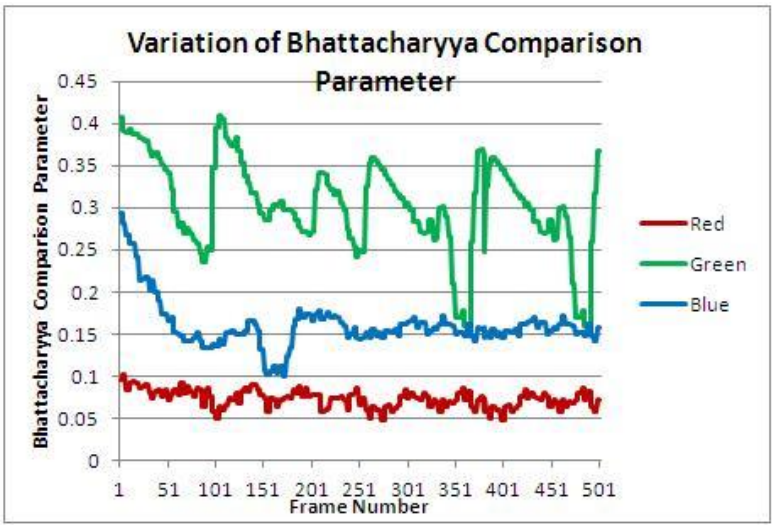

Figure. 6.12 Variation of Bhattacharyya red, green and blue histogram comparison parameter between the first frame of the polyurethane laser image sequence and the frames of the kerosene laser image sequence

Discussion:

The light of exposed red, green and blue laser beams were scattered by all the test particles with a significant intensity (e.g., Figure 6.8). The intensity of each individual red, green and blue scattered light is heavily dependent on the particle density and the density distribution pattern inside the particle chamber. As illustrated by Figure 6.9, more scattered light can be seen in the areas with high particle density and less scattered light in the areas of low particle densities along each laser beam. Even though, Figure 6.9 shows only ten frames of the polyurethane sequence, this behaviour was observed in every frame of each particle sequence. This irregular intensity variation in each red, green and blue colour in each frame explains the unpredictable variation of histogram comparison parameters in Figure 6.11. According to Figure 6.11, it is clear that there are significant variations even between the histograms of the images of same particle image sequence (e.g., fig 6.10 shows only the variation between Polyurethane particle images), and owing to the same fact, histogram comparisons between the frames of different particle sequences becomes more insignificant and it is clearly shown in Figure 6.12.

As described in Chapter 2 - Section 2.3, theoretically, the comparison of intensities of scattered light with different wavelengths (e.g., red, green and blue intensities in this experiment) is the best method to classify different sized particles. But owing to the unpredictable movement behaviour of particles illuminated with laser beams, the existing histogram comparison methods (Correlation method, Chi-square method, Intersect method and Bhattacharyya method) did not accurately classify the test particles. Therefore, a different parameter which is independent of the particle density should be constructed to compare the scattered intensities of light of different wavelengths.

6.3.2 RESULTS WITH DIGITAL MICROSCOPE AND WHITE LED LIGHT

Eight video streams from each of the six monotype particles were captured and total 24,000 images (500 frames from each video stream) were used in this smoke classification experiment. Half of the randomly selected frames in each video stream were used to train the classification algorithm and the other half were used as test data.

Colour and single channelled (separate red, green and blue) smoke-only images were used to extract the features. Each image of the captured colour video sequence was divided into its red, green and blue single-channel images. Smoke-only images were constructed for both colour images and their three single channel images according to equation-5.5. For an example, fig. 6.13 shows a smoke image caused by kerosene smoke on the white background (a), the thresholded (black and white) difference image (b) using equation-5.4, the noise-only image (c) using equation-5.5 and the corresponding intensity histogram of smoke pixels (d).

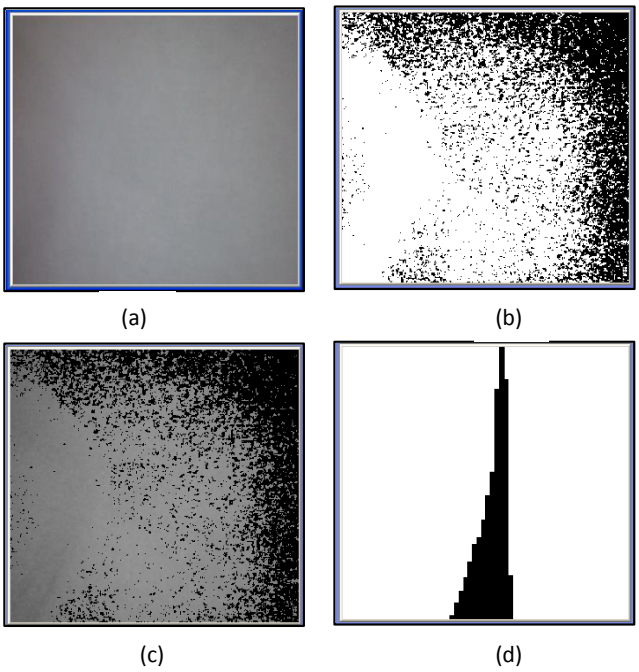

Figure 6.13 The noise caused by kerosene smoke particles on a white background (a), thresholded (black and white) difference image (b), the noise (smoke) – only image (c) and the corresponding intensity histogram of smoke pixels (d)

6.3.2.1 CLASSIFICATION WITH SINGLE CHANNEL IMAGES

Particle intensity histograms were calculated and the *MVI*s were obtained for the red, green and blue single channel images of all 500 frames of each image sequence. Figure 6.14 shows an example RGB colour image of polyurethane smoke with its separate red, green and blue channel images. It also shows the histograms of these single channel images. As illustrated in Figure 6.14, it is clear that noticeably different histograms can be obtained from the three single channel images, even though there is no visible difference between the single channel images. Some example calculated values of $MVI_{Intensity,R}$, $MVI_{Intensity,G}$, and $MVI_{Intensity,B}$ of eight frames (frame 141 to frame 148 of the first set of image sequences of each particle type) captured with digital microscope are shown in table 6.2. The variation of $MVI_{Intensity,R}$, $MVI_{Intensity,G}$, and $MVI_{Intensity,B}$, of all particles over 500 frames (first set of sequences) with a digital microscope are shown in Figure 6.15, 6.16 and 6.17 respectively. Placing a Moving window of a fixed number of frames (50, 100, 150 and 200) over the distribution $MVI_{k,l}$ of all 500 frames of each image sequence, enabled the running mode, mean and standard deviation of *MVI*s (mode, mean and standard deviation of *MVI*s inside the moving window) of the calculated histograms to be obtained.

Two mutually independent feature vector sets (one with running means and standard deviations, and the other with running modes) were constructed as described in Chapter III for every temporal window. For example, Figure 6.18 shows the calculations of feature vector $F_{Steam,200}$ for N=100. ($F_{Steam,200}$ is the feature vector of the 200th window of the steam sequence and x_1 (=146.68) is the mean of noise histogram maximum value indexes for the frames of R-layer in that window).

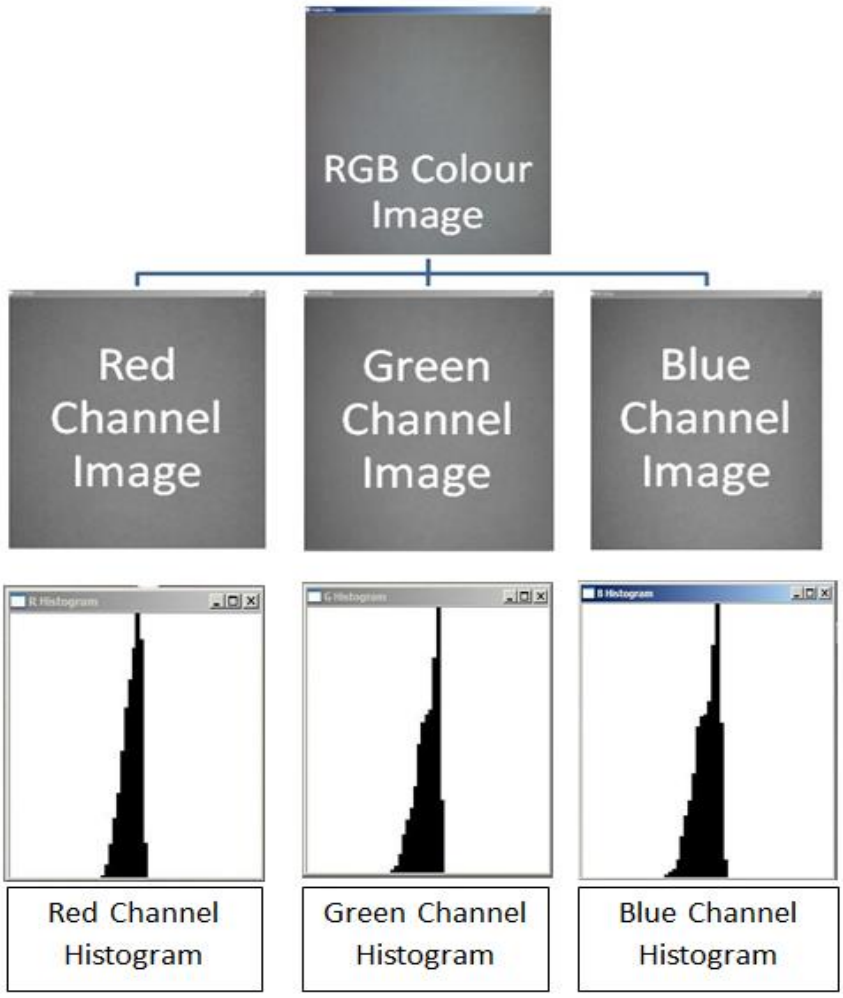

Figure 6.14 An RGB colour image and its separate Red, Green and Blue channel images with image histograms of polyurethane smoke

TABLE 6.2 CALCULATED $MVI_{INTENSITY,R}$, $MVI_{INTENSITY,G}$, AND $MVI_{INTENSITY,B}$ VALUES OF TEN FRAMES (FRAME 141 TO FRAME 150) OF EACH PARTICLE IMAGE SEQUENCE WITH DIGITAL MICROSCOPE

Particle type	Frame Number	$MVI_{Intensity,R}$	$MVI_{Intensity,G}$	$MVI_{Intensity,B}$
Polyurethane	141	134	142	142
Polyurethane	142	128	134	132
Polyurethane	143	128	133	132
Polyurethane	144	134	142	142
Polyurethane	145	131	136	136
Polyurethane	146	131	136	138
Polyurethane	147	132	136	138
Polyurethane	148	132	137	136
Kerosene	141	128	134	132
Kerosene	142	128	133	132
Kerosene	143	134	142	142
Kerosene	144	131	136	138
Kerosene	145	131	136	136
Kerosene	146	131	136	136
Kerosene	147	131	136	136
Kerosene	148	131	136	136
Steam	141	147	151	156
Steam	142	147	151	155
Steam	143	146	151	156
Steam	144	147	151	156
Steam	145	147	151	156
Steam	146	147	151	156
Steam	147	147	151	156
Steam	148	147	151	156
Cooking oil	141	150	149	157
Cooking oil	142	149	150	156
Cooking oil	143	149	149	156
Cooking oil	144	149	149	156
Cooking oil	145	149	150	155
Cooking oil	146	149	149	156
Cooking oil	147	149	149	156
Cooking oil	148	149	149	156
Cotton wool	141	138	159	165
Cotton wool	142	138	159	165
Cotton wool	143	139	160	166
Cotton wool	144	138	160	166
Cotton wool	145	139	159	165
Cotton wool	146	139	161	164
Cotton wool	147	136	161	165
Cotton wool	148	138	159	166
Test Smoke	141	124	127	128
Test Smoke	142	124	127	129
Test Smoke	143	125	128	130
Test Smoke	144	124	127	129
Test Smoke	145	125	129	131
Test Smoke	146	124	129	131
Test Smoke	147	125	127	130

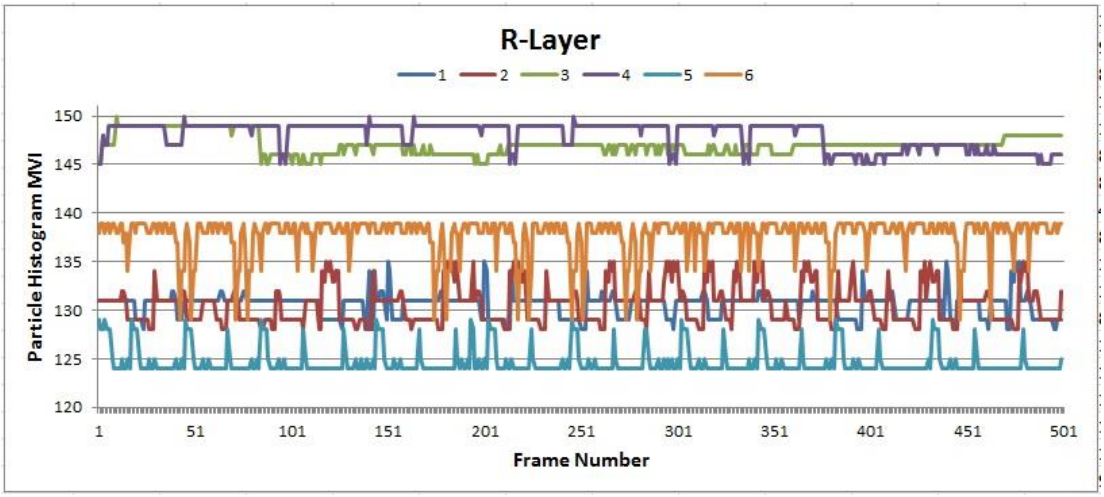

Figure 6.15 The smoke histogram *MVI* for the R-layer sequences of all monotype particle

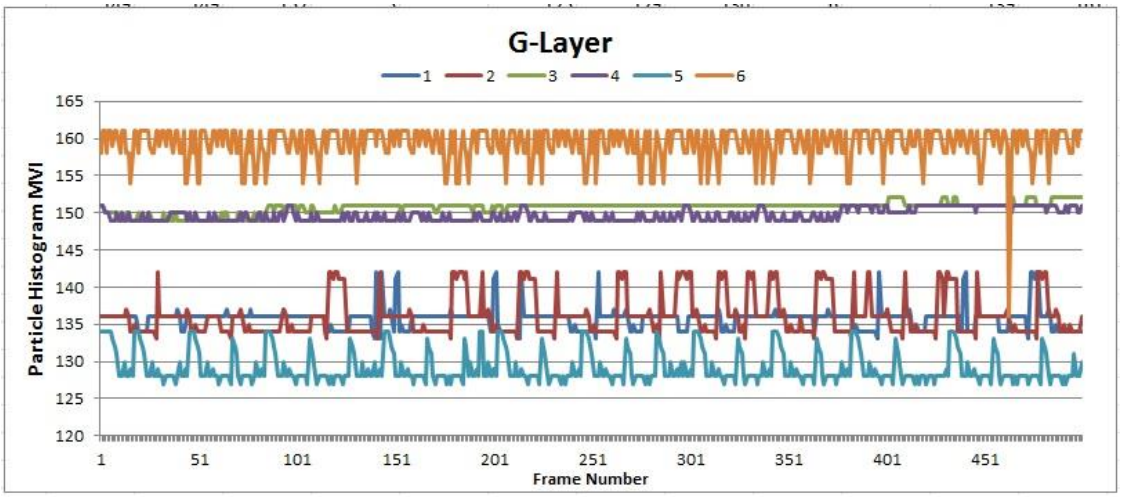

Figure 6.16 The smoke histogram *MVI* for the G-layer sequences of all monotype particle

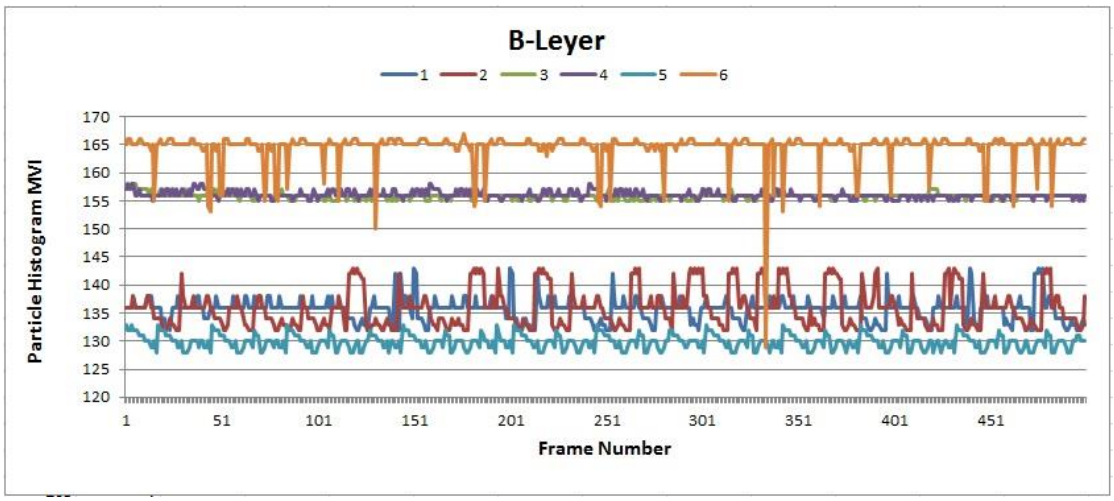

Figure 6.17 The smoke histogram *MVI* for the B-layer sequences of all monotype particle

Note: In the legends of figures 6.15, 6.16 and 6.17, 1, 2, 3, 4, 5 and 6 represent polyurethane, kerosene, steam, cooking oil, test smoke and cotton wool smoke particles respectively.

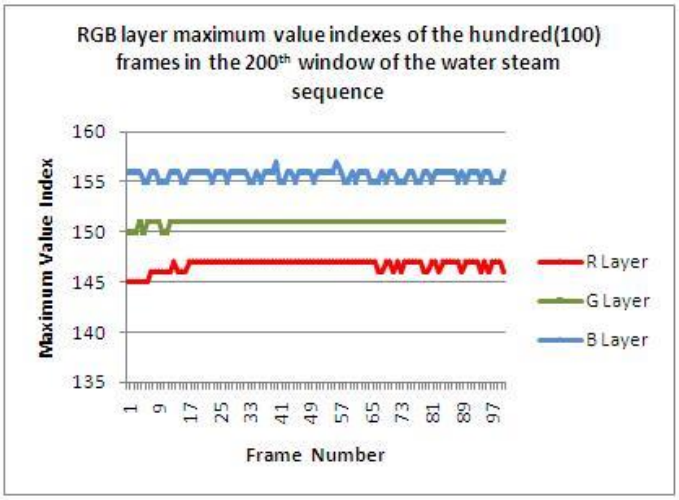

	R Layer	G Layer	B Layer
Mean	146.68	150.94	155.67
STD	0.583961	0.238683	0.513554

Figure 6.18 Window for calculation of feature vector $_{FSteam,200}$

Feature vectors were classified using two widely used supervised classification algorithms; Linear Discriminant Analysis (LDA) (Tang and Tao, 2006; Hamsici and Martinez, 2008; Cazzanti and Gupta, 2007) and K-Nearest Neighbour algorithm (KNN) (Hastie *et al*., 2001; Chen *et al*. 2010; Yu and Yu 2007). KNN and LDA are very simple, commonly used and easy to implement. With Knn, the value of K is extremely training-data dependent and use of a predefined K is one of the major disadvantage of KNN. In the present experiment several K values have been tested and K=10 gave the optimum performance for the selected data set.

The total number of test instances and the correctly classified instances of all the monotype particles classified by the two classification algorithms with four different window sizes, are shown in table 6.3. Here, correctly identified instances are classified into two categories according to the used feature vectors.

Discussion:

As illustrated in Table 6.3, the feature vectors constructed with the running mode classified the test instances more accurately than the feature vectors constructed with the running mean and the standard deviation by both classification algorithms. Again, the classification algorithm LDA gave more accurate results compared to KNN.

TABLE 6.3 TOTAL NUMBER OF TEST INSTANCES AND THE CORRECTLY CLASSIFIED INSTANCES CLASSIFIED BY THE TWO CLASSIFICATION ALGORITHMS

Histogram Type	Window Size	Test Instances	Correctly classified Instances							
			With KNN (K = 10)				With LDA			
			With Mode		With Mean and Standard Deviation		With Mode		With Mean and Standard Deviation	
			Instances	%	Instances	%	Instances	%	Instances	%
Single chanelled Intensity Histograms	50	4050	3025	74.69	3009	74.30	3040	75.06	3018	74.52
	100	3600	2826	78.50	2784	77.33	2845	79.03	2793	77.58
	150	3150	2769	87.90	2682	85.14	2784	88.38	2693	85.49
	200	2700	2700	100.00	2644	97.93	2700	100.00	2652	98.22

As illustrated in Figures 6.15, 6.16 and 6.17, noise histogram maximum value indexes vary slightly around the average in consecutive frames. Therefore, lesser fluctuations of averages of maximum value indexes can be obtained by increasing the size of the moving window. For an example, Figure 6.19 shows the variation of moving averages with window size 50 and 200 for R layer kerosene data in Figure 6.15. According to Figure 6.19, it is clear that the number of overlaps of average values between different particle types can be reduced significantly by increasing the moving window size. This explains the increase in classification accuracy with higher window sizes in table 6.3.

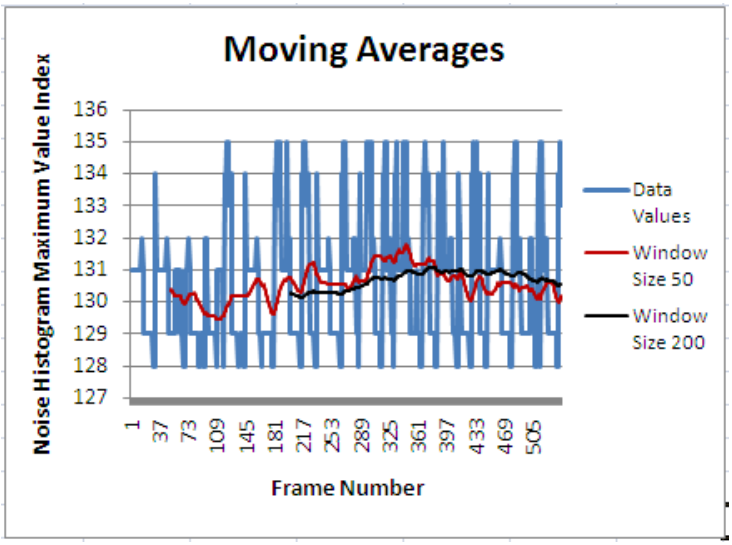

Figure 6.19 Moving averages with window size 50 and 200 for R layer kerosene data in figure 6.15

According to Figures 6.15, 6.16 and 6.17, in most frames, each *MVI* tends to stay in a fixed value rather than varying randomly around its average. Therefore, less fluctuating more separable feature vectors can be obtained with signatures with mode values, rather than with signatures with means and standard deviations. Again, increasing the size of the moving window also results in less fluctuations of running modes. For example, the variation of running modes with window size 50 and 200 for R layer kerosene data is shown in Figure 6.20.

As in the previous feature extraction and testing studies (e.g. Andrew at al., 2014 with only KNN, Truong & Kim, 2011 with only KNN, Narwade and Chakkarwar, 2013 with only SVM, Lalli & V. Palanisamy, 2014 with only KNN etc), the objective of the present study is to find out how accurately the constructed feature vectors classify the particles. According to the output of the KNN classifier the constructed feature vectors able to classify the particles with 100% accuracy (with window size = 200 and K=10) and so decided that there was nothing to be gained by pursuing the significantly higher complexity of SVM. For

a comparison, the data were fed into another classifier LDA and that also classified particles with extracted features effectively.

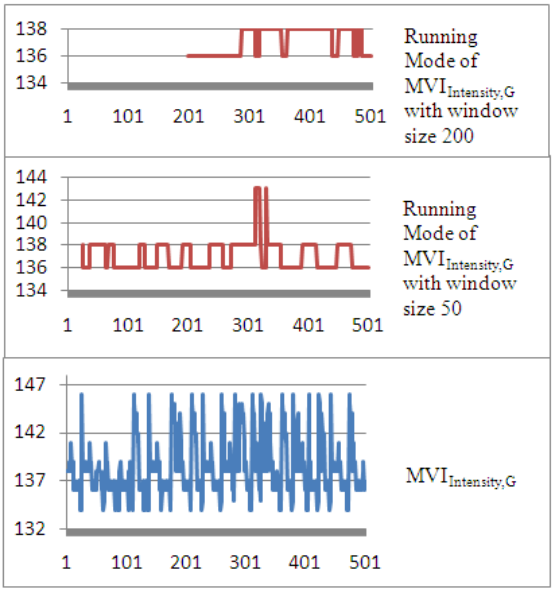

Figure 6.20 variation of running modes with window size 50 and 200 for R layer kerosene data

6.3.2.2 CLASSIFICATION WITH RGB COLOUR IMAGES

The $MVI_{k,l}$ values for k =colour and l ϵ {red, green, blue} were calculated for each isolated particle image of the image sequences. For comparison, the variation of $MVI_{k,l}$ for both k ϵ {intensity and colour} and l ϵ {red, green, blue}, over the first 100 frames of the polyurethane smoke image sequence are shown in fig. 6.21(a) and fig. 6.21(b) respectively.

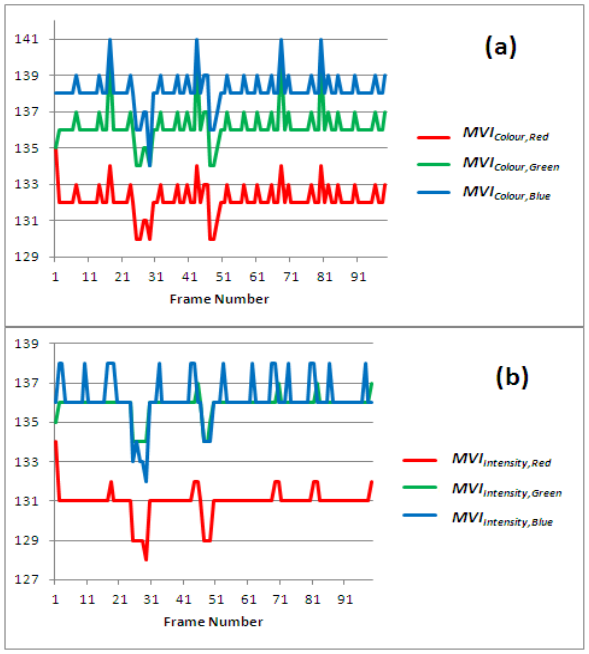

Figure 6.21 Variation of $MVI_{k,l}$ for each *k* ϵ {intensity, colour} and each *l* ϵ {red, green, blue} of polyurethane particle images

The variation of running averages of $MVI_{Colour,G}$ of test particles with a moving window of 100 frames is shown in Figure 6.22(b) together with the running averages of $MVI_{Intensity,G}$ for the same particles (Figure 6.22(a)), as a comparison. Again, with a moving window of size 100 frames, a comparison of running modes of $MVI_{Colour,R}$ (Fig. 6.22(d)), $MVI_{Colour,G}$ (fig. 6.22(f)) and $MVI_{Colour,B}$ (fig. 6.22(h)) with the running modes of $MVI_{Intensity,R}$ (Fig. 6.22(c)), $MVI_{Intensity,G}$ (Fig. 6.22(e)) and $MVI_{Intensity,B}$ (Fig. 6.22(g)) are shown in Figure 6.22 for the same particles (only four randomly selected particle types: 1- polyurethane; 2- kerosene; 4- cooking oil; 5- test smoke, are shown in Figure 6.22 for clarity).

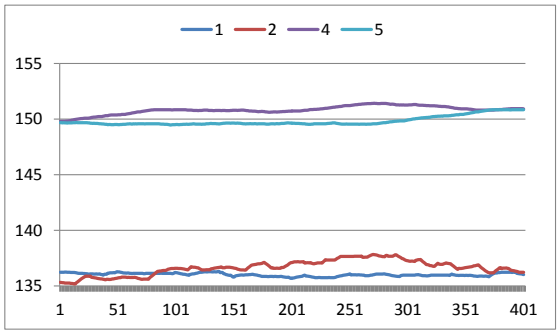

(a) Running averages of $MVI_{intensity,G}$ of first 400 windows of four particle types with window size 100.

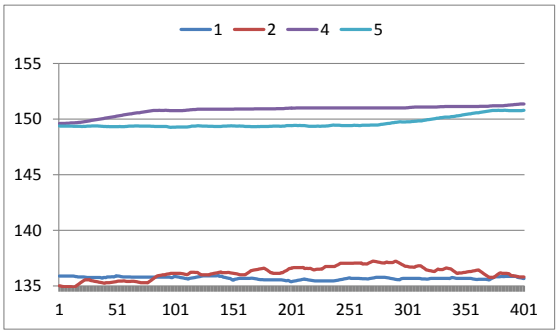

(b) Running averages of $MVI_{colour,G}$ of first 400 windows of four particle types with window size 100.

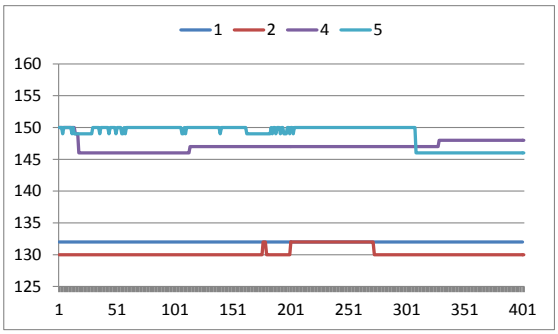

(c) Running modes of $MVI_{intensity,R}$ of first 400 windows of four particle types with window size 100.

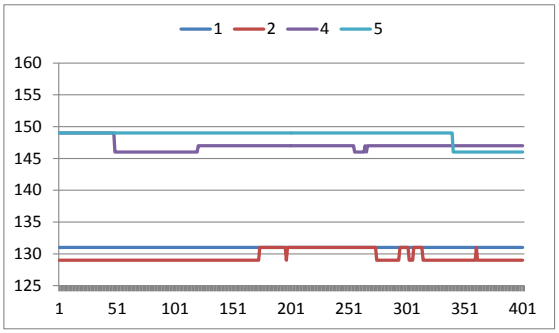

(d) Running modes of $MVI_{colour,R}$ of first 400 windows of four particle types with window size 100.

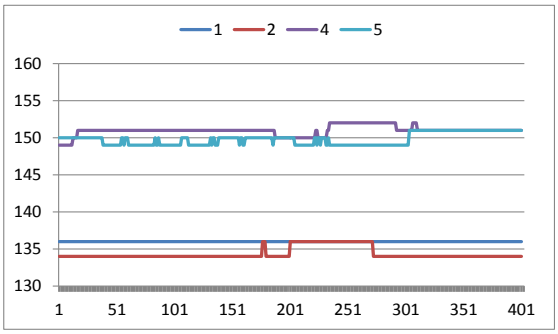

(e) Running modes of $MVI_{intensity,G}$ of first 400 windows of four particle types with window size 100.

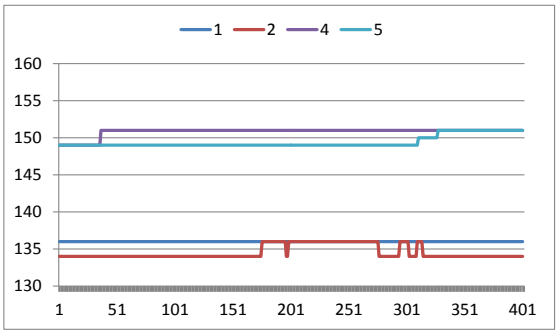

(f) Running modes of $MVI_{colour,G}$ of first 400 windows of four particle types with window size 100.

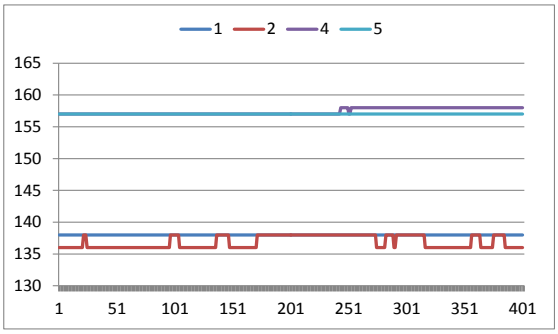

(g) Running modes of $MVI_{intensity,B}$ of first 400 windows of four particle types with window size 100.

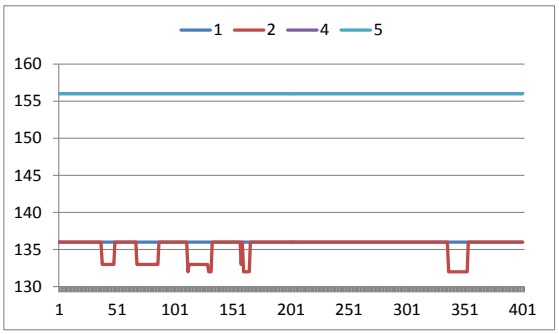

(h) Running modes of $MVI_{colour,B}$ of first 400 windows of four particle types with window size 100.

Figure 6.22 Comparison of the variation of running modes and running averages of *MVI*s. Only four particle types (1- polyurethane; 2- kerosene; 4- cooking oil; 5- test smoke) are shown here for clarity

Feature vectors constructed with $MVI_{Colour,l}$, where l ϵ {red, green, blue} were classified again using the two classification algorithms, Linear Discriminant Analysis (LDA) and K-Nearest Neighbour algorithm (KNN). Total number of test instances and the correctly classified instances of all the monotype particles classified by the two classification algorithms with four different window sizes are shown in table 6.4 (correctly classified instances are divided into two categories according to the used feature vectors).

TABLE 6.4 TOTAL NUMBER OF TEST INSTANCES AND THE CORRECTLY CLASSIFIED INSTANCES CLASSIFIED BY THE TWO CLASSIFICATION ALGORITHMS

Histogram Type	Window Size	Test Instances	Correctly classified Instances							
			With KNN (K = 10)				With LDA			
			With Mode		With Mean and Standard Deviation		With Mode		With Mean and Standard Deviation	
			Instances	%	Instances	%	Instances	%	Instances	%
Colour Histograms	50	4050	3603	88.96	3580	88.40	3630	89.63	3601	88.91
	100	3600	3520	97.78	3322	92.28	3544	98.44	3426	95.17
	150	3150	3150	100.00	3118	98.98	3150	100.00	3122	99.11
	200	2700	2700	100.00	2700	100.00	2700	100.00	2700	100.00

Discussion

According to Table 6.4, again, the feature vectors constructed with the running mode classified the test instances more accurately than the feature vectors constructed with the running mean and the standard deviation by both classification algorithms. Again, the classification algorithm LDA gave more accurate results compared to KNN. The same reason for the higher classification accuracy with the growth of the window size and with the feature vectors constructed with mode rather than mean and standard deviation (which was described in section 6.3.2.1), can be used to explain the higher accuracies in table 6.4.

7 CONCLUSION

The major conclusions (section 7.1), further discussions (section 7.2) and future work (section 7.3) are presented in this chapter in detail.

7.1 MAJOR CONCLUSIONS

Smoke detection:

Image histograms of any of the single channel (red, green, blue or gray-scale) images captured with white LED light can effectively be used to detect the presence of any test particle. Compared to the effectiveness of detecting smaller smoke particles by common photoelectric smoke alarms, this can be considered as a significant achievement since common photoelectric smoke alarms do not respond to particles less than approximately 100 nm diameter.

Smoke classification:

The proposed method successfully used the maximum value indexes of three-channel colour histograms or single-channel red, green and blue histograms of the images of monotype particles (which were generated with Rayleigh scattered light), to correctly classify all the monotype test smoke particles accurately. Both feature vector sets (constructed with mode and, mean and standard deviation of $MVI_{k,l,}$ for $k \in$ {*intensity* and *colour*}) achieved their maximum accuracy of 100% with all the monotype particles

(polyurethane smoke, kerosene smoke, cooking oil smoke, cotton wool smoke, steam and test smoke) when the moving window size is greater than 200.

Compared to the classification speed of KNN with histograms of multi-channel images, MDA with histograms of single channel images performed the fastest classifications.

Overall, the proposed methodology based on the image histogram feature; maximum value indexes of three-channel colour histograms or single-channel red, green and blue histograms of the images which were captured with Rayleigh scattered light, can be considered as a promising solution to a new generation smoke detector which can overcome the limitations of both existing ionization and photoelectric smoke detectors. The results suggest that the proposed algorithm may enable a smoke detector to be safer by detecting a wider range of fires and reduce false alarms such as those caused by steam.

7.2 FURTHER DISCUSSIONS

It was also successfully demonstrated that the variation of maximum value index could also be used to detect impurities of a monotype particle cloud since its image histogram mode, mean and standard deviation vary widely and rapidly for particles of different dimensionalities (Figure 7.1 compares the variations of histogram *MVI*s between a monotype particle sequence (polyurethane) and a non-monotype particle sequence (pinewood)).

As expected, it was observed that the classification accuracy drops significantly with feature vectors of non-monotype particles (e.g. pinewood smoke) due to the variations in particle sizes distributed in the particle cloud over time as explained in Figure 7.1.

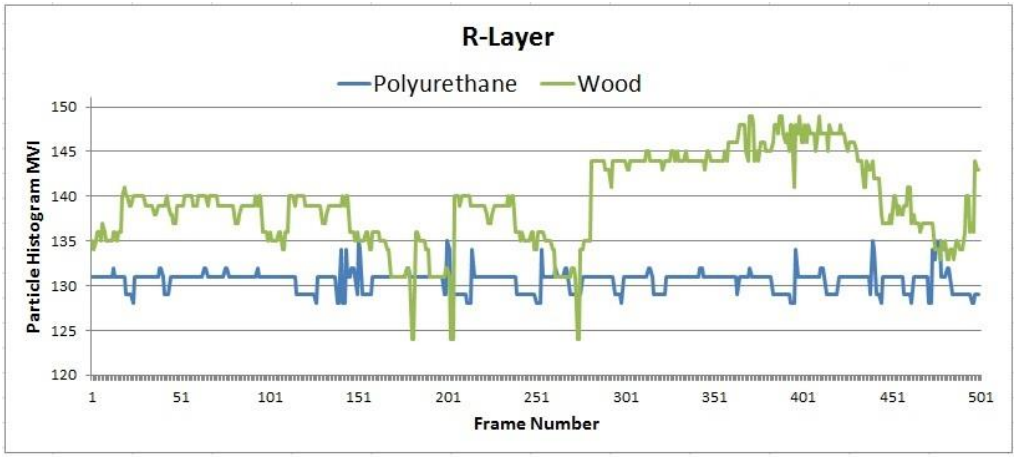

Figure 7.1 Variation of histogram MVIs of the images of polyurethane smoke image sequence and pinewood smoke image sequence

Analysis of the incorrectly identified instances showed that most of the test instances were incorrectly identified as wood smoke particles. For example, because of the wide variability of the average value of the moving window for wood smoke particles, all the time, K-nearest neighbour algorithm identified wood training instances as the closest neighbours for these test instances (Confusion table with 675 classified instances from each particle type with a running window size 50 is shown in table 7.1).

TABLE 7.1 CONFUSION TABLE

Test / **Classified**	Pinewood	Cooking Oil	Polyurethane	Kerosene	Steam	Cotton wool	Test smoke
Pinewood	501	63	59	49	41	55	43
Cooking Oil	25	534	21	28	32	24	31
Polyurethane	34	13	512	21	12	28	22
Kerosene	22	24	24	503	16	41	39
Steam	20	5	14	25	520	20	19
Cotton wool	39	11	23	18	31	480	28
Test smoke	34	25	22	31	23	27	493

All the results are depending on the camera spectral sensitivity function. For smoke detection, three camera types: simple web camera, cyber-shot camera and a digital microscope were used. For example, the used digital microscope and its spectral sensitivity curves are shown in Figure 7.2.

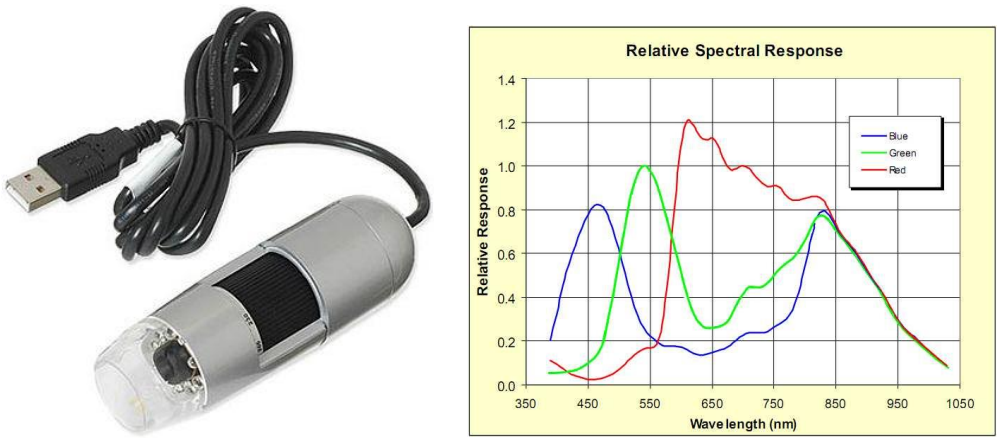

Figure 7.2 The digital microscope and its spectral sensitivity curve (http://www.dinolite.us/support/faq#465)

Results showed that all the three cameras were able to detect the smoke particles effectively. For smoke classification only a digital microscope was used and accurate classification results were obtained. With the cameras with different sensitivities (compared to the used cameras), we would expect it to still work but calibration may be required.

7.3 FUTURE RESEARCH

a) A low cost smoke detector

According to the fact that the whole range of smoke particle sizes (40 nm to 1200 nm) can be detected with both captured Rayleigh and Mie scattering light, a low cost smoke detector that detects the whole range of smoke types can be constructed with a simple silicon photodiode and a white LED (simply replacing the infra-red LED with a white LED in

the existing photoelectric smoke detector) even though, it does not classify the smoke particles. In addition, the sensitivity of the smoke detector to small smoke particles can be improved with additional blue/green enhanced photodiodes (regular silicon photodiodes are more suitable for near IR applications -see Figure 7.3).

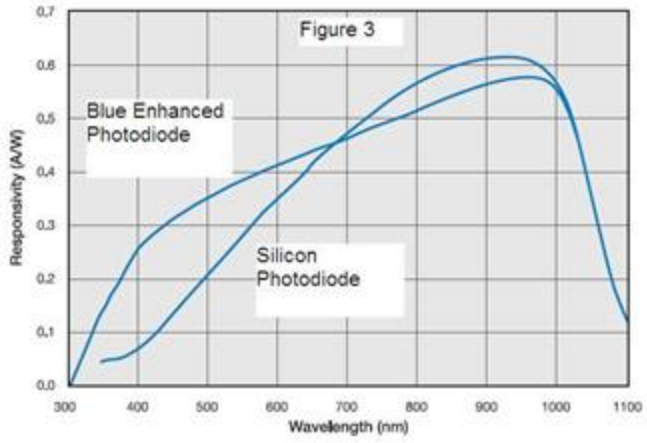

Figure 7.3 Responsivity of blue enhanced photodiode and silicon photodiode to different wavelengths of light

b) Commercial grade smoke classifier

The proposed smoke classification program was tested using a laptop computer with 2.53 GHz processor and 2.9 GB of RAM. The total memory usage by the program is around 22,000 k. At present, the commercially available processor that provides the minimum requirements to run this program can be considered as the Raspberry Pi (priced at US$25), a single-board credit card sized computer (Figure 4) developed in the UK by the Raspberry Pi Foundation (Figure 7.4). This design includes an ARM1176JZF-S 700 MHz processor, VideoCore IV GPU, and 256 Megabytes of RAM. The peripheral devices can be connected with a USB hub.

Figure 7.4 Raspberry Pi

REFERENCES:

Ahmadi, A., Daliri, M. R., Nodehi, A., Qorbani, A., 2012. "Objects Recognition Using the Histogram Based on Descriptors of SIFT and SURF", *Journal of Basic and Applied Scientific Research,* 2 (9), pp. 8612 - 8616.

Ahrens, M., 1998. "U.S. Experience with Smoke Alarms and Other Fire Alarms. Who Has Them? How Well Do They Work? When Don't They Work?", *Report, Fire Analysis and Research Division, National Fire Protection Association*, Quincy, Ma.

Ahrens, M., 2004. ""False Alarms and Unwanted Activations" From: U.S. Experience with Smoke Alarms and Other Fire Detection/Alarm Equipment", *Report, Fire Analysis and Research Division, National Fire Protection Association*, Quincy, Ma.

Ahuja, K., Tuli, P., 2013. "Object Recognition by Template Matching Using Correlations and Phase Angle Method", *International Journal of Advanced Research in Computer and Communication Engineering*, 2 (3), pp. 1368 - 1373.

Andrew A., Kamarudin K., Mamduh S. M., Shakaff A. Y. M., Zakaria A., Adom A. H., Ndzi D., Ragunathan S., 2014. "Classification of domestic burning smell using covariance k- nearest neighbour algorithm for early fire detection application", *Chemical Engineering Transactions*, 40, pp. 271 – 276. DOI: 10.3303/CET1440046.

Bach, J. R., Fuller, C., Gupta, A., Hampapur, A., Horowitz, B., Humphrey, R., Jain, R. C., and Shu. C., 1996. "Virage image search engine: an open framework for image management", *Symposium on Electronic Imaging: Science and Technology - Storage and Retrieval for Image and Video Databases IV*, pp. 76 - 87.

Belhumeur, P. N., Hespanha, J. P., Kriegman, D. J., 1997. "Eigenface vs. Fisherface: recognition using class specific linear projection", *IEEE Transactions on Pattern Analysis and Machine Intelligence*, 19 (7), pp. 711 – 720.

Bloomberg, D. S., 2008. "Color quantization using octrees", *Leptonica*. (http://www.leptonica.org/papers/colorquant.pdf, visited on 05/03/2014).

Bottou, L., Cortes, C., Denker, J. S., Drucker, H., Guyon, I., Jackel, L. D., LeCun, Y., Muller, U. A., Sackinger, E., Simard, P., Vapnik, V., 1994. "Comparison of classifier methods: a case study in handwritten digit recognition", *Proceedings of the 12th IAPR International Conference on Pattern Recognition*, vol. 2, pp. 77 - 82.

Bradski, G. R., Kaehler, A., 2008. *Learning OpenCV: Computer Vision with the OpenCV Library*, Sebastopol, CA: O'Reilly.

Brammer, D.R., 2002. "A comparison between predicted and actual behaviour of domestic smoke detectors in a realistic house fire", Master's Thesis, Department of Civil Engineering, University of Canterbury, New Zealand.

Brunelli, R., Poggio, T., 1993. "Face recognition: features versus templates", *IEEE Transactions on Pattern Analysis and Machine Intelligence*, 15 (10), pp. 1042 – 1052.

Capitan, J., Mantecon, D., Soriano, P., Ollero, A., 2007. "Autonomous perception techniques for urban and industrial fire scenarios", *Proceedings of the IEEE International Workshop on Safety, Security and Rescue Robotics*, Rome, Italy, pp. 1 – 6.

Cappellini, V., Mattii, L., Mecocci, A., 1989. "An Intelligent System for Automatic Fire Detection in Forests" *Lecture Notes in Computer Science*, 399, pp. 351 - 364.

Cazzanti, L., Gupta, M. R., 2007. "Local Similarity Discriminant Analysis", *Proceedings of the 24th International Conference on Machine Learning*, Omni Press, pp. 137 – 144.

Çelik, T., Özkaramanli, H., Demirel, H., 2007. “Fire and smoke detection without sensors: Image processing based approach”, *15th European Signal Processing Conference (EUSIPCO)*, Poznań, Poland, pp. 1794 - 1798.

Chapelle, O., Haffner P., Vapnik, V., 1999. “SVMs for Histogram-Based Image Classification”, *IEEE Transactions on Neural Networks,* Vol.10 , Issue: 5, pp. 1055 – 1064.

Chapelle, O., Haffner, P., Vapnik, V. N., 1999. “Support Vector Machines for Histogram-Based Image Classification”, *IEEE Transactions on Neural Networks*, 10 (5), pp. 1055 – 1064.

Chen, H.-T., Chen, F.-T., Buthpitiya, S., Zhang, Y., Nefian, A. V., 2010. "Lunar Image Classification for Terrain Detection", *Proceeding of the 6th international conference on Advances in visual computing* - Part III, pp. 1 – 8.

Chen,T. -H., Yin, Y. -H., Huang, S. -F., Ye, Y. -T., 2006. “The smoke Detection for Early Fire-Alarming System Based on Video Processing”, *IEEE proceedings of the International conference on Intelligent Information Hiding and Multimedia Signal Processing*, pp. 427 - 430.

Clark, D., 1995. “The popularity algorithm,” *Dr. Dobb’s Journal*, pp. 121-127.

Clark, D., 1996. “Color quantization using octrees,” *Dr. Dobb’s Journal*, pp. 54-57 and 102-104.

Darmakusuma, R., Prihatmanto, A. S., Indrayanto, A., Mengko, T. L., 2012. “Pattern recognition of finger movement detection using Support Vector Machine”, *International Conference on System Engineering and Technology (ICSET),* pp. 1 – 3.

Dedeoğlu, Töreyin, B.U., Güdükbay, U., Çetin, A.E., 2005. “Real-time Fire and Flame Detection in Video”, *IEEE Proceedings of 30th Int. Conf. on Acoustics, Speech and Signal Processing*, 2, ICASSP’05, Philadelphia, USA. Pp. 669 – 672.

Dubuisson, S., 2010. “The computation of the Bhattacharyya distance between histograms without histograms”, *2nd International Conference on Image Processing Theory Tools and Applications (IPTA)*, pp. 373 - 378.

Fabian, T. Z., Gandhi, P. D., 2007. “Smoke Characterization Project, Technical report”, Underwriter Laboratories Inc, Northbrook, IL 60062.

Flickner, M., Sawhney, H., Niblack, W., Ashley, J., Huang, Q., Dom, B., Gorkani, M., Hafner, J., Lee, D., Petkovic, D., Steele, D., and Yanker, P., 1995. “Query by image and video content: The QBIC system”, *IEEE Computer*, 28 (9), pp. 23 - 32.

Furay, T. S., Cristianini, N., Duffy, N., Bednarski, D. W., Schummer, M., Haussler, D., 2000. “Support vector machine classification and validation of cancer tissue samples using microarray expression data”, *Bioinformatics*, Vol. 16, pp. 906 – 914.

Georgara, D., Kermanidis, K. L., Mariolis, I., 2012. “Support Vector Machine Classification of Protein Sequences to Functional Families Based on Motif Selection*”, Proceedings of 8th International Federation for Information Processing (IFIP WG 12.5) International Conference*, pp. 27 - 30.

Gervautz, M., Purgathofer, W., 1988. "A Simple Method for Color Quantization: Octree Quantization", *New Trends in Computer Graphics*, Springer-Verlag Berlin Heidelberg, pp 219 – 231.

Grimson, W. E. L., Stau_er, C., Romano, R., Lee, L., 1998. “Using adaptive tracking to classify and monitor activities in a site”, *Computer Vision and Pattern Recognition*, Santa Barbara, California, pp. 1 - 8.

Hamsici, O. C., Martinez, A. M., 2008. “Bayes Optimality in Linear Discriminant Analysis”, *IEEE Transactions on Pattern Analysis and Machine Intelligence*, Vol. 30, pp. 647 - 657.

Han, D., Lee, B., 2006. “Development of Early Tunnel Fire Detection Algorithm using the Image processing ”, *Lecture Notes in Computer Science*, 4292, pp. 39 - 48.

Hastie, T., Tibshirani, R., Friedman, J., 2001. *The Elements of Statistical Learning — Data Mining, Interface and Prediction*. Canada: Springer, pp. 415 - 426.

He, X., Yan, S., Hu, Y., Niyogi, P., Zhang, H., 2005. “Face recognition using Laplacianfaces”, *IEEE Transactions on Pattern Analysis and Machine Intelligence*, 27 (3), pp. 328 – 340.

Heckbert, P. 1982. "Color Image Quantization for Frame Buffer Display", *Computer Graphics*, Vol 16, 3, pp. 297 – 303.

http://en.wikipedia.org/wiki/Phototransistor#Other_modes_of_operation (visited on 11/03/2014).

http://en.wikipedia.org/wiki/Smoke_detector (visited on 11/03/2014).

http://home.howstuffworks.com/smoke3.htm (visited on 11/03/2014).

http://sales.hamamatsu.com/en/products/solid-state-division/si-photodiode-series.php (visited on 11/03/2014).

http://www.agu.org/pubs/sample_articles/ae/2000JD000190/2.html (visited on 11/03/2014).

http://www.electronics-manufacturers.com/info/sensors-and-detectors/smoke-detectors.html (visited on 11/03/2014).

http://www.nist.gov/public_affairs/releases/smoke_detectors.htm (visited on 01/02/2010)

http://www.sas.org/tcs/weeklyIssues/2004-07-16/feature1/ (visited on 01/02/2010).

Information Report, 2005. Are photoelectric smoke alarms better than ionization smoke alarms for “adjacent to kitchen” installations, to minimize nuisance alarms?, Applied Research Office of the Fire Marshal, (http://www.kingsvillefire.ca/review_on_best_sensor_type_for_kitchens.pdf, visited on 11/03/2014).

Ivanov, Y., Stau_er, C., Bobick, A., Grimson, W. E. L., 1999. “Video surveillance of interactions”, *Second IEEE Workshop on Visual Surveillance*, Fort Collins, Colorado, pp. 82 - 90.

Jain, R., Kasturi, R., Schunck, B. G., 1995. *Machine Vision*, McGraw-Hill, Inc,USA.

Kekre, H. B., Sarode, T. K., Thepade, S. D., Suryavanshi,V., 2010(a). "Improved Texture Feature Based Image Retrieval using Kekre's Fast Codebook Generation Algorithm", *Springer-International Conference on Contours of Computing Technology (Thinkquest-2010)*, Babasaheb Gawde Institute of Technology, Mumbai. Pp. 143 - 149.

Kekre, H. B., Thepade, S. D., 2010(b). "Image Retrieval using Color-Texture Features Extracted from Walshlet Pyramid", *ICGST International Journal on Graphics, Vision and Image Processing (GVIP)*, 10 (I), pp. 9 – 18.

Kekre, H. B., Thepade, S. D., Mukherjee, P., Kakaiya, M., Wadhwa, S., Singh, S., 2010. "Image Retrieval with Shape Features Extracted using Gradient Operators and Slope Magnitude Technique with BTC", *International Journal of Computer Applications* (0975 – 8887), 6 (8), pp. 28 - 33.

Koller, D., Weber, J., Huang, T., Malik, J., Ogasawara, G., Rao, B., Russel. S., 1994. "Towards robust automatic traffic scene analysis in real-time", *Proceedings of the 33rd IEEE Conference on Decision and Control*, Vol. 4, pp. 3776 – 3781.

Kopeika, N. S., 1998. *A system engineering approach to imaging*, SPIE Optical Engineering Press, Bellingham, pp. 446-451.

Kruger, A., 1994. "Median-cut color quantization," *Dr. Dobb's Journal*, pp. 46-54 and 91-92.

Laptev, I., 2010. "Improving object detection with boosted histograms", *Computer Vision and Image Understanding*, 114, pp. 400 – 408.

Lee, B., Han, D., 2007. "Real-Time Fire Detection Using Camera Sequence Image in Tunnel Environment", *Lecture Notes in Computer Science*, 4861, pp. 1209 - 1220.

Li, J., Wang, S., Dou, Z., Yang, Z., 2001. "Discrimination of Smoke Particles Using Infrared Photoelectrical Detection", *International journal of Infrared and Millimetre Waves*, 22 (1), pp. 141 - 151.

Malathi, G., Shanthi, V., 2010. “Histogram based Classification of Ultrasound Images of Placenta”, *International Journal of Computer Applications*, 1 (16), pp. 0975 – 8887.

Mulholland, G. W., Choi, M. Y., 1998. “Measurements of the mass specific extinction coefficient for acetylene and ethylene smoke using the large agglomerate optics facility”, *Twenty-Seventh symposium (international) on Combustion*, The Combustion Institute, Pittsburgh, pp. 1515 - 1522.

Narwade, A. A., Chakkarwar, V. A., 2013. “Smoke detection in video for early warning using static and dynamic features”, *International Journal of Research in Engineering and Technology (IJRET)*, Vol. 02 (11), pp. 610 – 614.

Ogle, V., Stonebraker, M., 1995. “Chabot: Retrieval from a relational database of images”, *IEEE Computer*, 28 (9), pp. 40 – 48.

OpenCV, 2.4.8.0 documentation, 2013. (http://docs.opencv.org/doc/tutorials/ml/introduction_to_svm/introduction_to_svm.html, visited on 14/02/2014).

Photodiode, Wikipedia, http://en.wikipedia.org/wiki/photodiode (visited on 19 September 2012).

Qualey III, J. R., Desmarais, L., Pratt, J., 2001. “Response-Time Comparisons of Ionization and Photoelectric/Heat Detectors”, *Proceedings of International Conference on Automatic Fire Detection* "AUBE '01", 12th., National Institute of Standards and Technology, pp 283 – 299.

Ridder, C., Munkelt, O., Kirchner, H., 1995. “Adaptive Background Estimation and Foreground Detection using Kalman-Filtering”, *Proceedings of International Conference on recent Advances in Mechatronics*, ICRAM’95, UNESCO Chair on Mechatronics, pp. 193 - 199.

Science Magazine: http://news.sciencemag.org/2013/07/smart-knife-sniffs-out-cancer-cells (visited on 12/08/2013).

Sergyan, S., 2008. “Color histogram features based image classification in content-based image retrieval systems”, *6th IEEE International Symposium on Applied Machine Intelligence and Informatics*, pp. 221 - 224.

Shixin, Y., De Backer, S., Scheunders, P. , 2000. “Genetic feature selection combined with fuzzy kNN for hyperspectral satellite imagery”, *IEEE Proceedings of the International Geoscience and Remote Sensing Symposium, IGARSS,* Vol. 2, pp. 702 – 704.

Smith, C. L., 1993. “Smoke detector operability survey – Report on Findings”, Bethesda, MD: *U.S. Consumer Product Safety Commission*, November, Appendix B, pp. 20-21 (not sighted).

Stauffer, C., Grimson, W. E. L., 1999. “Adaptive background mixture models for real-time tracking*”, Computer Vision and Pattern Recognition*, Fort Collins, Colorado, pp. 246-252.

Swain, M. J., Ballard, D. H., 1990. “Indexing via color histograms”, *Proceedings of the 3rd International Conference on Computer Vision*, pp 390 – 393.

Swain, M. J., Ballard, D. H., 1991. “Color indexing”, *International Journal of Computer Vision*, 7(1), pp. 11 – 32.

Tang, F., Tao, H., 2006. “Fast Linear Discriminant Analysis Using Binary Bases”, *18th International Conference on Pattern Recognition (ICPR)*, Vol. 2, pp. 52 - 55.

Toreyin, B.U., and Cetin, A.E., 2007. “Online Detection of Fire in Video”, *IEEE Comp. Soc. Conf. on Computer Vision and Pattern Recognition (CVPR 2007)*, Online Learning for Classification Workshop, MN, USA.

Toreyin, B.U., Dedeoglu, Y., Gudukbay, U., Cetin, A.E., 2006. “Computer Vision Based System for Real-time Fire and Flame Detection”, *Pattern Recognition Letters*, 27 pp. 49-58.

Truong, T. X., Kim, J-M., 2011. “A Smoke Detection Method based on Video for Early Fire-Alarming System”, *The Korea Information Processing Society (KIPS) transactions*, Part B / v.18B no.4, pp. 213 – 220.

Turk, M. A., Pentland, A. P., 1991. “Eigenfaces for recognition”, *Journal of Cognitive Neuroscience*, 3 (1), pp. 71 – 96.

Weinert, D., Cleary, T. G., Mulholland, G. W., Beever, P. F., 2003. “Light Scattering Characteristics and Size Distribution of Smoke and Nuisance Aerosols”, *Fire Safety Science*, 7, pp. 209 - 220.

Wiskott, L., Fellous, J., Kruger, N., Malsburg, C., 1997, “Face recognition by elastic bunch graph matching”, *IEEE Transactions on Pattern Analysis and Machine Intelligence*, 19 (7), pp. 775 – 779.

Wren, C. R., Azarbayejani, A., Darrell, T., Pentland. A., 1997. “Pfinder: Real-Time Tracking of the Human Body”, *IEEE Transactions on Pattern Analysis And Machine Intelligence*, 19 (7), pp. 780 – 785.

www.firesafetycouncil.com/pdf/review_on_best_sensor_type_for_kitchens.pdf (visited on 01/02/2010).

Xia, J., Wu, J., Zhai, H., Cui, Z., 2009. “Moving Vehicle Tracking Based on Double Difference and CAMShift”, *Proceedings of the International Symposium on Information Processing*, Huangshan, P.R. China, pp. 29 – 32.

Xiong Z., Caballero R., Wang H., Finn A.M., Lelic M.A., and Peng P.-Y., 2007. “Video-based Smoke Detection: Possibilities, Techniques, and Challenges”, *Proceedings, National Fire Protection Association, Fire Suppression and Detection Research and Applications - A Technical Working Conference (SUPDET)*, Orlando, Florida,

Xu, Z. Xu, J., 2007. “Automatic Fire Detection Based on Image Visual Features”, *IEEE International Conference on Computational Intelligence and Security Workshops*, pp. 316 - 319.

Yu, X.-g., Yu, X.-p., 2007. “Locally Adaptive Text Classification Based K-Nearest Neighbours”, *International Conference on Wireless Communications*, Networking and Mobile Computing, pp. 5651 – 5654.

Zanchettin, C., Bezerra, B. L. D., Azevedo, W. W., 2012. "A KNN-SVM hybrid model for cursive handwriting recognition", *The International Joint Conference on Neural Networks (IJCNN),* pp. 1 – 8.

Zhang, Z., Li, W., Li, B., 2009. "An Improving Technique of Color Histogram in Segmentation-based Image Retrieval", *Fifth IEEE International Conference on Information Assurance and Security*, Vol. 2, pp. 381 - 384.

Zhong, D., Defee, I., 2007. "Performance of similarity measures based on histograms of local image feature vectors", *Pattern Recognition Letters*, 28(15), pp. 2003 – 2010.

Zisserman, 2014. Lecture 2: The SVM classifier (http://www.robots.ox.ac.uk/~az/lectures/ml/lect2.pdf, visited on 14/02/2014)